

Parallel Algorithms for Monte Carlo Particle Transport Simulation on Exascale Computing Architectures

by

Paul Kollath Romano

B.S., Rensselaer Polytechnic Institute (2007)

M.S., Massachusetts Institute of Technology (2009)

Submitted to the Department of Nuclear Science and Engineering
in partial fulfillment of the requirements for the degree of
Doctor of Philosophy in Nuclear Science and Engineering

at the

MASSACHUSETTS INSTITUTE OF TECHNOLOGY

February 2013

© Massachusetts Institute of Technology 2013. All rights reserved.

Author 

Department of Nuclear Science and Engineering

January 11, 2013

Certified by 

Benoit Forget

Assistant Professor of Nuclear Science and Engineering

Thesis Supervisor

Certified by 

Kord S. Smith

KEPCO Professor of the Practice of Nuclear Science and Engineering

Thesis Reader

Accepted by

Mujid S. Kazimi

TEPCO Professor of Nuclear Engineering

Chairman, Department Committee on Graduate Students

Parallel Algorithms for Monte Carlo Particle Transport Simulation on Exascale Computing Architectures

by

Paul Kollath Romano

Submitted to the Department of Nuclear Science and Engineering
on January 11, 2013, in partial fulfillment of the
requirements for the degree of
Doctor of Philosophy in Nuclear Science and Engineering

Abstract

Monte Carlo particle transport methods are being considered as a viable option for high-fidelity simulation of nuclear reactors. While Monte Carlo methods offer several potential advantages over deterministic methods, there are a number of algorithmic shortcomings that would prevent their immediate adoption for full-core analyses. In this thesis, algorithms are proposed both to ameliorate the degradation in parallel efficiency typically observed for large numbers of processors and to offer a means of decomposing large tally data that will be needed for reactor analysis.

A nearest-neighbor fission bank algorithm was proposed and subsequently implemented in the OpenMC Monte Carlo code. A theoretical analysis of the communication pattern shows that the expected cost is $O(\sqrt{N})$ whereas traditional fission bank algorithms are $O(N)$ at best. The algorithm was tested on two supercomputers, the Intrepid Blue Gene/P and the Titan Cray XK7, and demonstrated nearly linear parallel scaling up to 163,840 processor cores on a full-core benchmark problem.

An algorithm for reducing network communication arising from tally reduction was analyzed and implemented in OpenMC. The proposed algorithm groups only particle histories on a single processor into batches for tally purposes — in doing so it prevents all network communication for tallies until the very end of the simulation. The algorithm was tested, again on a full-core benchmark, and shown to reduce network communication substantially.

A model was developed to predict the impact of load imbalances on the performance of domain decomposed simulations. The analysis demonstrated that load imbalances in domain decomposed simulations arise from two distinct phenomena: non-uniform particle densities and non-uniform spatial leakage. The dominant performance penalty for domain decomposition was shown to come from these physical effects rather than insufficient network bandwidth or high latency. The model predictions were verified with measured data from simulations in OpenMC on a full-core benchmark problem.

Finally, a novel algorithm for decomposing large tally data was proposed, analyzed, and implemented/tested in OpenMC. The algorithm relies on disjoint sets of compute

processes and tally servers. The analysis showed that for a range of parameters relevant to LWR analysis, the tally server algorithm should perform with minimal overhead. Tests were performed on Intrepid and Titan and demonstrated that the algorithm did indeed perform well over a wide range of parameters.

Thesis Supervisor: Benoit Forget

Title: Assistant Professor of Nuclear Science and Engineering

Thesis Reader: Kord S. Smith

Title: KEPCO Professor of the Practice of Nuclear Science and Engineering

Acknowledgments

This research was performed under appointment to the Rickover Fellowship Program in Nuclear Engineering sponsored by Naval Reactors Division of the U.S. Department of Energy. This work was also supported in part by the Office of Advanced Scientific Computing Research, Office of Science, US Department of Energy, under Contract DE-AC02-06CH11357 and by the Consortium for Advanced Simulation of Light Water Reactors, an Energy Innovation Hub for Modeling and Simulation of Nuclear Reactors under US Department of Energy Contract No. DE-AC05-00OR22725.

I would like to express my most sincere gratitude to my advisor, Ben Forget, for his unconditional support over the years, for granting me pretty much complete autonomy in pursuing my research, and yet still providing the vision and necessary guidance to work towards a tangible goal. I could not have asked for a better advisor, mentor, or friend to have during my years as a graduate student.

I have been most fortunate to also have Kord Smith serve in an advisory capacity in my work. Kord has helped us tremendously with keeping a focus on realistic problems and one day bringing OpenMC to a point where it could be used for real analysis. I am certainly indebted to him, not only for his advice, lectures, and inspiration, but also for the many drinks that he has subsidized.

It has truly been an honor working closely with Andrew Siegel on the development of parallel algorithms. His guidance was instrumental in the successful analysis and implementation of our tally server methodology. I also thank him for his mentorship on various issues, and look forward to future collaborations together.

Also deserving acknowledgment are Tom Sutton, Tim Trumbull, and Forrest Brown for their patience and willingness to answer my many questions on Monte Carlo methods. My growth as a competent methods developer would not have been possible without their counsel. I would also like to thank Tim Donovan for his help in navigating the public utterance process.

Feedback from the nascent OpenMC user and developer community has significantly improved the usability and performance of the code — a big thanks to Andrew Siegel,

Bryan Herman, Katie Biegel, Jed Phillips, Steven Fine, Nick Horelik, and Adam Nelson for all that they've done in this respect.

The five and a half years that I've spent in graduate school have been incredible thanks to my friends and family all over the country who have provided constant encouragement in all my pursuits. Finally, I want to thank my wife and best friend, Audrey, without whose love, understanding, and support, this would have not been possible. She has pushed me out of my zone of comfort and opened my eyes to the world, quite literally.

Table of Contents

| | |
|--|-----------|
| Table of Contents | 7 |
| List of Figures | 11 |
| List of Tables | 13 |
| 1 Introduction | 15 |
| 1.1 The Monte Carlo Method | 15 |
| 1.2 History of Parallel Algorithms | 17 |
| 1.3 Motivation | 19 |
| 1.4 Challenge Problems | 20 |
| 1.4.1 NEA Monte Carlo Performance Benchmark | 20 |
| 1.4.2 MIT PWR Benchmark | 23 |
| 1.5 Summary of Issues | 23 |
| 1.5.1 Source Convergence | 25 |
| 1.5.2 Cross Section Memory Requirements | 26 |
| 1.5.3 Tally Memory Requirements | 27 |
| 1.5.4 Degradation of Parallel Efficiency | 29 |
| 1.6 Objectives | 31 |
| 2 The OpenMC Monte Carlo Code | 33 |
| 2.1 Background | 33 |
| 2.2 Overview of Program Flow | 34 |
| 2.3 Geometry | 36 |
| 2.3.1 Constructive Solid Geometry | 36 |
| 2.3.1.1 Universes | 37 |
| 2.3.1.2 Lattices | 39 |
| 2.3.2 Computing the Distance to Nearest Boundary | 39 |
| 2.3.3 Finding a Cell Given a Point | 41 |
| 2.3.4 Determining if a Coordinate is in a Cell | 41 |
| 2.3.5 Handling Surface Crossings | 42 |
| 2.3.6 Building Neighbor Lists | 43 |
| 2.3.7 Reflective Boundary Conditions | 43 |
| 2.4 Cross Section Representation | 44 |
| 2.4.1 Energy Grid Methods | 45 |

| | | |
|----------|---|----|
| 2.4.1.1 | Unionized Energy Grid | 45 |
| 2.4.1.2 | Unionized Energy Grid with Nuclide Pointers | 46 |
| 2.5 | Random Number Generation | 46 |
| 2.6 | Physics | 48 |
| 2.6.1 | Sampling Distance to Next Collision | 48 |
| 2.6.2 | (n, γ) and Other Disappearance Reactions | 49 |
| 2.6.3 | Elastic Scattering | 49 |
| 2.6.4 | Inelastic Scattering | 51 |
| 2.6.5 | (n, xn) Reactions | 51 |
| 2.6.6 | Fission | 52 |
| 2.6.7 | Sampling Secondary Angle Distributions | 53 |
| 2.6.7.1 | Isotropic Angular Distribution | 54 |
| 2.6.7.2 | Equiprobable Angle Bin Distribution | 54 |
| 2.6.7.3 | Tabular Angular Distribution | 55 |
| 2.6.8 | Sampling Secondary Energy and Correlated Angle/Energy Distributions | 57 |
| 2.6.8.1 | ACE Law 1 - Tabular Equiprobable Energy Bins | 58 |
| 2.6.8.2 | ACE Law 3 - Inelastic Level Scattering | 59 |
| 2.6.8.3 | ACE Law 4 - Continuous Tabular Distribution | 59 |
| 2.6.8.4 | ACE Law 7 - Maxwell Fission Spectrum | 60 |
| 2.6.8.5 | ACE Law 9 - Evaporation Spectrum | 61 |
| 2.6.8.6 | ACE Law 11 - Energy-Dependent Watt Spectrum | 61 |
| 2.6.8.7 | ACE Law 44 - Kalbach-Mann Correlated Scattering | 62 |
| 2.6.8.8 | ACE Law 61 - Correlated Energy and Angle Distribution | 63 |
| 2.6.8.9 | ACE Law 66 - N-Body Phase Space Distribution | 64 |
| 2.6.9 | Transforming a Particle's Coordinates | 65 |
| 2.6.10 | Effect of Thermal Motion on Cross Sections | 66 |
| 2.6.11 | $S(\alpha, \beta, T)$ Tables | 72 |
| 2.6.11.1 | Calculating Integrated Cross Sections | 73 |
| 2.6.11.2 | Outgoing Angle for Coherent Elastic Scattering | 74 |
| 2.6.11.3 | Outgoing Angle for Incoherent Elastic Scattering | 74 |
| 2.6.11.4 | Outgoing Energy and Angle for Inelastic Scattering | 75 |
| 2.6.12 | Unresolved Resonance Region Probability Tables | 75 |
| 2.6.13 | Variance Reduction Techniques | 77 |
| 2.6.13.1 | Survival Biasing | 77 |
| 2.7 | Tallies | 78 |
| 2.7.1 | Filters and Scores | 78 |
| 2.7.2 | Using Maps for Filter-Matching | 79 |
| 2.7.3 | Volume-Integrated Flux and Reaction Rates | 80 |
| 2.7.3.1 | Analog Estimator | 80 |
| 2.7.3.2 | Collision Estimator | 80 |
| 2.7.3.3 | Track-length Estimator | 81 |
| 2.7.4 | Statistics | 83 |
| 2.7.4.1 | Law of Large Numbers | 83 |
| 2.7.4.2 | Central Limit Theorem | 83 |

| | | |
|----------|--|------------|
| 2.7.4.3 | Estimating Statistics of a Random Variable | 84 |
| 2.8 | Eigenvalue Calculations | 88 |
| 2.8.1 | Method of Successive Generations | 88 |
| 2.8.2 | Shannon Entropy | 89 |
| 3 | Fission Bank Algorithms | 91 |
| 3.1 | Introduction | 91 |
| 3.2 | Master-Slave Algorithm | 92 |
| 3.3 | Nearest-Neighbor Algorithm | 95 |
| 3.4 | Validation of Theoretical Analysis | 105 |
| 3.5 | Results | 108 |
| 3.5.1 | Communication Time | 108 |
| 3.5.2 | Parallel Scaling | 109 |
| 3.6 | Other Considerations | 110 |
| 3.6.1 | Load Balancing | 110 |
| 3.6.2 | Fault Tolerance | 111 |
| 3.7 | Conclusions | 112 |
| 4 | Tally Reduction Algorithms | 113 |
| 4.1 | Batch Statistics | 114 |
| 4.2 | Reduction of Tally Scores | 116 |
| 4.3 | Results | 119 |
| 4.4 | Conclusions | 122 |
| 5 | Domain Decomposition | 125 |
| 5.1 | Background | 125 |
| 5.1.1 | Review of Prior Work | 126 |
| 5.1.2 | Recent Developments | 127 |
| 5.2 | Analysis | 128 |
| 5.2.1 | Problem definition | 128 |
| 5.2.2 | Basic properties | 130 |
| 5.2.3 | Expression for τ | 132 |
| 5.2.4 | Expression for τ' | 134 |
| 5.2.5 | Expression for Δ | 135 |
| 5.3 | Variable leakage rates | 136 |
| 5.4 | Evaluation of model | 139 |
| 5.4.1 | Leakage rates | 140 |
| 5.4.2 | Evaluation of correction factor C and penalty Δ | 143 |
| 5.5 | Conclusions | 145 |
| 6 | Data Decomposition | 149 |
| 6.1 | Background | 149 |
| 6.1.1 | Data decomposition | 150 |
| 6.1.2 | Tally Server Algorithm | 151 |
| 6.2 | Analysis | 153 |

| | | |
|----------|---|------------|
| 6.2.1 | Derivation of performance model | 153 |
| 6.2.1.1 | Blocking Communication | 153 |
| 6.2.1.2 | Non-blocking communication | 156 |
| 6.2.2 | Performance predictions | 158 |
| 6.2.3 | Implications of total memory requirements | 161 |
| 6.2.4 | Dependence of μ on d | 163 |
| 6.3 | Implementation | 164 |
| 6.3.1 | Description of algorithm | 164 |
| 6.3.2 | Potential optimizations | 165 |
| 6.3.2.1 | Explicit buffering | 165 |
| 6.3.2.2 | Combining successive scoring events | 167 |
| 6.3.2.3 | Topologically-aware layouts | 168 |
| 6.4 | Results | 168 |
| 6.5 | Conclusions | 173 |
| 7 | Conclusions | 177 |
| 7.1 | Source Convergence | 178 |
| 7.1.1 | Status | 178 |
| 7.1.2 | Future Work | 179 |
| 7.2 | Parallel Efficiency | 180 |
| 7.2.1 | Contributions of Present Work | 180 |
| 7.2.2 | Future Work | 181 |
| 7.3 | Cross Section Memory | 182 |
| 7.3.1 | Status | 182 |
| 7.3.2 | Future Work | 182 |
| 7.4 | Tally Memory — Domain Decomposition | 183 |
| 7.4.1 | Contributions of Present Work | 183 |
| 7.4.2 | Future Work | 184 |
| 7.5 | Tally Memory — Data Decomposition | 185 |
| 7.5.1 | Contributions of Present Work | 185 |
| 7.5.2 | Future Work | 185 |
| 7.6 | Other Future Work | 186 |
| | References | 189 |

List of Figures

| | | |
|-----|--|-----|
| 1-1 | Geometry layout of the NEA Monte Carlo performance benchmark. . . . | 21 |
| 1-2 | Geometry plot of a preliminary model of the MIT PWR Benchmark generated with the OpenMC Monte Carlo code. | 24 |
| 2-1 | Example of an ellipse and its associated half-spaces. | 37 |
| 2-2 | The shaded region represents a cell bounded by three surfaces. | 38 |
| 2-3 | Mapping of union energy grid to nuclide energy grid through pointers. . | 46 |
| 3-1 | Typical master-slave algorithm. | 93 |
| 3-2 | Nearest-neighbor communication pattern. | 95 |
| 3-3 | Example illustrating nearest-neighbor fission bank algorithm. | 98 |
| 3-4 | Expected number of fission bank sites sent to neighboring processes using 8 processes. | 106 |
| 3-5 | Expected number of fission bank sites sent to neighboring processes using 16 processes. | 106 |
| 3-6 | Q-Q plot of M_1 for Case 1 | 107 |
| 3-7 | Execution time for fission bank algorithms. | 108 |
| 3-8 | Parallel scaling for the Monte Carlo Performance Benchmark on the Cray XK6 (Jaguar) and Blue Gene/P (Intrepid) supercomputers. | 110 |
| 4-1 | Summation of tally scores across processors when doing statistics based on a single particle history or single generation. | 116 |
| 4-2 | Summation of tally scores across processors when doing statistics based on a single batch with $M = 4$ | 118 |
| 4-3 | Summation of tally scores across processors when doing statistics based on a batch combining realizations from a single processor with $M = 4$. . | 120 |
| 4-4 | Percentage CPU usage of entire cluster during two simulations of the Monte Carlo Performance Benchmark. | 122 |
| 4-5 | Network bandwidth during two simulations of the Monte Carlo Performance Benchmark. | 122 |
| 5-1 | Leakage rate distributions for the full, quarter, and ninth assembly experiments. | 141 |
| 5-2 | Average values of leakage rate λ at each stage for the full, quarter, and ninth assembly experiments. | 142 |

| | | |
|------|--|-----|
| 5-3 | Computed values of p^{max} for each stage versus the value predicted by (5.29). | 143 |
| 6-1 | Estimated tally server overhead for Intrepid Blue Gene/P supercomputer based on (6.10) and (6.17). | 160 |
| 6-2 | Estimated tally server overhead for Titan Cray XK7 supercomputer based on (6.10) and (6.17). | 161 |
| 6-3 | Observed dependence of μ on the amount of data tallied, d , on Intrepid and Titan. | 169 |
| 6-4 | Tally server overhead on Intrepid Blue Gene/P as a function of data per event with $c/s = 1$ | 170 |
| 6-5 | Tally server overhead on Intrepid Blue Gene/P as a function of data per event with $c/s = 3$ | 170 |
| 6-6 | Tally server overhead on Intrepid Blue Gene/P as a function of data per event with $c/s = 7$ | 170 |
| 6-7 | Tally server overhead on Intrepid Blue Gene/P as a function of data per event with $c/s = 15$ | 170 |
| 6-8 | Tally server overhead on Intrepid Blue Gene/P as a function of p for $d = 15360$ | 171 |
| 6-9 | Tally server overhead on Titan Cray XK7 as a function of data per event with $c/s = 1$ | 172 |
| 6-10 | Tally server overhead on Titan Cray XK7 as a function of data per event with $c/s = 3$ | 172 |
| 6-11 | Tally server overhead on Titan Cray XK7 as a function of data per event with $c/s = 7$ | 172 |
| 6-12 | Tally server overhead on Titan Cray XK7 as a function of data per event with $c/s = 15$ | 172 |
| 6-13 | Tally server overhead on Titan Cray XK7 as a function of p for $d = 15360$ | 173 |

List of Tables

| | | |
|-----|--|-----|
| 2.1 | Surface types available in OpenMC. | 38 |
| 3.1 | Test cases for nearest-neighbor fission bank algorithm. | 105 |
| 4.1 | Elapsed wall-clock time for Monte Carlo Performance Benchmark with 8,352,100 tally bins. | 121 |
| 5.1 | The number of stages M for the three numerical experiments vs. the value predicted by (5.37). | 142 |
| 5.2 | Values of Δ and the various terms which contribute to it for each of the three numerical experiments using the Monte Carlo performance benchmark. | 145 |
| 6.1 | Parameters used for tally server overhead models in (6.10) and (6.17). . | 160 |

Chapter 1

Introduction

1.1 The Monte Carlo Method

At the heart of nuclear engineering and many associated fields is the study of the behavior of subatomic particles interacting with matter. Reactor engineers are interested in the distribution of power and other reaction rates at each point in a nuclear reactor; medical physicists are interested in energy deposition in the human body due to radiation treatments; nuclear astrophysicists are interested in how nuclear reactions can produce elements heavier than hydrogen in stars; and so on. In order to determine such quantities, one generally needs knowledge of two things:

1. An understanding of how individual particles interact with the matter through which they're traveling; and
2. A mathematical description for how a distribution of particles evolves in time.

The study of particle interactions is of primary concern to nuclear physicists. The advent of quantum mechanics in the early 20th century greatly advanced the state of understanding of particle interactions, especially with respect to the scattering of particles, a subject which can not be understood well without considering quantum effects. The latter subject, i.e. the theory of particle transport, came to maturity in the middle and later parts of the 20th century, with many advances coming from the

nuclear reactor engineering community which was focused on studying the behavior of fissionable systems.

The physical transport of particles is stochastic and non-deterministic; a free particle moving through a medium, after being born from some nuclear, chemical, or other process, will have a trajectory consisting of a number of successive random steps (a random walk). At the end of this random walk, the particle is absorbed, transmuted, or otherwise “killed”. To cast the problem into a strictly mathematical form, it is necessary to make a continuum hypothesis. This hypothesis implies that the particle density is high enough such that over the length scales (be it in space, energy, or time) one is interested in, the average behavior of particles will be observed. In certain situations, e.g. a reactor operating at very low power, the continuum hypothesis may not be valid, and the actual behavior of particles at any given point in phase space may deviate significantly from its average. However, for most practical cases of interest in nuclear engineering, the particle densities are indeed high enough to justify the continuum hypothesis. The equation that results from this hypothesis is known as the Boltzmann transport equation.

There are two fundamentally different approaches for determining the distribution of particles in a system:

1. *Monte Carlo methods* model particle transport¹ by mimicking the actual physical transport of particles using fictitious “particles” — variables stored in computer memory representative of a position, direction, and energy. At each stage in an actual particle’s life, there is a known probability distribution for the distance it travels between collisions, the probability of undergoing a certain reaction, and the energy and angle following a collision/reaction. By successively sampling these known probability distributions, the life of a particle can be simulated from birth to death. This process is repeated until enough particles have been simulated to obtain the average behavior with sufficiently low statistical uncertainty.
2. *Deterministic methods* determine the average behavior of particles in a system by numerically solving the Boltzmann transport equation. This requires discretizations

¹It is to be understood that while the term *Monte Carlo* applies to a very wide class of statistical simulation techniques, we will be focusing solely on Monte Carlo methods as applied to particle transport.

of each of the phase space variables: space, angle, and energy.

While these two approaches can be shown to be equivalent to one another, there are various trade-offs and incentives for using one method or the other. It should also be noted that deterministic methods encompass a wide variety of solution and discretization techniques, e.g. discrete ordinates [1], spherical harmonics [2], and the method of characteristics [3].

In this thesis, we will focus specifically on the transport of neutrons through a multiplying (fissionable) medium — a topic that is central to the study of energy production in nuclear reactors. When a fissionable medium is present, a source of neutrons is introduced that is itself proportional to the neutron population. As a result, the steady-state neutron transport equation is generally solved as an eigenvalue equation where the eigenvalue represents a scaling factor on the fission source that forces the equation to balance. More specifically, the solution of the neutron transport equation via Monte Carlo methods will be studied in the context of massively parallel simulations on supercomputers. Neutron transport has a few desirable characteristics. Neutrons, being neutral particles, are generally not subject to external forces when traveling between collisions. Moreover, it is not necessary to consider collisions between neutrons since the density of the host medium is generally much greater than the density of neutrons². This property enables the simulation of neutrons via Monte Carlo methods to be parallelized quite easily since the trajectory of each particle is completely independent of all others.

1.2 History of Parallel Algorithms

The ability to simulate complex transport phenomena using stochastic methods was recognized early on in the development of multiplying fission systems. Also recognized was the fact that while providing an elegant means of computing functionals, such methods would require a great amount of computation as well. The development of Monte Carlo methods has thus gone hand-in-hand with the development of computers

²Another way of thinking about this is that the particles and the host medium can be considered mutually exclusive.

over the course of the last half century.

Due to the computationally-intensive nature of Monte Carlo methods, there has been an ever-present interest in parallelizing such simulations. Even in the first paper on the Monte Carlo method [4], John Metropolis and Stanislaw Ulam recognized that solving the Boltzmann equation with the Monte Carlo method could be done in parallel very easily whereas the deterministic counterparts for solving the Boltzmann equation did not offer such a natural means of parallelism. With the introduction of vector computers in the early 1970s, general-purpose parallel computing became a reality. In 1972, Troubetzkoy et al. designed a Monte Carlo code to be run on the first vector computer, the ILLIAC-IV [5]. The general principles from that work were later refined and extended greatly through the work of Forrest Brown in the 1980s [6]. However, as Brown's work shows, the single-instruction multiple-data (SIMD) parallel model inherent to vector processing does not lend itself to the parallelism on particles in Monte Carlo simulations. Troubetzkoy et al. recognized this, remarking that "the order and the nature of these physical events have little, if any, correlation from history to history," and thus following independent particle histories simultaneously using a SIMD model is difficult.

The difficulties with vector processing of Monte Carlo codes led to the adoption of the single program, multiple data (SPMD) technique for parallelization, first proposed in general form in 1984 at IBM [7]. In this model, multiple processors simultaneously execute a program independently of one another. As applied to Monte Carlo particle transport, this means that each different process tracks a particle independently of other processes. However, it is still necessary to exchange some data between processes. For example, tally results from each process need to be added together to obtain a final result. This and other data can be exchanged between processes through a *message-passing* interface.

The SPMD technique became widespread once message-passing standards were introduced in the late 1980s and early 1990s such as PVM [8] and MPI [9]. Over time, the SPMD model has proved much easier to use than vectorization methods in practice and takes advantage of the inherent parallelism on particles rather than instruction-level

parallelism. As a result, it has since become ubiquitous for Monte Carlo simulations of transport phenomena. The SPMD parallel model has enabled high parallel efficiencies in Monte Carlo codes using small clusters.

1.3 Motivation

At the present time, Monte Carlo neutron transport simulations are primarily used for benchmarking and validation purposes. In some cases, research or test reactors can also reasonably be simulated directly using Monte Carlo [10]. For these types of applications, simulation on a small cluster (via SPMD parallelism) is usually sufficient to obtain a solution with acceptably low statical uncertainties within a short amount of time. However, the use of Monte Carlo methods to directly simulate large commercial nuclear reactors has been viewed as impractical due to the excessive computational burden. Instead, reactor core analysis codes have traditionally been based on deterministic methods. Furthermore, at the level of full-core simulation, nodal diffusion methods are typically employed.

The use of diffusion theory introduces approximations that are sometimes not very accurate, particularly with respect to leakage and the presence of strong absorbers. To overcome these approximations, one solution is to simply avoid the diffusion approximation and use deterministic transport methods such as discrete ordinates or method of characteristics. However, these methods are, in practice, quite difficult to use at the level of full-core simulation. Again, these methods rely on discretization — this means that the discretized mesh over which the problem must be solved will grow in proportion to the physical size of the problem. Ergo, the solution time and memory requirements will also grow with increases in the physical size of the problem. Seen this way, accurate solution of full-core reactor problems using transport theory, regardless of whether it is by Monte Carlo or deterministic methods, will require large-scale high-performance computing (HPC) resources coupled with parallel algorithms that will scale to thousands or possibly millions of processors.

Monte Carlo methods offer several potential advantages over deterministic methods,

particularly in areas that tend to encumber the practical adoption of transport tools to new classes of problems: the avoidance of complex meshing for complicated geometries, the simplification of the cumbersome multigroup cross section generation process, and, perhaps most importantly, the potentially easier adaptability to the extreme levels of concurrency that are likely to characterize beyond-petascale HPC architectures. Notwithstanding these advantages, there are a number of algorithmic shortcomings that would prevent the immediate adoption of Monte Carlo methods for full-core analyses. Before discussing explicitly the algorithmic shortcomings related to full-core reactor simulation using Monte Carlo and potential solutions, it helps first to set the stage by introducing contemporary “challenge problems”. With these problems as a reference point, the limitations of present parallel methods should then become evident.

1.4 Challenge Problems

1.4.1 NEA Monte Carlo Performance Benchmark

In 2003, Kord Smith issued a challenge by predicting that the solution to a full-core reactor problem using Monte Carlo methods would not be possible on a single CPU in under an hour until the year 2030 [11]. In his lecture, Smith specified that the local power in each pin subdivided into 100 axial and 10 radial zones be calculated to within 1% statistical uncertainty. Smith’s 2030 estimate was later refined by Martin in an invited talk at the M&C 2007 conference [12], who estimated that it would take until year 2019. Hoogenboom and Martin then proposed a full-core benchmark problem [13] at the M&C 2009 conference called the Monte Carlo performance benchmark that would serve as a reference for monitoring progress towards reaching the Kord Smith challenge. The benchmark model consists of a pressurized water reactor with 241 assemblies, each containing a 17 by 17 square rod array. The original version of the benchmark also included five fuel pins with Gadolinium within each assembly as well as two different assembly types having asymmetric positions. However, a later specification of the benchmark [14] removed the five Gadolinium pins in each assembly (instead,

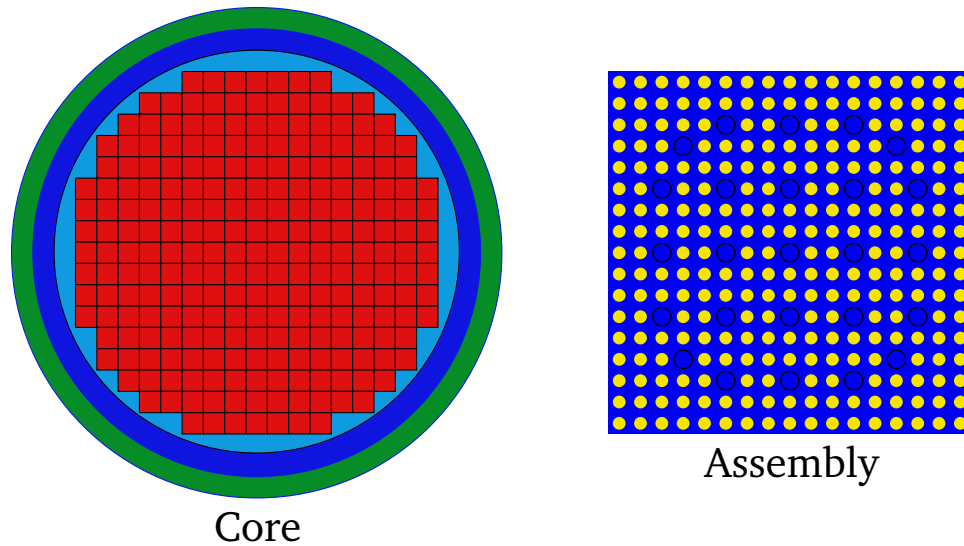


Figure 1-1: Geometry layout of the NEA Monte Carlo performance benchmark.

every pin has Gd) and the asymmetries by having only one assembly type. The later specification also included 25 control rod guide tubes in each assembly. Figure 1-1 shows the general geometric layout of the revised benchmark.

There are a number of simplifications in the Monte Carlo performance benchmark model that make it quite unrealistic as far as light-water reactor (LWR) design is concerned. There are no control rods, no core baffle, no grid spacers, and very limited ex-core detail. Furthermore, the fact that all fuel pins are the same enrichment and composition results in a roughly cosine distribution in the axial direction and a Bessel distribution in the radial direction. All materials in the problem are also specified to use cross sections at a single temperature. Nevertheless, even this simplified problem is computationally challenging due to the number of unknowns to be solved for. In this benchmark, the aim is to compute the power distribution for every fuel pin subdivided into 100 evenly spaced axial nodes (note that the 10 radial rings per pin originally specified by Smith were not included). With 264 fuel pins in each assembly and 241 assemblies, this means there are 6,362,400 unique regions that need to be tallied over.

At the PHYSOR 2010 conference, Kelly et al. presented the first credible solution to the Monte Carlo Performance benchmark [15] using the MC21 Monte Carlo code [16] developed by the Knolls and Bettis Atomic Power Laboratories. To solve for the local power distribution, a simulation was run with 40 billion active neutron histories and the

flux, total absorption rate, and total fission rate were tallied over a pin cell mesh with 100 axial mesh cells. They faced a number of challenges and problems in their solution:

- Even with 40 billion neutrons, virtually none of the local tallies had 95% confidence intervals with half-widths of less than 1% of the mean as required by the Kord Smith Challenge.
- Due to the highly non-uniform nature of the power distribution, regions of the problem with low fission rate density had correspondingly large variances.
- Although the tallies in their simulation required about 0.5 GB of memory, the problem overall took over 6 GB. Since the SPMD method implies that all memory is replicated across different processes, the memory requirements could easily exceed that available on a single node. In their case, they had at least 24 GB of memory shared among four cores.
- Since the benchmark model has a dominance ratio close to unity, Kelly et al. had to use 300 inactive batches before tallies even began to accumulate.

Their simulation ran for 18 hours on 400 processors, implying that on a single processor it would have taken about 300 days.

Leppänen analyzed the Monte Carlo performance benchmark using the Serpent Monte Carlo code [17] and presented results at the SNA + MC2010 conference [18]. In his simulation, 100 billion active neutron histories were used. Thanks to use of delta tracking and various methods that enable a faster simulation at the expense of more memory in Serpent, the simulation took about 21 days on 7 processor cores, a rate twice as fast as that obtained in Kelly et al.'s 2010 analysis. No mention was made of the exact memory requirements for the simulation.

At the PHYSOR 2012 conference, Kelly et al. gave an updated solution to the Monte Carlo performance benchmark, again using MC21 but incorporating a few new methods [19]. The first modification was that they used multiple fission generations per batch to eliminate the systematic underprediction of confidence intervals. In addition, they introduced a new methodology for weighting the fission source sites at each batch to

achieve a flatter variance distribution. With these two methods, they ran a simulation with 200 billion active neutron histories and succeeded in reaching the criterion of having 95% of tallies with 95% confidence intervals with half widths of less than 1% of their respective means. This simulation took 75.6 hours on 750 processor cores.

1.4.2 MIT PWR Benchmark

The introduction of the NEA Monte Carlo performance benchmark was an important first step in encouraging the Monte Carlo community to start addressing problems related to the ability to perform full-core simulations. The analyses by Kelly et al. and Leppänen have shown that obtaining a solution is indeed possible given the availability of large computing resources. However, as previously mentioned, the benchmark model contains many model simplifications that make the problem unrealistic.

To move towards simulation of actual reactor models, MIT is currently developing a PWR full-core benchmark that includes details and dimensions from an actual operating PWR plant. Many of the simplifications that were present in the NEA Monte Carlo performance benchmark are not part of the MIT benchmark; features that are explicitly modeled include radial enrichment zoning, guide tubes and instrument tubes, burnable absorbers and control rods, grid spacers, core support, core baffle, core barrel, thermal shield pads, and the reactor pressure vessel. A geometry plot of the benchmark model is shown in Figure 1-2. The level of detail and complexity in the MIT benchmark will only exacerbate the challenges encountered when simulating the Monte Carlo performance benchmark including high memory requirements, poor source convergence, and the requirement to run possibly trillions of particles to reach convergence of local tallies.

1.5 Summary of Issues

As we see from the preceding considerations, there are a number of formidable challenges to simulating full-core reactor problems directly using Monte Carlo. Perhaps the most important point to recognize (as it indirectly or directly causes all other problems), is that to obtain a converged solution for the spatial distribution of power in a full-core

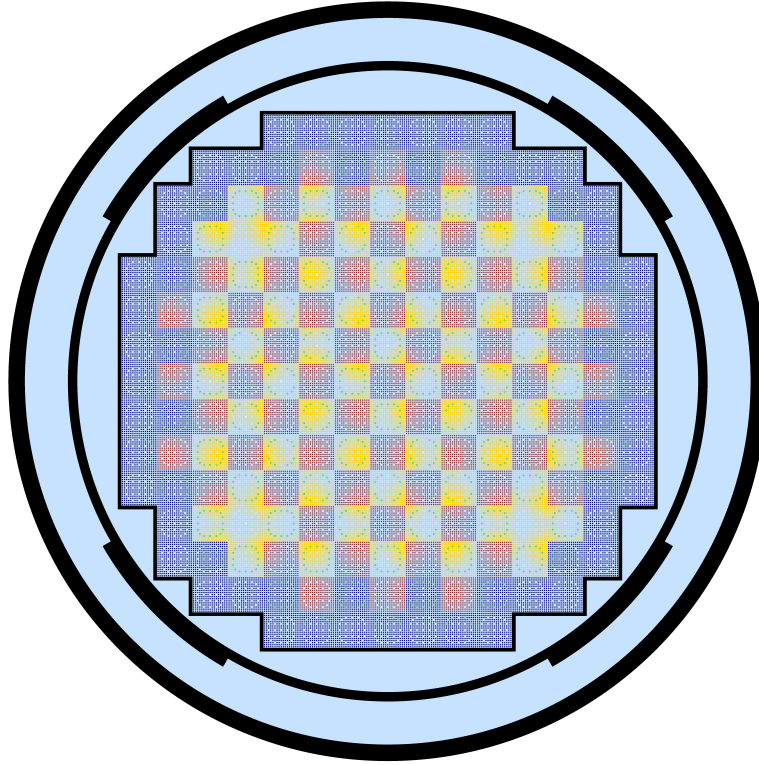


Figure 1-2: Geometry plot of a preliminary model of the MIT PWR Benchmark generated with the OpenMC Monte Carlo code.

model will likely require an unprecedented number of particle histories. The study of Kelly et al. [19] showed that even for the simplified NEA Monte Carlo performance benchmark, 200 billion active neutron histories were required to converge the local tallies. To accurately model changes in material compositions due to depletion, it is likely that as many as 500 axial nodes will be required instead of 100; on top of that, 10 radial rings per pin may be necessary. Thus, assuming the number of particles needed to reach the desired uncertainty criterion scales with the number of tally regions, we would need $200 \cdot 10^9 \times 5 \times 10 = 10 \cdot 10^{12}$, or ten trillion, neutrons to fully converge all tallies.

Barring a huge increase in the efficiency of single processor cores, the expedient solution of a full-core reactor problem will in turn require millions of processors running simultaneously. To-date, only a few studies in the literature have demonstrated the use of even thousands of processors in parallel in a Monte Carlo neutron transport simulation [20, 21].

Let us now discuss each algorithmic issue in further detail to assess 1) whether

solutions to these problems already exist, 2) the status of current work towards their resolution, and 3) what areas need further work. It is the last point that motivates the objective of this thesis.

1.5.1 Source Convergence

In a Monte Carlo k -eigenvalue calculation, we start with some assumed guess of the actual fission source distribution. Before tallies can begin accumulating, it is necessary to first iterate on the fission source to obtain a converged distribution. The rate at which the fission source distribution will converge depends on a quantity known as the *dominance ratio*, the ratio of the first higher harmonic eigenvalue to the fundamental mode eigenvalue. The closer the dominance ratio is to one, the more difficult it is to converge the fission source distribution.

In a typical commercial light-water reactor, the width and height of the reactor core are very large relative to the mean free path of neutrons. As a result, full-core reactor models typically have dominance ratios close to unity. Converging on the fission source distribution can consequently require hundreds of iterations if using standard power iteration. With a small batch size, this might not be much of a concern. However, in a simulation with possibly millions of processor cores, each one must be occupied with sufficient work. As a result, batch sizes with many billions of particles would be needed in practice. If we are to discard hundreds of batches, each composed of billions of particles, at the beginning of every simulation, a great amount of processor time may be wasted.

A number of solutions have been proposed to obtain faster fission source convergence in Monte Carlo k -eigenvalue calculations. These include the fission matrix method [22, 23], Wielandt's method [24, 25], extrapolation methods [26, 27], and acceleration via low-order operators (e.g. coarse mesh finite difference [28, 29, 30]), to name a few. Lee et al. [30] have demonstrated that the CMFD formulation can reduce the number of inactive batches in an eigenvalue calculation to less than 20 with effectively no overhead from solving the low-order CMFD system. With this and other viable solutions at hand,

source convergence is now considered by many in the Monte Carlo community to be a solved problem. Methods to accelerate fission source convergence have been or are currently being implemented in a number of Monte Carlo codes including MCNP [31], MC21, and OpenMC [32].

While source convergence may now be of less concern than it was years ago thanks to effective acceleration methods, the diagnosis and suppression of tally bias due to undersampling [33, 34, 35] is still an outstanding problem. However, this is primarily a physics problem that will not impede the successful implementation of scalable parallel algorithms. As such, it is not explored in this thesis.

1.5.2 Cross Section Memory Requirements

One of the simplifications in the NEA Monte Carlo performance benchmark is that all materials are to be treated at the same temperature. This was done for practical purposes as it allows someone simulating the benchmark to use cross section data processed at a single temperature (in this case room temperature). However, for problems containing nuclides at many temperatures (e.g. a reactor at full power), or with time-varying temperatures, it is necessary to store cross sections at many temperatures.

The next natural question is then — how many temperatures are necessary? This question was studied in some depth by Trumbull [36]. He concluded that for many nuclides, cross sections would need to be stored at increments of less than 28 K. Assuming that even a 28 K interval were sufficient, this means that over the range of temperatures found in a light-water reactor (typically 293 K up to at least 1300 K for steady state calculations and 2500 K for transients), cross sections would be needed at over 75 different temperatures. Thus, potentially hundreds of GB of memory are needed to accommodate cross sections for a truly temperature-dependent model. The reader should once again recall that, in the standard SPMD parallel model, this memory requirement is to be multiplied by the number of processes used in the simulation. It is thus anticipated that special techniques will need to be employed in order to perform massively-parallel full-core LWR simulations given that the memory requirements will almost certainly

exceed the available node memory.

Two solutions for reducing cross section memory requirements have thus far been proposed. The first method is known as on-the-fly Doppler broadening [37, 38]. The basic idea is that the cross section at any temperature can be represented as a series expansion. As a result, only the 0 K cross sections and a series of expansion coefficients need be stored in memory. While this method does show some promise, it may not ultimately be an adequate solution for LWR simulation since the range of temperatures and required accuracy could necessitate that the series expansion contain at least 13 terms and possibly more for certain nuclides [39]. Thus, the problem is merely shifted from storing cross sections at a multitude of temperatures to storing a multitude of series expansion coefficients.

Another method that may potentially solve the cross section memory requirements is the work of Viitanen on explicit temperature treatment [40, 41]. This method would enable simulation using 0 K cross sections via a rejection technique based on Woodcock delta tracking. The downside is that the method may incur a performance penalty. However, from the perspective of massively parallel simulations, the trade-off of a slower calculational rate in return for drastically reduced memory requirement is quite tolerable. It is often said that “flops are free” [42]; on the other hand, memory is an increasingly scarce resource for high fidelity simulations. Given that excellent progress has been made towards reducing cross section memory requirements, it is a topic that will not be further explored as part of the current work.

1.5.3 Tally Memory Requirements

Kelly et al. [19] found that the memory required in their simulation of the Monte Carlo performance benchmark was so large that they were unable to use all processors on a single node. For that problem, the tallies consumed about 0.5 GB on each process — a number that actually may not, at first glance, seem that prohibitive. However, we must keep in mind the following facts: 1) they were only solving for a few (three) physical quantities for each tally region, and 2) the number of regions they used may be 50 times

smaller than that needed for a realistic reactor simulation.

If we were really only interested in a steady-state problem, it would suffice to calculate just the total energy deposition in each tally region and perhaps a few more quantities. However, the fuel composition will slowly change over time due to irradiation and depletion of the fuel. Furthermore, while fresh fuel in a reactor may be composed of only a few nuclides, over time hundreds of actinides and fission product nuclides will appear in the fuel due to nuclear transmutation. This process is governed by a set of equations called the Bateman equations [43]. In order to solve the Bateman equations, one needs to know various reaction rates in each nuclide in the fuel: the fission reaction rate, the (n, γ) reaction rate, the $(n, 2n)$ reaction rate, the $(n, 3n)$ reaction rate, the (n, α) reaction rate, and the (n, p) reaction rate.

To get an idea for just how large the memory requirements for tallies might be, let us consider a depletion simulation of the MIT PWR benchmark. This benchmark has 193 assemblies, each having 264 pins. With 500 axial and 10 radial zones within each fuel pin for depletion purposes, the total number of depletable materials would be 254,760,000. With approximately 300 nuclides and six reaction rates needed for each nuclide, the total memory for tallies would be $254,760,000 \times 300 \times 6 \times 24 \text{ bytes}^3 = 11,005,632,000,000 \text{ bytes}$ or **11 terabytes**. Again, in the SPMD parallel model, this amount of memory would be required for each process. This is clearly a major problem and one that has no easy resolution.

One of the primary objectives of this thesis is to study algorithms for decomposing tally memory and provide guidance on the best path going forward for realistic LWR analysis. Two classes of strategies have been proposed to address this problem — what we loosely refer to as *data decomposition* and *domain decomposition*. Data decomposition could take many forms, but the basic approach would involve the same naturally parallel by-particle parallelization strategy as is currently employed together with a set of dedicated *tally servers* that continuously receive tally updates from the tracking processors (e.g. with one-side operations or by running a continuous receive loop). The spatial decomposition

³We have chosen the last multiplier as 24 bytes for the following reason; for each tally bin we need to store the accumulated sum, the accumulated sum of squares, and also a temporary variable that is used for a single batch. Thus there are three 8-byte floating point numbers.

of the tallies is in general arbitrary and the data sent from the tracking processors could be carried out with non-blocking MPI send operations to maximize overlap in communication/computation.

Domain decomposition on the other hand associates a contiguous region of physical space with each processing element (or node). Each processor then owns the subset of tallies for the corresponding region of physical space. This approach is potentially made efficient with a more complex parallelization strategy where each processor only tracks the particles that are passing through its own portion of the domain. However, new complexities emerge — fast neutrons travel long distances before absorption, and thus the local leakage rates (probability of a neutron leaving a partition before being absorbed) are relatively large. This requires intermediate data exchange *stages* where particles are moved to adjacent processors, potentially leading to significant communication costs and non-trivial load imbalances.

1.5.4 Degradation of Parallel Efficiency

Thus far, we have discussed algorithmic problems that arise when simulating full-core reactor models, regardless of how many processors are utilized. The full-core LWR simulations that have been performed to date [18, 19] have generally used under 1000 processors. With this many processors, overhead from network communication is generally small compared to the overall computation time, especially when using a high-speed network interconnect. However, more realistic reactor simulations will require trillions of particles and hence orders of magnitude greater processor core counts. That being the case, the network communication from message-passing can quickly become prohibitive if scalable algorithms are not utilized. Until recently, Monte Carlo particle transport simulations using this many processors had not been attempted — in fact, the first attempts at such large runs are presented in this thesis.

It has been fairly well-documented that current production Monte Carlo codes, such as MCNP [44], do not scale well to large numbers of processors. So bad is the problem that a prominent researcher has recently questioned whether Monte Carlo truly “is ...

embarrassingly parallel” [45]. The inability to achieve scaling can be traced to one fundamental design flaw. Most parallel algorithms in Monte Carlo codes are commonly implemented in the form of a *master-slave* algorithms. This means that one process acts as the *master*, assigning and coordinating work between all other *slave* processes. While master-slave algorithms can be beneficial from the perspective of maintaining good load balancing, they can also unfortunately create a bottleneck at the master process. In practice, poor scaling can result from two distinct algorithms:

1. *Fission source synchronization* — in an eigenvalue calculation, it is necessary to iterate over the fission source to obtain a converged distribution. During each fission source iteration, source sites are generated as fission occurs and are stored in an array called the *fission bank*. As the generation of these sites is stochastic, we may end up with fewer or more sites than particles requested per source iteration. Thus the specified number of sites must be sampled from the fission bank. Common implementations rely on a single master processor to sort/re-order⁴, sample, and redistribute all source sites.
2. *Tally reduction* — in many Monte Carlo codes, each process responsible for tracking particles accumulates its own estimates of the tally random variables. At the end of every realization, these estimates are added together to obtain a single estimate (with lower variance). In terms of network communication, this requires that the tallies be *reduced* from all processors to one, a process which can take $O(p \log_2 p)$ steps where p is the number of processes. This generally affects both fixed source and eigenvalue calculations, but is only a problem when many tally bins are used. We saw earlier that for realistic reactor calculations, terabytes of memory corresponding to many billions of tally bins would be necessary.

For the time being, we will defer further discussion regarding these algorithms to the chapters where they are analyzed thoroughly. However, we remark that not only are these problems unsolved, they are not even widely recognized by many in the community.

⁴This is done for the sake of maintaining reproducibility, which is discussed at length in chapter 3.

A major objective of this thesis will be to propose, analyze, and demonstrate scalable algorithms for tally reduction and fission source synchronization.

1.6 Objectives

The preceding summary identified a number of challenges that must be overcome before Monte Carlo simulation of full-core light-water reactors is possible. While some of these challenges have either been solved or are currently being researched substantially elsewhere, other areas have received very little attention. The major objectives of this thesis are threefold:

1. To demonstrate a method for collecting tally results without massive network communication that erodes scalability for large tallies and processor counts;
2. To analyze and implement a nearest-neighbor algorithm for sampling and distributing source sites in k -eigenvalue calculations; and
3. To study algorithms for decomposing tally memory in light-water reactor simulations, namely domain decomposition and data decomposition, and evaluate the inherent trade-offs.

The studies and results being presented here would not have been possible without a substantial level of code development within a production Monte Carlo code that employs realistic geometry and physics models. Unfortunately, many production Monte Carlo codes that are widely used in the community, such as MCNP and KENO [46], have a long legacy attached to them and are not written using modern programming paradigms. This, combined with the complexity of these codes, often makes them ill-suited for research purposes. As part of the present work, a modern, high-performance, extensible, open source Monte Carlo code called OpenMC has been developed and released to the public. The development and methodology of the OpenMC Monte Carlo code is discussed thoroughly in chapter 2.

In chapter 3, we present a theoretical analysis of both the traditional parallel fission bank algorithm used in Monte Carlo eigenvalue calculations as well as a novel algorithm

based on nearest-neighbor exchanges of source sites. The novel algorithm is implemented in the OpenMC Monte Carlo code and tested to validate the theoretical analysis. Finally, possible concerns including load balancing, ordering of the fission bank, and fault tolerance are discussed.

In chapter 4, we begin by demonstrating why reducing tallies at every realization during a Monte Carlo simulation may incur significant network communication. A means of reducing communication by using the concept of *batching* is proposed and compared to techniques used to eliminate correlation between successive realizations in eigenvalue calculations. The method is implemented in OpenMC, tested on a problem with large tallies, and demonstrated to reduce communication substantially.

In chapter 5, a model is developed to predict the impact of particle load imbalances on the performance of domain decomposition algorithms for Monte Carlo neutron transport, specifically as applied to LWR analysis. Expressions for upper bound performance “penalties” are derived in terms of simple machine characteristics, material characterizations, and initial particle distributions. Important limitations for domain decomposed simulations are identified and discussed based on the upper bound penalties.

In chapter 6, an algorithm for decomposing large tally data in Monte Carlo particle simulations is developed, analyzed and implemented in OpenMC. The algorithm is based on a non-overlapping decomposition of compute nodes into tracking processors and tally servers. The former are used to simulate the movement of particles through the domain while the latter continuously receive and update tally data. A performance model for this approach is developed, showing that, for a range of parameters relevant to LWR analysis, the tally server algorithm should perform with minimal overhead on contemporary supercomputers. An implementation of the algorithm in OpenMC is then tested on the Intrepid and Titan supercomputers, supporting the key predictions of the model over a wide range of parameters.

Chapter 2

The OpenMC Monte Carlo Code

2.1 Background

As part of the present work, a general Monte Carlo neutron transport code was written from scratch with an emphasis on high performance algorithms, accurate physics capabilities, and modern software design practices. The development of the code started as a simplistic platform, first mentioned in [47], within which algorithms could be easily tested. At that stage, the geometry was limited to a simple structured mesh and all physics were based on predefined fictitious multigroup cross sections. However, as further studies of domain and data decomposition schemes, described in chapter 5 and chapter 6, demanded that realistic geometry and physics be present, a decision was made to greatly expand the capabilities of the code.

In early 2011, the geometry and physics from the original structured-mesh, multigroup code was gutted and replaced with constructive solid geometry routines and physics based on continuous-energy cross sections. In Fall 2011, the input file format was changed to an XML format and a basic outline of the current tally system was introduced. Since then, improvements have been made in physics methods, geometry capabilities, and input/output options.

OpenMC has been described in a recent paper in *Annals of Nuclear Energy* [21]. Further developments will be reported in a paper at the M&C 2013 conference [32].

2.2 Overview of Program Flow

OpenMC performs a Monte Carlo simulation one particle at a time — at no point is more than one particle being tracked on a single program instance¹. Before any particles are tracked, the problem must be initialized. This involves the following steps:

- Read input files and build data structures for the geometry, materials, tallies, and other associated variables.
- Initialize the pseudorandom number generator.
- Read ACE format cross sections specified in the problem.
- If using a special energy grid treatment such as a union energy grid with pointers, that must be initialized as well.
- In a fixed source problem, source sites are sampled from the specified source. In an eigenvalue problem, source sites are sampled from some initial source distribution or from a source file. The source sites consist of coordinates, a direction, and an energy.

Once initialization is complete, the actual transport simulation can proceed. The life of a single particle will proceed as follows:

1. The particle's properties are initialized from a source site previously sampled.
2. Based on the particle's coordinates, the current cell in which the particle resides is determined.
3. The energy-dependent cross sections for the material that the particle is currently in are determined. Note that this includes the total cross section, which is not pre-calculated.
4. The distance to the nearest boundary of the particle's cell is determined based on the bounding surfaces to the cell.

¹When executed in parallel, each program instance tracks one particle at a time.

5. The distance to the next collision is sampled. If the total material cross section is Σ_t , this can be shown to be

$$d = -\frac{\ln \xi}{\Sigma_t} \quad (2.1)$$

where ξ is a pseudorandom number sampled from a uniform distribution on $[0, 1)$.

6. If the distance to the nearest boundary is less than the distance to the next collision, the particle is moved forward to this boundary. Then, the process is repeated from step 2. If the distance to collision is closer than the distance to the nearest boundary, then the particle will undergo a collision. In either case, track-length estimate tallies are scored to based on the closest distance.
7. The material at the collision site may consist of multiple nuclides. First, the nuclide with which the collision will happen is sampled based on the total cross sections. If the total cross section of material i is $\Sigma_{t,i}$, then the probability that any nuclide is sampled is

$$P(i) = \frac{\Sigma_{t,i}}{\Sigma_t}. \quad (2.2)$$

8. Once the specific nuclide is sampled, a reaction for that nuclide is randomly sampled based on the microscopic cross sections. If the microscopic cross section for some reaction x is σ_x and the total microscopic cross section for the nuclide is σ_t , then the probability that reaction x will occur is

$$P(x) = \frac{\sigma_x}{\sigma_t}. \quad (2.3)$$

9. If the sampled reaction is elastic or inelastic scattering, the outgoing energy and angle is sampled from the appropriate distribution. Reactions of type (n, xn) are treated as scattering and the weight of the particle is increased by the multiplicity of the reaction. The particle then continues from step 3. If the reaction is absorption or fission, the particle dies and if necessary, fission sites are created and stored in the fission bank.

After all particles have been simulated, there are a few final tasks that must be performed

before the run is finished. This include the following:

- With the accumulated sum and sum of squares for each tally, the sample mean and its variance is calculated.
- All tallies and other results are written to disk.
- If requested, a source file is written to disk.
- All allocatable arrays are deallocated.

2.3 Geometry

2.3.1 Constructive Solid Geometry

OpenMC uses a technique known as constructive solid geometry (CSG) to build arbitrarily complex three-dimensional models in Euclidean space. In a CSG model, every unique object is described as the union, intersection, or difference of *half-spaces* created by bounding surfaces. Every surface divides all of space into exactly two half-spaces. We can mathematically define a surface as a collection of points that satisfy an equation of the form $f(x, y, z) = 0$ where $f(x, y, z)$ is a given function. All coordinates for which $f(x, y, z) < 0$ are referred to as the negative half-space (or simply the *negative side*) and coordinates for which $f(x, y, z) > 0$ are referred to as the positive half-space.

Let us take the example of a sphere centered at the point (x_0, y_0, z_0) with radius R . One would normally write the equation of the sphere as

$$(x - x_0)^2 + (y - y_0)^2 + (z - z_0)^2 = R^2. \quad (2.4)$$

By subtracting the right-hand term from both sides of (2.4), we can then write the surface equation for the sphere:

$$f(x, y, z) = (x - x_0)^2 + (y - y_0)^2 + (z - z_0)^2 - R^2 = 0 \quad (2.5)$$

One can confirm that any point inside this sphere will correspond to $f(x, y, z) < 0$ and any point outside the sphere will correspond to $f(x, y, z) > 0$.

In OpenMC, every surface defined by the user is assigned an integer to uniquely identify it. We can then refer to either of the two half-spaces created by a surface by a combination of the unique ID of the surface and a positive/negative sign. Figure 2-1 shows an example of an ellipse with unique ID 1 dividing space into two half-spaces.

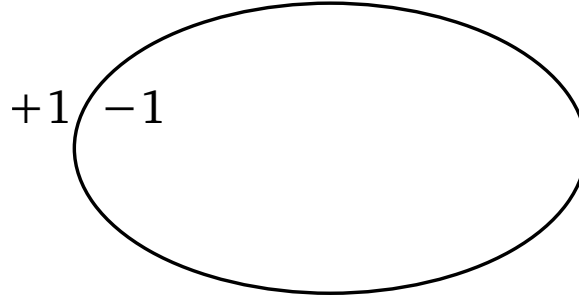


Figure 2-1: Example of an ellipse and its associated half-spaces.

References to half-spaces created by surfaces are used to define regions of space of uniform composition, known as *cells*. While some codes allow regions to be defined by intersections, unions, and differences or half-spaces, OpenMC is currently limited to cells defined only as intersections of half-spaces. Thus, the specification of the cell must include a list of half-space references whose intersection defines the region. The region is then assigned a material defined elsewhere. Figure 2-2 shows an example of a cell defined as the intersection of an ellipse and two planes.

The ability to form regions based on bounding quadratic surfaces enables OpenMC to model arbitrarily complex three-dimensional objects. In practice, one is limited only by the different surface types available in OpenMC. Table 2.1 lists the available surface types, the identifier used to specify them in input files, the corresponding surface equation, and the input parameters needed to fully define the surface.

2.3.1.1 Universes

OpenMC supports universe-based geometry similar to the likes of MCNP [48] and Serpent [17]. This capability enables users to model any identical repeated structures once and

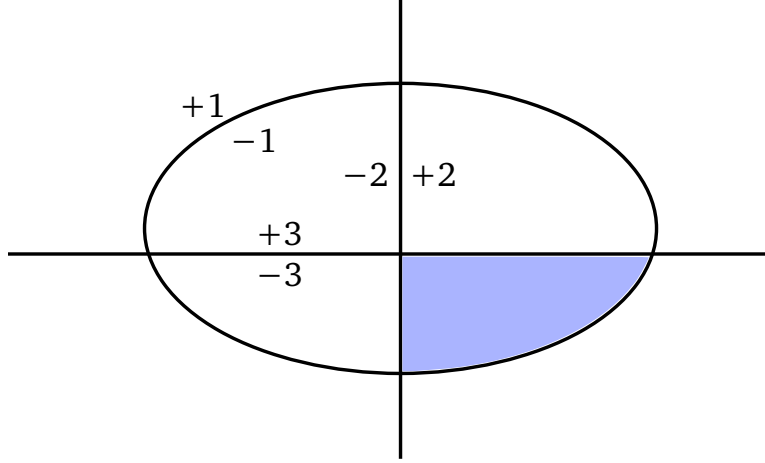


Figure 2-2: The shaded region represents a cell bounded by three surfaces.

Table 2.1: Surface types available in OpenMC.

| Surface | Identifier | Equation | Parameters |
|---|------------|---|-------------------|
| Plane perpendicular to x -axis | x-plane | $x - x_0 = 0$ | x_0 |
| Plane perpendicular to y -axis | y-plane | $y - y_0 = 0$ | y_0 |
| Plane perpendicular to z -axis | z-plane | $z - z_0 = 0$ | z_0 |
| Arbitrary plane | plane | $Ax + By + Cz = D$ | $A B C D$ |
| Infinite cylinder parallel to x -axis | x-cylinder | $(y - y_0)^2 + (z - z_0)^2 = R^2$ | $y_0 z_0 R$ |
| Infinite cylinder parallel to y -axis | y-cylinder | $(x - x_0)^2 + (z - z_0)^2 = R^2$ | $x_0 z_0 R$ |
| Infinite cylinder parallel to z -axis | z-cylinder | $(x - x_0)^2 + (y - y_0)^2 = R^2$ | $x_0 y_0 R$ |
| Sphere | sphere | $(x - x_0)^2 + (y - y_0)^2 + (z - z_0)^2 = R^2$ | $x_0 y_0 z_0 R$ |
| Cone parallel to the x -axis | x-cone | $(y - y_0)^2 + (z - z_0)^2 = R^2(x - x_0)^2$ | $x_0 y_0 z_0 R^2$ |
| Cone parallel to the y -axis | y-cone | $(x - x_0)^2 + (z - z_0)^2 = R^2(y - y_0)^2$ | $x_0 y_0 z_0 R^2$ |
| Cone parallel to the z -axis | z-cone | $(x - x_0)^2 + (y - y_0)^2 = R^2(z - z_0)^2$ | $x_0 y_0 z_0 R^2$ |

then fill them in various spots in the geometry. A prototypical example of a repeated structure would be a fuel pin within a fuel assembly or a fuel assembly within a core.

Each cell in OpenMC can either be filled with a normal material or with a universe. If the cell is filled with a universe, only the region of the universe that is within the defined boundaries of the parent cell will be present in the geometry. That is to say, even though a collection of cells in a universe may extend to infinity, not all of the universe will be “visible” in the geometry since it will be truncated by the boundaries of the cell that contains it.

When a cell is filled with a universe, it is possible to specify that the universe filling the cell should be rotated and translated. This is done through the rotation and translation attributes on a cell (note though that these can only be specified on a cell

that is filled with a universe, not a material).

It is not necessary to use or assign universes in a geometry if there are no repeated structures. Any cell in the geometry that is not assigned to a specified universe is automatically part of the *base universe* whose coordinates are just the normal coordinates in Euclidean space.

2.3.1.2 Lattices

Often times, repeated structures in a geometry occur in a regular pattern such as a rectangular or hexagonal lattice. In such a case, it would be cumbersome for a user to have to define the boundaries of each of the cells to be filled with a universe. Thus, OpenMC provides a lattice capability similar to that used in MCNP and Serpent.

The implementation of lattices is similar in principle to universes — instead of a cell being filled with a universe, the user can specify that it is filled with a finite lattice. The lattice is then defined by a two-dimensional array of universes that are to fill each position in the lattice. A good example of the use of lattices and universes can be seen in the OpenMC model for the Monte Carlo Performance benchmark [49].

2.3.2 Computing the Distance to Nearest Boundary

One of the most basic algorithms in any Monte Carlo code is determining the distance to the nearest surface within a cell. Since each cell is defined by the surfaces that bound it, if we compute the distance to all surfaces bounding a cell, we can determine the nearest one.

With the possibility of a particle having coordinates on multiple levels (universes) in a geometry, we must exercise care when calculating the distance to the nearest surface. Each different level of geometry has a set of boundaries with which the particle's direction of travel may intersect. Thus, it is necessary to check the distance to the surfaces bounding the cell in each level. This should be done starting at the highest (most global) level going down to the lowest (most local) level. That ensures that if two surfaces on different levels are coincident, by default the one on the higher level will

be selected as the nearest surface. Although they are not explicitly defined, it is also necessary to check the distance to surfaces representing lattice boundaries if a lattice exists on a given level.

The following procedure is used to calculate the distance to each bounding surface. Suppose we have a particle at (x_0, y_0, z_0) traveling in the direction u_0, v_0, w_0 . To find the distance d to a surface $f(x, y, z) = 0$, we need to solve the equation:

$$f(x_0 + du_0, y_0 + dv_0, z_0 + dw_0) = 0. \quad (2.6)$$

Since $f(x, y, z)$ in general is quadratic in x, y , and z , this implies that $f(x_0 + du_0, y_0 + dv_0, z_0 + dw_0)$ is quadratic in d . Thus we expect at most two real solutions to (2.6). If no solutions to (2.6) exist or the only solutions are complex, then the particle's direction of travel will not intersect the surface. If the solution to (2.6) is negative, this means that the surface is “behind” the particle, i.e. if the particle continues traveling in its current direction, it will not hit the surface.

Once a distance has been computed to a surface, we need to check if it is closer than previously-computed distances to surfaces. Unfortunately, we cannot just use the minimum function because some of the calculated distances, which should be the same in theory (e.g. coincident surfaces), may be slightly different due to the use of floating-point arithmetic. Consequently, we should first check for floating-point equality of the current distance calculated and the minimum found thus far. This is done by checking if

$$\frac{|d - d_{min}|}{d_{min}} < \epsilon \quad (2.7)$$

where d is the distance to a surface just calculated, d_{min} is the minimum distance found thus far, and ϵ is a small number. In OpenMC, this parameter is set to $\epsilon = 10^{-14}$ since all floating calculations are done on 8-byte floating point numbers.

2.3.3 Finding a Cell Given a Point

Another basic algorithm is to determine which cell contains a given point in the global coordinate system, i.e. if the particle's position is (x, y, z) , what cell is it currently in. This is done in the following manner in OpenMC. With the possibility of multiple levels of coordinates, we must perform a recursive search for the cell. First, we start in the highest (most global) universe, which we call the base universe, and loop over each cell within that universe. For each cell, we check whether the specified point is inside the cell using the algorithm described in subsection 2.3.4. If the cell is filled with a normal material, the search is done and we have identified the cell containing the point. If the cell is filled with another universe, we then search all cells within that universe to see if any of them contain the specified point. If the cell is filled with a lattice, the position within the lattice is determined, and then whatever universe fills that lattice position is recursively searched. The search ends once a cell containing a normal material is found that contains the specified point.

2.3.4 Determining if a Coordinate is in a Cell

To determine which cell a particle is in given its coordinates, we need to be able to check whether a given cell contains a point. The algorithm for determining if a cell contains a point is as follows. For each surface that bounds a cell, we determine the particle's sense with respect to the surface. As explained earlier, if we have a point (x_0, y_0, z_0) and a surface $f(x, y, z) = 0$, the point is said to have negative sense if $f(x_0, y_0, z_0) < 0$ and positive sense if $f(x_0, y_0, z_0) > 0$. If for all surfaces, the sense of the particle with respect to the surface matches the specified sense that defines the half-space within the cell, then the point is inside the cell. Note that this algorithm works only for *simple cells* defined as intersections of half-spaces.

It may help to illustrate this algorithm using a simple example. Let's say we have a cell defined as²

```
<surface id="1" type="sphere" coeffs="0 0 0 10" />
```

²The input file syntax is defined in detail in the OpenMC User's Guide [50].

```

<surface id="2" type="x-plane" coeffs="-3" />
<surface id="3" type="y-plane" coeffs="2" />
<cell id="1" surfaces="-1 2 -3" />

```

This means that the cell is defined as the intersection of the negative half space of a sphere, the positive half-space of an x-plane, and the negative half-space of a y-plane. Said another way, any point inside this cell must satisfy the following equations

$$\begin{aligned}
 x^2 + y^2 + z^2 - 10^2 &< 0 \\
 x - (-3) &> 0 \\
 x - 2 &< 0
 \end{aligned} \tag{2.8}$$

In order to determine if a point is inside the cell, we would substitute its coordinates into (2.8). If the resulting inequalities are satisfied, then the point is indeed inside the cell.

2.3.5 Handling Surface Crossings

A particle will cross a surface if the distance to the nearest surface is closer than the distance sampled to the next collision. A number of things happen when a particle hits a surface. First, we need to check if a non-transmissive boundary condition has been applied to the surface. If a vacuum boundary condition has been applied, the particle is killed and any surface current tallies are scored to as needed. If a reflective boundary condition has been applied to the surface, surface current tallies are scored to and then the particle's direction is changed according to the procedure in subsection 2.3.7.

Next, we need to determine what cell is beyond the surface in the direction of travel of the particle so that we can evaluate cross sections based on its material properties. At initialization, a list of neighboring cells is created for each surface in the problem as described in subsection 2.3.6. The algorithm outlined in subsection 2.3.3 is used to find a cell containing the particle with one minor modification; rather than searching all cells in the base universe, only the list of neighboring cells is searched. If this search is unsuccessful, then a search is done over every cell in the base universe.

2.3.6 Building Neighbor Lists

After the geometry has been loaded and stored in memory from an input file, OpenMC builds a list for each surface containing any cells that are bounded by that surface in order to speed up processing of surface crossings. The algorithm to build these lists is as follows. First, we loop over all cells in the geometry and count up how many times each surface appears in a specification as bounding a negative half-space and bounding a positive half-space. Two arrays are then allocated for each surface, one that lists each cell that contains the negative half-space of the surface and one that lists each cell that contains the positive half-space of the surface. Another loop is performed over all cells and the neighbor lists are populated for each surface.

2.3.7 Reflective Boundary Conditions

If the velocity of a particle is \mathbf{v} and it crosses a surface of the form $f(x, y, z) = 0$ with a reflective boundary condition, it can be shown based on geometric arguments that the velocity vector will then become

$$\mathbf{v}' = \mathbf{v} - 2(\mathbf{v} \cdot \hat{\mathbf{n}})\hat{\mathbf{n}} \quad (2.9)$$

where $\hat{\mathbf{n}}$ is a unit vector normal to the surface at the point of the surface crossing. The rationale for this can be understood by noting that $(\mathbf{v} \cdot \hat{\mathbf{n}})\hat{\mathbf{n}}$ is the projection of the velocity vector onto the normal vector. By subtracting two times this projection, the velocity is reflected with respect to the surface normal. Since the magnitude of the velocity will not change as it undergoes reflection, we can work with the direction of the particle instead, simplifying (2.9) to

$$\boldsymbol{\Omega}' = \boldsymbol{\Omega} - 2(\boldsymbol{\Omega} \cdot \hat{\mathbf{n}})\hat{\mathbf{n}} \quad (2.10)$$

where $\mathbf{v} = \|\mathbf{v}\|\boldsymbol{\Omega}$. The direction of the surface normal will be the gradient of the surface at the point of crossing, i.e. $\mathbf{n} = \nabla f(x, y, z)$. Substituting this into (2.10), we get

$$\boldsymbol{\Omega}' = \boldsymbol{\Omega} - \frac{2(\boldsymbol{\Omega} \cdot \nabla f)}{\|\nabla f\|^2} \nabla f \quad (2.11)$$

If we write the initial and final directions in terms of their vector components, $\Omega = (u, v, w)$ and $\Omega' = (u', v', w')$, this allows us to represent (2.11) as a series of equations:

$$\begin{aligned} u' &= u - \frac{2(\Omega \cdot \nabla f)}{\|\nabla f\|^2} \frac{\partial f}{\partial x} \\ v' &= v - \frac{2(\Omega \cdot \nabla f)}{\|\nabla f\|^2} \frac{\partial f}{\partial y} \\ w' &= w - \frac{2(\Omega \cdot \nabla f)}{\|\nabla f\|^2} \frac{\partial f}{\partial z}. \end{aligned} \tag{2.12}$$

One can then use (2.12) to develop equations for transforming a particle's direction given the equation of the surface.

2.4 Cross Section Representation

The data governing the interaction of neutrons with various nuclei are represented using the ACE format [51] which is used by MCNP [48] and Serpent [17]. ACE-format data can be generated with the NJOY nuclear data processing system [52] which converts raw ENDF/B data [53] into linearly-interpolable data as required by most Monte Carlo codes. The use of a standard cross section format allows for a direct comparison of OpenMC with other codes since the same cross section libraries can be used.

The ACE format contains continuous-energy cross sections for the following types of reactions: elastic scattering, fission (or first-chance fission, second-chance fission, etc.), inelastic scattering, (n, xn) , (n, γ) , and various other absorption reactions. For those reactions with one or more neutrons in the exit channel, secondary angle and energy distributions may be provided. In addition, fissionable nuclides have total, prompt, and/or delayed ν as a function of energy and neutron precursor distributions. Many nuclides also have probability tables to be used for accurate treatment of self-shielding in the unresolved resonance range. For bound scatterers, separate tables with $S(\alpha, \beta, T)$ scattering law data can be used.

2.4.1 Energy Grid Methods

The method by which continuous energy cross sections for each nuclide in a problem are stored as a function of energy can have a substantial effect on the performance of a Monte Carlo simulation. Since the ACE format is based on linearly-interpolable cross sections, each nuclide has cross sections tabulated over a wide range of energies. Some nuclides may only have a few points tabulated (e.g. ^1H) whereas other nuclides may have hundreds or thousands of points tabulated (e.g. ^{238}U).

At each collision, it is necessary to sample the probability of having a particular type of interaction whether it be elastic scattering, $(n, 2n)$, level inelastic scattering, etc. This requires looking up the microscopic cross sections for these reactions for each nuclide within the target material. Since each nuclide has a unique energy grid, it would be necessary to search for the appropriate index for each nuclide at every collision. This can become a very time-consuming process, especially if there are many nuclides in a problem as there would be for burnup calculations. Thus, there is a strong motive to implement a method of reducing the number of energy grid searches in order to speed up the calculation.

2.4.1.1 Unionized Energy Grid

The most naïve method to reduce the number of energy grid searches is to construct a new energy grid that consists of the union of the energy points of each nuclide and use this energy grid for all nuclides. This method is computationally very efficient as it only requires one energy grid search at each collision as well as one interpolation between cross section values since the interpolation factor can be used for all nuclides. However, it requires redundant storage of cross section values at points which were added to each nuclide grid. This additional burden on memory storage can become quite prohibitive. To lessen that burden, the unionized energy grid can be thinned with cross sections reconstructed on the thinned energy grid. This method is currently used by default in the Serpent Monte Carlo code [54].

2.4.1.2 Unionized Energy Grid with Nuclide Pointers

While having a unionized grid that is used for all nuclides allows for very fast lookup of cross sections, the burden on memory is in many circumstances unacceptable. The OpenMC Monte Carlo code utilizes a method that allows for a single energy grid search to be performed at every collision while avoiding the redundant storage of cross section values. Instead of using the unionized grid for every nuclide, the original energy grid of each nuclide is kept and a list of pointers (of the same length as the unionized energy grid) is constructed for each nuclide that gives the corresponding grid index on the nuclide grid for a given grid index on the unionized grid. One must still interpolate on cross section values for each nuclide since the interpolation factors will generally be different. Figure 2-3 illustrates this method. All values within the dashed box would need to be stored on a per-nuclide basis, and the union grid would need to be stored once. This method is also referred to as *double indexing* [55] and is available as an option in Serpent.

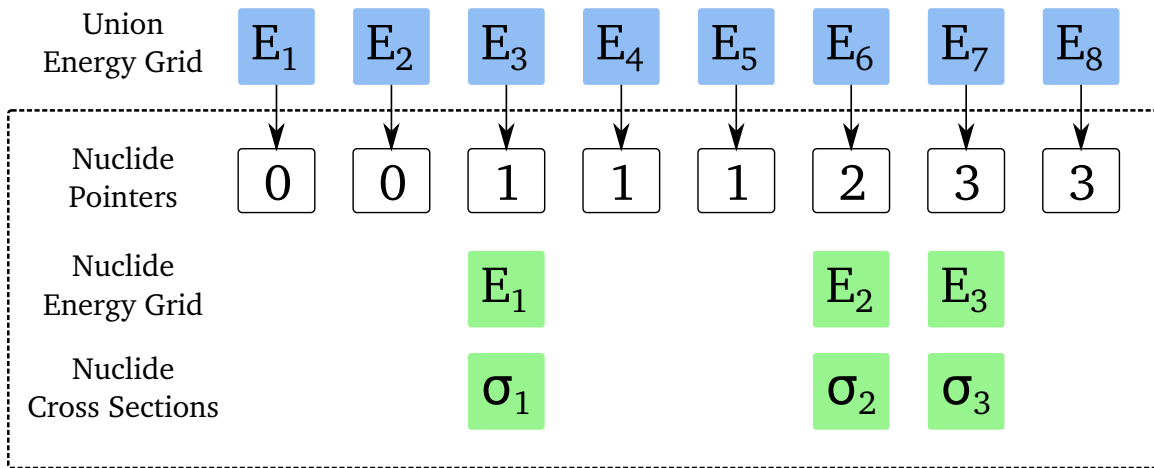


Figure 2-3: Mapping of union energy grid to nuclide energy grid through pointers.

2.5 Random Number Generation

In order to sample probability distributions, one must be able to produce random numbers. The standard technique to do this is to generate numbers on the interval $[0, 1)$

from a deterministic sequence that has properties that make it appear to be random, e.g. being uniformly distributed and not exhibiting correlation between successive terms. Since the numbers produced this way are not truly “random” in a strict sense, they are typically referred to as pseudorandom numbers, and the techniques used to generate them are pseudorandom number generators (PRNGs). Numbers sampled on the unit interval can then be transformed for the purpose of sampling other continuous or discrete probability distributions.

There are a great number of algorithms for generating random numbers. One of the simplest and commonly used algorithms is called a linear congruential generator (LCG). We start with a random number *seed* ξ_0 and a sequence of random numbers can then be generated using the following recurrence relation:

$$\xi_{i+1} = g\xi_i + c \mod M \quad (2.13)$$

where g , c , and M are constants. The choice of these constants will have a profound effect on the quality and performance of the generator, so they should not be chosen arbitrarily. As Donald Knuth stated in his seminal work *The Art of Computer Programming* [56], “random numbers should not be generated with a method chosen at random. Some theory should be used.” Typically, M is chosen to be a power of two as this enables $x \mod M$ to be performed using the bitwise AND operator with a bit mask. The constants for the linear congruential generator used by default in OpenMC are $g = 2806196910506780709$, $c = 1$, and $M = 2^{63}$ [57].

One of the important capabilities for a random number generator is to be able to skip ahead in the sequence of random numbers. Without this capability, it would be very difficult to maintain reproducibility in a parallel calculation. If we want to skip ahead N random numbers and N is large, the cost of sampling N random numbers to get to that position may be prohibitively expensive. Fortunately, algorithms have been developed that allow us to skip ahead in $O(\log_2 N)$ operations instead of $O(N)$. One algorithm to do so is described in a paper by Brown [58]. This algorithm relies on the

following relationship:

$$\xi_{i+k} = g^k \xi_i + c \frac{g^k - 1}{g - 1} \mod M \quad (2.14)$$

Note that (2.14) has the same general form as (2.13), so the idea is to determine the new multiplicative and additive constants in $O(\log_2 N)$ operations.

2.6 Physics

2.6.1 Sampling Distance to Next Collision

As a particle travels through a homogeneous material, the probability distribution function for the distance to its next collision ℓ is

$$p(\ell)d\ell = \Sigma_t e^{-\Sigma_t \ell} d\ell \quad (2.15)$$

where Σ_t is the total macroscopic cross section of the material. Equation (2.15) tells us that the further the distance is to the next collision, the less likely the particle will travel that distance. In order to sample the probability distribution function, we first need to convert it to a cumulative distribution function

$$\int_0^\ell d\ell' p(\ell') = \int_0^\ell d\ell' \Sigma_t e^{-\Sigma_t \ell'} = 1 - e^{-\Sigma_t \ell}. \quad (2.16)$$

By setting the cumulative distribution function equal to ξ , a random number on the unit interval, and solving for the distance ℓ , we obtain a formula for sampling the distance to next collision:

$$\ell = -\frac{\ln(1 - \xi)}{\Sigma_t} \quad (2.17)$$

Since ξ is uniformly distributed on $[0, 1)$, this implies that $1 - \xi$ is also uniformly distributed on $[0, 1)$ as well. Thus, the formula used to calculate the distance to next collision in OpenMC is

$$\ell = -\frac{\ln \xi}{\Sigma_t}. \quad (2.18)$$

2.6.2 (n, γ) and Other Disappearance Reactions

All absorption reactions other than fission do not produce any secondary neutrons. As a result, these are the easiest type of reactions to handle. When a collision occurs, the first step is to sample a nuclide within a material. Once the nuclide has been sampled, then a specific reaction for that nuclide is sampled. Since the total absorption cross section is pre-calculated at the beginning of a simulation, the first step in sampling a reaction is to determine whether a “disappearance” reaction occurs where no secondary neutrons are produced. This is done by sampling a random number ξ on the interval $[0, 1)$ and checking whether

$$\xi \sigma_t(E) < \sigma_a(E) - \sigma_f(E) \quad (2.19)$$

where σ_t is the total cross section, σ_a is the absorption cross section (this includes fission), and σ_f is the total fission cross section. If this condition is met, then the neutron is killed and we proceed to simulate the next neutron from the source bank.

No secondary particles from disappearance reactions such as photons or alpha-particles are produced or tracked in OpenMC. To truly capture the affects of gamma heating, it would be necessary to explicitly track photons originating from (n, γ) and other reactions.

2.6.3 Elastic Scattering

Elastic scattering refers to the process by which a neutron scatters off a nucleus and does not leave it in an excited state. It is referred to as “elastic” because in the center-of-mass system, the neutron does not actually lose energy. However, in lab coordinates, the neutron does indeed lose energy. Elastic scattering can be treated exactly in a Monte Carlo code thanks to its simplicity.

Let us discuss how OpenMC handles two-body elastic scattering kinematics. The first step is to determine whether the target nucleus has any associated motion. Above a certain energy threshold (400 kT by default), all scattering is assumed to take place with the target at rest. Below this threshold though, we must account for the thermal motion of the target nucleus. Methods to sample the velocity of the target nucleus are

described later in subsection 2.6.10. For the time being, let us assume that we have sampled the target velocity \mathbf{v}_t . The velocity of the center-of-mass system is calculated as

$$\mathbf{v}_{cm} = \frac{\mathbf{v}_n + A\mathbf{v}_t}{A + 1} \quad (2.20)$$

where \mathbf{v}_n is the velocity of the neutron and A is the atomic mass of the target nucleus measured in neutron masses (commonly referred to as the *atomic weight ratio*). With the velocity of the center-of-mass calculated, we can then determine the neutron's velocity in the center-of-mass system:

$$\mathbf{V}_n = \mathbf{v}_n - \mathbf{v}_{cm} \quad (2.21)$$

where we have used uppercase \mathbf{V} to denote the center-of-mass system. The direction of the neutron in the center-of-mass system is

$$\boldsymbol{\Omega}_n = \frac{\mathbf{V}_n}{\|\mathbf{V}_n\|}. \quad (2.22)$$

At low energies, elastic scattering will be isotropic in the center-of-mass system, but for higher energies, there may be p-wave and higher order scattering that leads to anisotropic scattering. Thus, in general, we need to sample a cosine of the scattering angle which we will refer to as μ . For elastic scattering, the secondary angle distribution is always given in the center-of-mass system and is sampled according to the procedure outlined in subsection 2.6.7. After the cosine of the angle of scattering has been sampled, we need to determine the neutron's new direction $\boldsymbol{\Omega}'_n$ in the center-of-mass system. This is done with the procedure in subsection 2.6.9. The new direction is multiplied by the speed of the neutron in the center-of-mass system to obtain the new velocity vector in the center-of-mass:

$$\mathbf{V}'_n = \|\mathbf{V}_n\| \boldsymbol{\Omega}'_n. \quad (2.23)$$

Finally, we transform the velocity in the center-of-mass system back to lab coordinates:

$$\mathbf{v}'_n = \mathbf{V}'_n + \mathbf{v}_{cm}. \quad (2.24)$$

In OpenMC, the angle and energy of the neutron are stored rather than the velocity vector itself, so the post-collision angle and energy can be inferred from the post-collision velocity of the neutron in the lab system.

For tallies that require the scattering cosine, it is important to store the scattering cosine in the lab system. If we know the scattering cosine in the center-of-mass, the scattering cosine in the lab system can be calculated as

$$\mu_{lab} = \frac{1 + A\mu}{\sqrt{A^2 + 2A\mu + 1}}. \quad (2.25)$$

However, (2.25) is only valid if the target was at rest. When the target nucleus does have thermal motion, the cosine of the scattering angle can be determined by simply taking the dot product of the neutron's initial and final direction in the lab system.

2.6.4 Inelastic Scattering

The major algorithms for inelastic scattering are described in the following subsections. First, a scattering cosine is sampled using the algorithms in subsection 2.6.7. Then an outgoing energy is sampled using the algorithms in subsection 2.6.8. If the outgoing energy and scattering cosine were given in the center-of-mass system, they are transformed to laboratory coordinates using the algorithm described in subsection 2.6.9. Finally, the direction of the particle is changed also using the procedure in subsection 2.6.9.

Although inelastic scattering leaves the target nucleus in an excited state, no secondary photons from nuclear de-excitation are tracked in OpenMC.

2.6.5 (n, xn) Reactions

These types of reactions are just treated as inelastic scattering and as such are subject to the same procedure as described in subsection 2.6.4. Rather than tracking multiple secondary neutrons, the weight of the outgoing neutron is multiplied by the number of secondary neutrons, e.g. for $(n, 2n)$, only one outgoing neutron is tracked but its weight is doubled.

2.6.6 Fission

While fission is normally considered an absorption reaction, from the perspective of a Monte Carlo simulation it actually bears more similarities to inelastic scattering since fission results in secondary neutrons in the exit channel. Other absorption reactions like (n, γ) or (n, α) , on the contrary, produce no neutrons. There are a few other idiosyncrasies in treating fission. In an eigenvalue calculation, secondary neutrons from fission are only “banked” for use in the next generation rather than being tracked as secondary neutrons from elastic and inelastic scattering would be. On top of this, fission is sometimes broken into first-chance fission, second-chance fission, etc. An ACE table either lists the partial fission reactions with secondary energy distributions for each one, or a total fission reaction with a single secondary energy distribution.

When a fission reaction is sampled in OpenMC (either total fission or, if data exists, first- or second-chance fission), the following algorithm is used to create and store fission sites for the following generation. First, the average number of prompt and delayed neutrons must be determined to decide whether the secondary neutrons will be prompt or delayed. This is important because delayed neutrons have a markedly different spectrum from prompt neutrons, one that has a lower average energy of emission. The total number of neutrons emitted ν_t is given as a function of incident energy in the ACE format. Two representations exist for ν_t . The first is a polynomial of order N with coefficients c_0, c_1, \dots, c_N . If ν_t has this format, we can evaluate it at incoming energy E by using the equation

$$\nu_t(E) = \sum_{i=0}^N c_i E^i. \quad (2.26)$$

The other representation is just a tabulated function with a specified interpolation law. The number of prompt neutrons released per fission event ν_p is also given as a function of incident energy and can be specified in a polynomial or tabular format. The number of delayed neutrons released per fission event ν_d can only be specified in a tabular format. In practice, we only need to determine ν_t and ν_d . Once these have been determined,

we can calculate the delayed neutron fraction

$$\beta = \frac{\nu_d}{\nu_t}. \quad (2.27)$$

We then need to determine how many total neutrons should be emitted from fission. If survival biasing is not being used, then the number of neutrons emitted is

$$\nu = \frac{w \nu_t}{k_{eff}} \quad (2.28)$$

where w is the statistical weight and k_{eff} is the effective multiplication factor from the previous generation. The number of neutrons produced is biased in this manner so that the expected number of fission neutrons produced is the number of source particles that we started with in the generation. Since ν is not an integer, we use the following procedure to obtain an integral number of fission neutrons to produce. If $\xi > \nu - \lfloor \nu \rfloor$, then we produce $\lfloor \nu \rfloor$ neutrons. Otherwise, we produce $\lfloor \nu \rfloor + 1$ neutrons. Then, for each fission site produced, we sample the outgoing angle and energy according to the algorithms given in subsection 2.6.7 and subsection 2.6.8 respectively. If the neutron is to be born delayed, then there is an extra step of sampling a delayed neutron precursor group since they each have an associated secondary energy distribution.

The sampled outgoing angle and energy of fission neutrons along with the position of the collision site are stored in an array called the fission bank. In a subsequent generation, these fission bank sites are used as starting source sites.

2.6.7 Sampling Secondary Angle Distributions

For any reactions with secondary neutrons, it is necessary to sample secondary angle and energy distributions. This includes elastic and inelastic scattering, fission, and (n, xn) reactions. In some cases, the angle and energy distributions may be specified separately, and in other cases, they may be specified as a correlated angle-energy distribution. In the following sections, we will outline the methods used to sample secondary distributions as well as how they are used to modify the state of a particle.

For elastic scattering, it is only necessary to specify a secondary angle distribution since the outgoing energy can be determined analytically. Other reactions may also have separate secondary angle and secondary energy distributions that are uncorrelated. In these cases, the secondary angle distribution is represented as either

- An isotropic angular distribution,
- An equiprobable distribution with 32 bins, or
- A tabular distribution.

2.6.7.1 Isotropic Angular Distribution

In the first case, no data needs to be stored on the ACE table, and the cosine of the scattering angle is simply calculated as

$$\mu = 2\xi - 1 \quad (2.29)$$

where μ is the cosine of the scattering angle and ξ is a random number sampled uniformly on $[0, 1)$.

2.6.7.2 Equiprobable Angle Bin Distribution

For a 32 equiprobable bin distribution, we select a random number ξ to sample a cosine bin i such that

$$i = 1 + \lfloor 32\xi \rfloor. \quad (2.30)$$

The same random number can then also be used to interpolate between neighboring μ values to get the final scattering cosine:

$$\mu = \mu_i + (32\xi - i)(\mu_{i+1} - \mu_i) \quad (2.31)$$

where μ_i is the i th scattering cosine.

2.6.7.3 Tabular Angular Distribution

As the MCNP manual points out [48], using an equiprobable bin distribution works well for high-probability regions of the scattering cosine, but for low-probability regions it is not very accurate. Thus, a more accurate method is to represent the scattering cosine with a tabular distribution. In this case, we have a table of cosines and their corresponding values for a probability distribution function and cumulative distribution function. For each incoming neutron energy E_i , let us call $p_{i,j}$ the j th value in the probability distribution function and $c_{i,j}$ the j th value in the cumulative distribution function. We first find the interpolation factor on the incoming energy grid:

$$f = \frac{E - E_i}{E_{i+1} - E_i} \quad (2.32)$$

where E is the incoming energy of the particle. Then, statistical interpolation is performed to choose between using the cosines and distribution functions corresponding to energy E_i and E_{i+1} . Let ℓ be the chosen table where $\ell = i$ if $\xi_1 > f$ and $\ell = i + 1$ otherwise, and ξ_1 is a random number. Another random number ξ_2 is used to sample a scattering cosine bin j using the cumulative distribution function:

$$c_{\ell,j} < \xi_2 < c_{\ell,j+1}. \quad (2.33)$$

The final scattering cosine will depend on whether histogram or linear-linear interpolation is used. In general, we can write the cumulative distribution function as

$$c(\mu) = \int_{-1}^{\mu} p(\mu') d\mu' \quad (2.34)$$

where $c(\mu)$ is the cumulative distribution function and $p(\mu)$ is the probability distribution function. Since we know that $c(\mu_{\ell,j}) = c_{\ell,j}$, this implies that for $\mu > \mu_{\ell,j}$,

$$c(\mu) = c_{\ell,j} + \int_{\mu_{\ell,j}}^{\mu} p(\mu') d\mu' \quad (2.35)$$

For histogram interpolation, we have that $p(\mu') = p_{\ell,j}$ for $\mu_{\ell,j} \leq \mu' < \mu_{\ell,j+1}$. Thus, after integrating (2.35) we have that

$$c(\mu) = c_{\ell,j} + (\mu - \mu_{\ell,j})p_{\ell,j} = \xi_2. \quad (2.36)$$

Solving for the scattering cosine, we obtain the final form for histogram interpolation:

$$\mu = \mu_{\ell,j} + \frac{\xi_2 - c_{\ell,j}}{p_{\ell,j}}. \quad (2.37)$$

For linear-linear interpolation, we represent the function $p(\mu')$ as a first-order polynomial in μ' . If we interpolate between successive values on the probability distribution function, we have that

$$p(\mu') - p_{\ell,j} = \frac{p_{\ell,j+1} - p_{\ell,j}}{\mu_{\ell,j+1} - \mu_{\ell,j}}(\mu' - \mu_{\ell,j}). \quad (2.38)$$

Solving for $p(\mu')$ in (2.38) and inserting it into (2.35), we obtain

$$c(\mu) = c_{\ell,j} + \int_{\mu_{\ell,j}}^{\mu} \left[\frac{p_{\ell,j+1} - p_{\ell,j}}{\mu_{\ell,j+1} - \mu_{\ell,j}}(\mu' - \mu_{\ell,j}) + p_{\ell,j} \right] d\mu'. \quad (2.39)$$

Let us now make a change of variables using

$$\eta = \frac{p_{\ell,j+1} - p_{\ell,j}}{\mu_{\ell,j+1} - \mu_{\ell,j}}(\mu' - \mu_{\ell,j}) + p_{\ell,j}. \quad (2.40)$$

Equation (2.39) then becomes

$$c(\mu) = c_{\ell,j} + \frac{1}{m} \int_{p_{\ell,j}}^{m(\mu - \mu_{\ell,j}) + p_{\ell,j}} \eta d\eta \quad (2.41)$$

where we have used

$$m = \frac{p_{\ell,j+1} - p_{\ell,j}}{\mu_{\ell,j+1} - \mu_{\ell,j}}. \quad (2.42)$$

Integrating (2.41), we have

$$c(\mu) = c_{\ell,j} + \frac{1}{2m} \left([m(\mu - \mu_{\ell,j}) + p_{\ell,j}]^2 - p_{\ell,j}^2 \right) = \xi_2. \quad (2.43)$$

Solving for μ , we have the final form for the scattering cosine using a tabular distribution and linear-linear interpolation:

$$\mu = \mu_{\ell,j} + \frac{1}{m} \left(\sqrt{p_{\ell,j}^2 + 2m(\xi_2 - c_{\ell,j})} - p_{\ell,j} \right). \quad (2.44)$$

2.6.8 Sampling Secondary Energy and Correlated Angle/Energy Distributions

For a reaction with secondary neutrons, it is necessary to determine the outgoing energy of the neutrons. For any reaction other than elastic scattering, the outgoing energy must be determined based on tabulated or parameterized data. The ENDF-6 Format [59] specifies a variety of ways that the secondary energy distribution can be represented. ENDF File 5 contains uncorrelated energy distribution whereas ENDF File 6 contains correlated energy-angle distributions. The ACE format specifies its own representations based loosely on the formats given in ENDF-6. In this section, we will describe how the outgoing energy of secondary particles is determined based on each ACE law.

One of the subtleties in the ACE format is the fact that a single reaction can have multiple secondary energy distributions. This is mainly useful for reactions with multiple neutrons in the exit channel such as $(n, 2n)$ or $(n, 3n)$. In these types of reactions, each neutron is emitted corresponding to a different excitation level of the compound nucleus, and thus in general the neutrons will originate from different energy distributions. If multiple energy distributions are present, they are assigned probabilities that can then be used to randomly select one.

Once a secondary energy distribution has been sampled, the procedure for determining the outgoing energy will depend on which ACE law has been specified for the data.

2.6.8.1 ACE Law 1 - Tabular Equiprobable Energy Bins

In the tabular equiprobable bin representation, an array of equiprobable outgoing energy bins is given for a number of incident energies. While the representation itself is simple, the complexity lies in how one interpolates between incident as well as outgoing energies on such a table. If one performs simple interpolation between tables for neighboring incident energies, it is possible that the resulting energies would violate laws governing the kinematics, i.e. the outgoing energy may be outside the range of available energy in the reaction.

To avoid this situation, the accepted practice is to use a process known as scaled interpolation [60]. First, we find the tabulated incident energies which bound the actual incoming energy of the particle, i.e. find i such that $E_i < E < E_{i+1}$ and calculate the interpolation factor f via (2.32). Then, we interpolate between the minimum and maximum energies of the outgoing energy distributions corresponding to E_i and E_{i+1} :

$$\begin{aligned} E_{min} &= E_{i,1} + f(E_{i+1,1} - E_{i,1}) \\ E_{max} &= E_{i,M} + f(E_{i+1,M} - E_{i,M}) \end{aligned} \quad (2.45)$$

where E_{min} and E_{max} are the minimum and maximum outgoing energies of a scaled distribution, $E_{i,j}$ is the j th outgoing energy corresponding to the incoming energy E_i , and M is the number of outgoing energy bins. Next, statistical interpolation is performed to choose between using the outgoing energy distributions corresponding to energy E_i and E_{i+1} . Let ℓ be the chosen table where $\ell = i$ if $\xi_1 > f$ and $\ell = i + 1$ otherwise, and ξ_1 is a random number. Now, we randomly sample an equiprobable outgoing energy bin j and interpolate between successive values on the outgoing energy distribution:

$$\hat{E} = E_{\ell,j} + \xi_2(E_{\ell,j+1} - E_{\ell,j}) \quad (2.46)$$

where ξ_2 is a random number sampled uniformly on $[0, 1)$. Since this outgoing energy may violate reaction kinematics, we then scale it to the minimum and maximum energies

we calculated earlier to get the final outgoing energy:

$$E' = E_{min} + \frac{\hat{E} - E_{\ell,1}}{E_{\ell,M} - E_{\ell,1}}(E_{max} - E_{min}). \quad (2.47)$$

2.6.8.2 ACE Law 3 - Inelastic Level Scattering

It can be shown [61] that in inelastic level scattering, the outgoing energy of the neutron E' can be related to the Q-value of the reaction and the incoming energy:

$$E' = \left(\frac{A}{A+1} \right)^2 \left(E - \frac{A+1}{A} Q \right) \quad (2.48)$$

where A is the mass of the target nucleus measured in neutron masses.

2.6.8.3 ACE Law 4 - Continuous Tabular Distribution

This representation is very similar that in subsection 2.6.8.1 except that instead of equiprobable outgoing energy bins, the outgoing energy distribution for each incoming energy is represented with a probability distribution function. For each incoming neutron energy E_i , let us call $p_{i,j}$ the j th value in the probability distribution function, $c_{i,j}$ the j th value in the cumulative distribution function, and $E_{i,j}$ the j th outgoing energy.

We proceed first as we did for ACE Law 1, determining the bounding energies of the particle's incoming energy such that $E_i < E < E_{i+1}$ and calculating an interpolation factor f with (2.32). Next, statistical interpolation is performed to choose between using the outgoing energy distributions corresponding to energy E_i and E_{i+1} . Let ℓ be the chosen table where $\ell = i$ if $\xi_1 > f$ and $\ell = i + 1$ otherwise, and ξ_1 is a random number. Then, we sample an outgoing energy bin j using the cumulative distribution function:

$$c_{\ell,j} < \xi_2 < c_{\ell,j+1} \quad (2.49)$$

where ξ_2 is a random number sampled uniformly on $[0, 1)$. At this point, we need to interpolate between the successive values on the outgoing energy distribution using either histogram or linear-linear interpolation. The formulas for these can be derived

along the same lines as those found in subsubsection 2.6.7.3. For histogram interpolation, the interpolated outgoing energy on the ℓ th distribution is

$$\hat{E} = E_{\ell,j} + \frac{\xi_2 - c_{\ell,j}}{p_{\ell,j}}. \quad (2.50)$$

If linear-linear interpolation is to be used, the outgoing energy on the ℓ th distribution is

$$\hat{E} = E_{\ell,j} + \frac{E_{\ell,j+1} - E_{\ell,j}}{p_{\ell,j+1} - p_{\ell,j}} \left(\sqrt{p_{\ell,j}^2 + 2 \frac{p_{\ell,j+1} - p_{\ell,j}}{E_{\ell,j+1} - E_{\ell,j}} (\xi_2 - c_{\ell,j}) - p_{\ell,j}} \right). \quad (2.51)$$

Since this outgoing energy may violate reaction kinematics, we then scale it to minimum and maximum energies interpolated between the neighboring outgoing energy distributions to get the final outgoing energy:

$$E' = E_{min} + \frac{\hat{E} - E_{\ell,1}}{E_{\ell,M} - E_{\ell,1}} (E_{max} - E_{min}) \quad (2.52)$$

where E_{min} and E_{max} are defined the same as in (2.45).

2.6.8.4 ACE Law 7 - Maxwell Fission Spectrum

One representation of the secondary energies for neutrons from fission is the so-called Maxwell spectrum. A probability distribution for the Maxwell spectrum can be written in the form

$$p(E') dE' = c E'^{1/2} e^{-E'/T(E)} dE' \quad (2.53)$$

where E is the incoming energy of the neutron and T is the so-called nuclear temperature, which is a function of the incoming energy of the neutron. The ACE format contains a list of nuclear temperatures versus incoming energies. The nuclear temperature is interpolated between neighboring incoming energies using a specified interpolation law. Once the temperature T is determined, we then calculate a candidate outgoing energy based on rule C64 in the Monte Carlo Sampler [62]:

$$E' = -T \left[\log(\xi_1) + \log(\xi_2) \cos^2 \left(\frac{\pi \xi_3}{2} \right) \right] \quad (2.54)$$

where ξ_1, ξ_2, ξ_3 are random numbers sampled on the unit interval. The outgoing energy is only accepted if

$$0 \leq E' \leq E - U \quad (2.55)$$

where U is called the restriction energy and is specified on the ACE table. If the outgoing energy is rejected, it is resampled using (2.54).

2.6.8.5 ACE Law 9 - Evaporation Spectrum

Evaporation spectra are primarily used in compound nucleus processes where a secondary particle can “evaporate” from the compound nucleus if it has sufficient energy. The probability distribution for an evaporation spectrum can be written in the form

$$p(E')dE' = cE'e^{-E'/T(E)}dE' \quad (2.56)$$

where E is the incoming energy of the neutron and T is the nuclear temperature, which is a function of the incoming energy of the neutron. The ACE format contains a list of nuclear temperatures versus incoming energies. The nuclear temperature is interpolated between neighboring incoming energies using a specified interpolation law. Once the temperature T is determined, we then calculate a candidate outgoing energy based on rule C45 in the Monte Carlo Sampler [62]:

$$E' = -T \log(\xi_1 \xi_2) \quad (2.57)$$

where ξ_1, ξ_2 are random numbers sampled on the unit interval. The outgoing energy is only accepted according to a specified restriction energy as in (2.55).

2.6.8.6 ACE Law 11 - Energy-Dependent Watt Spectrum

The probability distribution for a Watt fission spectrum [63] can be written in the form

$$p(E')dE' = ce^{-E'/a(E)} \sinh \sqrt{b(E)E'} dE' \quad (2.58)$$

where a and b are parameters for the distribution and are given as tabulated functions of the incoming energy of the neutron. These two parameters are interpolated on the incoming energy grid using a specified interpolation law. Once the parameters have been determined, we sample a Maxwellian spectrum with nuclear temperature a using the algorithm described in subsubsection 2.6.8.4 to get an energy W . Then, the outgoing energy is calculated as

$$E' = W + \frac{a^2 b}{4} + (2\xi - 1)\sqrt{a^2 b W} \quad (2.59)$$

where ξ is a random number sampled on the interval $[0, 1)$. The outgoing energy is only accepted according to a specified restriction energy U as defined in (2.55).

This algorithm can be found in Forrest Brown's lectures on Monte Carlo methods [20] and is an unpublished sampling scheme based on the original Watt spectrum derivation.

2.6.8.7 ACE Law 44 - Kalbach-Mann Correlated Scattering

This law is very similar to ACE Law 4 except now the outgoing angle of the neutron is correlated to the outgoing energy and is not sampled from a separate distribution. For each incident neutron energy E_i tabulated, there is an array of precompound factors $R_{i,j}$ and angular distribution slopes $A_{i,j}$ corresponding to each outgoing energy bin j in addition to the outgoing energies and distribution functions as in ACE Law 4.

The calculation of the outgoing energy of the neutron proceeds exactly the same as in the algorithm described in subsubsection 2.6.8.3. In that algorithm, we found an interpolation factor f , statistically sampled an incoming energy bin ℓ , and sampled an outgoing energy bin j based on the tabulated cumulative distribution function. Once the outgoing energy has been determined with (2.52), we then need to calculate the outgoing angle based on the tabulated Kalbach-Mann parameters. These parameters themselves are subject to either histogram or linear-linear interpolation on the outgoing

energy grid. For histogram interpolation, the parameters are

$$\begin{aligned} R &= R_{\ell,j} \\ A &= A_{\ell,j} \end{aligned} \tag{2.60}$$

If linear-linear interpolation is specified, the parameters are

$$\begin{aligned} R &= R_{\ell,j} + \frac{\hat{E} - E_{\ell,j}}{E_{\ell,j+1} - E_{\ell,j}} (R_{\ell,j+1} - R_{\ell,j}) \\ A &= A_{\ell,j} + \frac{\hat{E} - E_{\ell,j}}{E_{\ell,j+1} - E_{\ell,j}} (A_{\ell,j+1} - A_{\ell,j}) \end{aligned} \tag{2.61}$$

where \hat{E} is defined in (2.51). With the parameters determined, the probability distribution function for the cosine of the scattering angle is

$$p(\mu)d\mu = \frac{A}{2 \sinh(A)} [\cosh(A\mu) + R \sinh(A\mu)] d\mu. \tag{2.62}$$

The rules for sampling this probability distribution function can be derived based on rules C39 and C40 in the Monte Carlo Sampler [62]. First, we sample two random numbers ξ_3, ξ_4 on the unit interval. If $\xi_3 > R$ then the outgoing angle is

$$\mu = \frac{1}{A} \ln \left(T + \sqrt{T^2 + 1} \right) \tag{2.63}$$

where $T = (2\xi_4 - 1) \sinh(A)$. If $\xi_3 \leq R$, then the outgoing angle is

$$\mu = \frac{1}{A} \ln \left(\xi_4 e^A + (1 - \xi_4) e^{-A} \right). \tag{2.64}$$

2.6.8.8 ACE Law 61 - Correlated Energy and Angle Distribution

This law is very similar to ACE Law 44 in the sense that the outgoing angle of the neutron is correlated to the outgoing energy and is not sampled from a separate distribution. In this case though, rather than being determined from an analytical distribution function, the cosine of the scattering angle is determined from a tabulated distribution. For each incident energy i and outgoing energy j , there is a tabulated angular distribution.

The calculation of the outgoing energy of the neutron proceeds exactly the same as in the algorithm described in subsubsection 2.6.8.3. In that algorithm, we found an interpolation factor f , statistically sampled an incoming energy bin ℓ , and sampled an outgoing energy bin j based on the tabulated cumulative distribution function. Once the outgoing energy has been determined with (2.52), we then need to decide which angular distribution to use. If histogram interpolation was used on the outgoing energy bins, then we use the angular distribution corresponding to incoming energy bin ℓ and outgoing energy bin j . If linear-linear interpolation was used on the outgoing energy bins, then we use whichever angular distribution was closer to the sampled value of the cumulative distribution function for the outgoing energy. The actual algorithm used to sample the chosen tabular angular distribution has been previously described in subsubsection 2.6.7.3.

2.6.8.9 ACE Law 66 - N-Body Phase Space Distribution

Reactions in which there are more than two products of similar masses are sometimes best treated by using what's known as an N-body phase distribution. This distribution has the following probability density function for outgoing energy of the i th particle in the center-of-mass system:

$$p_i(E')dE' = C_n \sqrt{E'} (E_i^{max} - E')^{(3n/2)-4} dE' \quad (2.65)$$

where n is the number of outgoing particles, C_n is a normalization constant, E_i^{max} is the maximum center-of-mass energy for particle i , and E' is the outgoing energy. The algorithm for sampling the outgoing energy is based on algorithms R28, C45, and C64 in the Monte Carlo Sampler [62]. First we calculate the maximum energy in the center-of-mass using the following equation:

$$E_i^{max} = \frac{A_p - 1}{A_p} \left(\frac{A}{A + 1} E + Q \right) \quad (2.66)$$

where A_p is the total mass of the outgoing particles in neutron masses, A is the mass of the original target nucleus in neutron masses, and Q is the Q-value of the reaction. Next we sample a value x from a Maxwell distribution with a nuclear temperature of one using the algorithm outlined in subsubsection 2.6.8.4. We then need to determine a value y that will depend on how many outgoing particles there are. For $n = 3$, we simply sample another Maxwell distribution with unity nuclear temperature. For $n = 4$, we use the equation

$$y = -\ln(\xi_1 \xi_2 \xi_3) \quad (2.67)$$

where ξ_i are random numbers sampled on the interval $[0, 1)$. For $n = 5$, we use the equation

$$y = -\ln(\xi_1 \xi_2 \xi_3 \xi_4) - \ln(\xi_5) \cos^2\left(\frac{\pi}{2} \xi_6\right) \quad (2.68)$$

After x and y have been determined, the outgoing energy is then calculated as

$$E' = \frac{x}{x + y} E_i^{max} \quad (2.69)$$

There are two important notes to make regarding the N-body phase space distribution. First, the documentation (and code) for MCNP5-1.60 has a mistake in the algorithm for $n = 4$. That being said, there are no existing nuclear data evaluations which use an N-body phase space distribution with $n = 4$, so the error would not affect any calculations. In the ENDF/B-VII.0 nuclear data evaluation, only one reaction uses an N-body phase space distribution at all, the $(n, 2n)$ reaction with ^2H .

2.6.9 Transforming a Particle's Coordinates

Once the cosine of the scattering angle μ has been sampled either from an angle distribution or a correlated angle-energy distribution, we are still left with the task of transforming the particle's coordinates. If the outgoing energy and scattering cosine were given in the center-of-mass system, then we first need to transform these into the laboratory system. The relationship between the outgoing energy in center-of-mass and

laboratory is

$$E' = E'_{cm} + \frac{E + 2\mu_{cm}(A+1)\sqrt{EE'_{cm}}}{(A+1)^2} \quad (2.70)$$

where E'_{cm} is the outgoing energy in the center-of-mass system, μ_{cm} is the scattering cosine in the center-of-mass system, E' is the outgoing energy in the laboratory system, and E is the incident neutron energy. The relationship between the scattering cosine in center-of-mass and laboratory is

$$\mu = \mu_{cm} \sqrt{\frac{E'_{cm}}{E'}} + \frac{1}{A+1} \sqrt{\frac{E}{E'}} \quad (2.71)$$

where μ is the scattering cosine in the laboratory system. The scattering cosine still only tells us the cosine of the angle between the original direction of the particle and the new direction of the particle. If we express the pre-collision direction of the particle as $\boldsymbol{\Omega} = (u, v, w)$ and the post-collision direction of the particle as $\boldsymbol{\Omega}' = (u', v', w')$, it is possible to relate the pre- and post-collision components. We first need to uniformly sample an azimuthal angle ϕ in $[0, 2\pi)$. After the azimuthal angle has been sampled, the post-collision direction is calculated as

$$\begin{aligned} u' &= \mu u + \frac{\sqrt{1-\mu^2}(uw \cos \phi - v \sin \phi)}{\sqrt{1-w^2}} \\ v' &= \mu v + \frac{\sqrt{1-\mu^2}(vw \cos \phi + u \sin \phi)}{\sqrt{1-w^2}} \\ w' &= \mu w - \sqrt{1-\mu^2} \sqrt{1-w^2} \cos \phi. \end{aligned} \quad (2.72)$$

2.6.10 Effect of Thermal Motion on Cross Sections

When a neutron scatters off of a nucleus, it may often be assumed that the target nucleus is at rest. However, the target nucleus will have motion associated with its thermal vibration, even at absolute zero³. Thus, the velocity of the neutron relative to the target nucleus is in general not the same as the velocity of the neutron entering the collision.

³This is due to the zero-point energy arising from quantum mechanical considerations.

The effect of the thermal motion on the interaction probability can be written as

$$v_n \bar{\sigma}(v_n, T) = \int d\mathbf{v}_T v_r \sigma(v_r) M(\mathbf{v}_T) \quad (2.73)$$

where v_n is the magnitude of the velocity of the neutron, $\bar{\sigma}$ is an effective cross section, T is the temperature of the target material, \mathbf{v}_T is the velocity of the target nucleus, $v_r = \|\mathbf{v}_n - \mathbf{v}_T\|$ is the magnitude of the relative velocity, σ is the cross section at 0 K, and $M(\mathbf{v}_T)$ is the probability distribution for the target nucleus velocity at temperature T (a Maxwellian). In a Monte Carlo code, one must account for the effect of the thermal motion on both the integrated cross section as well as secondary angle and energy distributions. For integrated cross sections, it is possible to calculate thermally-averaged cross sections by applying a kernel Doppler broadening algorithm to data at 0 K (or some temperature lower than the desired temperature). The most ubiquitous algorithm for this purpose is the SIGMA1 method [64] developed by Red Cullen and subsequently refined by others. This method is used in the NJOY [52] and PREPRO [65] data processing codes.

The effect of thermal motion on secondary angle and energy distributions can be accounted for on-the-fly in a Monte Carlo simulation. We must first qualify where it is actually used however. All threshold reactions are treated as being independent of temperature, and therefore they are not Doppler broadened in NJOY and no special procedure is used to adjust the secondary angle and energy distributions. The only non-threshold reactions with secondary neutrons are elastic scattering and fission. For fission, it is assumed that the neutrons are emitted isotropically (this is not strictly true, but is nevertheless a good approximation). This leaves only elastic scattering that needs a special thermal treatment for secondary distributions.

Fortunately, it is possible to directly sample the velocity of the target nuclide and use it in the kinematic calculations. However, this calculation is a bit more nuanced than it might seem at first glance. One might be tempted to simply sample a Maxwellian distribution for the velocity of the target nuclide. Careful inspection of (2.73) however tells us that target velocities that produce relative velocities which correspond to high

cross sections will have a greater contribution to the effective reaction rate. This is most important when the velocity of the incoming neutron is close to a resonance. For example, if the neutron's velocity corresponds to a local minimum in a resonance elastic scattering cross section, a very small target velocity can cause the relative velocity to correspond to the peak of the resonance, thus making a disproportionate contribution to the reaction rate. The conclusion is that if we are to sample a target velocity in the Monte Carlo code, it must be done in such a way that preserves the thermally-averaged reaction rate as per (2.73).

The method by which most Monte Carlo codes sample the target velocity for use in elastic scattering kinematics is outlined in detail by Gelbard [66]. The derivation here largely follows that of Gelbard. Let us first write the reaction rate as a function of the velocity of the target nucleus:

$$R(\mathbf{v}_T) = \|\mathbf{v}_n - \mathbf{v}_T\| \sigma(\|\mathbf{v}_n - \mathbf{v}_T\|) M(\mathbf{v}_T) \quad (2.74)$$

where R is the reaction rate. Note that this is just the right-hand side of (2.73). Based on the discussion above, we want to construct a probability distribution function for sampling the target velocity to preserve the reaction rate — this is different from the overall probability distribution function for the target velocity, $M(\mathbf{v}_T)$. This probability distribution function can be found by integrating (2.74) to obtain a normalization factor:

$$p(\mathbf{v}_T) d\mathbf{v}_T = \frac{R(\mathbf{v}_T) d\mathbf{v}_T}{\int d\mathbf{v}_T R(\mathbf{v}_T)} \quad (2.75)$$

Let us call the normalization factor in the denominator of (2.75) C .

It is normally assumed that $\sigma(v_r)$ is constant over the range of relative velocities of interest. This is a good assumption for almost all cases since the elastic scattering cross section varies slowly with velocity for light nuclei, and for heavy nuclei where large variations can occur due to resonance scattering, the moderating effect is rather small. Nonetheless, this assumption may cause incorrect answers in systems with low-lying resonances that can cause a significant amount of up-scatter that would be ignored by

this assumption (e.g. ^{238}U in commercial light-water reactors). Nevertheless, with this assumption, we write $\sigma(v_r) = \sigma_s$ which simplifies (2.75) to

$$p(\mathbf{v}_T)d\mathbf{v}_T = \frac{\sigma_s}{C} \|\mathbf{v}_n - \mathbf{v}_T\| M(\mathbf{v}_T) d\mathbf{v}_T. \quad (2.76)$$

The Maxwellian distribution in velocity is

$$M(\mathbf{v}_T) = \left(\frac{m}{2\pi kT} \right)^{3/2} \exp\left(\frac{-m\|\mathbf{v}_T\|^2}{2kT} \right) \quad (2.77)$$

where m is the mass of the target nucleus and k is Boltzmann's constant. Notice here that the term in the exponential is dependent only on the speed of the target, not on the actual direction. Thus, we can change the Maxwellian into a distribution for speed rather than velocity. The differential element of velocity is

$$d\mathbf{v}_T = v_T^2 dv_T d\mu d\phi. \quad (2.78)$$

Let us define the Maxwellian distribution in speed as

$$M(v_T)dv_T = \int_{-1}^1 d\mu \int_0^{2\pi} d\phi dv_T v_T^2 M(\mathbf{v}_T) = \sqrt{\frac{2}{\pi}} \left(\frac{m}{kT} \right)^3 v_T^2 \exp\left(\frac{-mv_T}{2kT} \right) dv_T. \quad (2.79)$$

To simplify things a bit, we'll define a parameter

$$\beta = \sqrt{\frac{m}{2kT}}. \quad (2.80)$$

Substituting (2.80) into (2.79), we obtain

$$M(v_T)dv_T = \frac{4}{\sqrt{\pi}} \beta^3 v_T^2 \exp(-\beta^2 v_T^2) dv_T. \quad (2.81)$$

Now, changing variables in (2.76) by using the result from (2.81), our new probability distribution function is

$$p(v_T, \mu)dv_T d\mu = \frac{4\sigma_s}{\sqrt{\pi}C'} \|\mathbf{v}_n - \mathbf{v}_T\| \beta^3 v_T^2 \exp(-\beta^2 v_T^2) dv_T d\mu. \quad (2.82)$$

Again, the Maxwellian distribution for the speed of the target nucleus has no dependence on the angle between the neutron and target velocity vectors. Thus, only the term $\|\mathbf{v}_n - \mathbf{v}_T\|$ imposes any constraint on the allowed angle. Our last task is to take that term and write it in terms of magnitudes of the velocity vectors and the angle rather than the vectors themselves. We can establish this relation based on the law of cosines which tells us that

$$2v_n v_T \mu = v_n^2 + v_T^2 - v_r^2. \quad (2.83)$$

Thus, we can infer that

$$\|\mathbf{v}_n - \mathbf{v}_T\| = \|\mathbf{v}_r\| = v_r = \sqrt{v_n^2 + v_T^2 - 2v_n v_T \mu}. \quad (2.84)$$

Inserting (2.84) into (2.82), we obtain

$$p(v_T, \mu) dv_T d\mu = \frac{4\sigma_s}{\sqrt{\pi}C'} \sqrt{v_n^2 + v_T^2 - 2v_n v_T \mu} \beta^3 v_T^2 \exp(-\beta^2 v_T^2) dv_T d\mu \quad (2.85)$$

This expression is still quite formidable and does not lend itself to any natural sampling scheme. We can divide this probability distribution into two parts as such:

$$p(v_T, \mu) = f_1(v_T, \mu) f_2(v_T) \quad (2.86)$$

$$f_1(v_T, \mu) = \frac{4\sigma_s}{\sqrt{\pi}C'} \frac{\sqrt{v_n^2 + v_T^2 - 2v_n v_T \mu}}{v_n + v_T} \quad (2.87)$$

$$f_2(v_T) = (v_n + v_T) \beta^3 v_T^2 \exp(-\beta^2 v_T^2). \quad (2.88)$$

In general, any probability distribution function of the form $p(x) = f_1(x)f_2(x)$ with $f_1(x)$ bounded can be sampled by sampling x' from the distribution

$$q(x)dx = \frac{f_2(x)dx}{\int f_2(x)dx} \quad (2.89)$$

and accepting it with probability

$$p_{\text{accept}} = \frac{f_1(x')}{\max f_1(x)} \quad (2.90)$$

The reason for dividing and multiplying the terms by $v_n + v_T$ is to ensure that the first term is bounded. In general, $\|\mathbf{v}_n - \mathbf{v}_T\|$ can take on arbitrarily large values, but if we divide it by its maximum value $v_n + v_T$, then it ensures that the function will be bounded. We now must come up with a sampling scheme for (2.89). To determine $q(v_T)$, we need to integrate f_2 in (2.88). Doing so we find that

$$\int_0^\infty dv_T (v_n + v_T) \beta^3 v_T^2 \exp(-\beta^2 v_T^2) = \frac{1}{4\beta} (\sqrt{\pi} \beta v_n + 2). \quad (2.91)$$

Thus, we need to sample the probability distribution function

$$q(v_T) dv_T = \left(\frac{4\beta^2 v_n v_T^2}{\sqrt{\pi} \beta v_n + 2} + \frac{4\beta^4 v_T^3}{\sqrt{\pi} \beta v_n + 2} \right) \exp(-\beta^2 v_T^2). \quad (2.92)$$

Now, let us do a change of variables with the following definitions

$$\begin{aligned} x &= \beta v_T \\ y &= \beta v_n. \end{aligned} \quad (2.93)$$

Substituting (2.93) into (2.92) along with $dx = \beta dv_T$ and doing some crafty rearranging of terms yields

$$q(x) dx = \left[\left(\frac{\sqrt{\pi} y}{\sqrt{\pi} y + 2} \right) \frac{4}{\sqrt{\pi}} x^2 e^{-x^2} + \left(\frac{2}{\sqrt{\pi} y + 2} \right) 2x^3 e^{-x^2} \right] dx. \quad (2.94)$$

It's important to note the following two facts. First, the terms outside the parentheses are properly normalized probability distribution functions that can be sampled directly. Secondly, the terms inside the parentheses are always less than unity. Thus, the sampling scheme for $q(x)$ is as follows. We sample a random number ξ_1 on the interval $[0, 1)$ and if

$$\xi_1 < \frac{2}{\sqrt{\pi} y + 2} \quad (2.95)$$

then we sample the probability distribution $2x^3 e^{-x^2}$ for x using rule C49 in the Monte Carlo Sampler [62] which we can then use to determine the speed of the target nucleus v_T from (2.93). Otherwise, we sample the probability distribution $\frac{4}{\sqrt{\pi}} x^2 e^{-x^2}$ for x using

rule C61 in the Monte Carlo Sampler.

With a target speed sampled, we must then decide whether to accept it based on the probability in (2.90). The cosine can be sampled isotropically as $\mu = 2\xi_2 - 1$ where ξ_2 is a random number on the unit interval. Since the maximum value of $f_1(v_T, \mu)$ is $4\sigma_s/\sqrt{\pi}C'$, we then sample another random number ξ_3 and accept the sampled target speed and cosine if

$$\xi_3 < \frac{\sqrt{v_n^2 + v_T^2 - 2v_n v_T \mu}}{v_n + v_T}. \quad (2.96)$$

If is not accepted, then we repeat the process and resample a target speed and cosine until a combination is found that satisfies (2.96).

2.6.11 $S(\alpha, \beta, T)$ Tables

For neutrons with thermal energies, generally less than 4 eV, the kinematics of scattering can be affected by chemical binding and crystalline effects of the target molecule. If these effects are not accounted for in a simulation, the reported results may be highly inaccurate. There is no general analytic treatment for the scattering kinematics at low energies, and thus when nuclear data is processed for use in a Monte Carlo code, special tables are created that give cross sections and secondary angle/energy distributions for thermal scattering that account for thermal binding effects. These tables are mainly used for moderating materials such as light or heavy water, graphite, hydrogen in ZrH, beryllium, etc.

The theory behind $S(\alpha, \beta, T)$ is rooted in quantum mechanics and is quite complex. Those interested in first principles derivations for formulae relating to $S(\alpha, \beta, T)$ tables should be referred to the excellent books by Williams [67] and Squires [68]. For our purposes here, we will focus only on the use of already processed data as it appears in the ACE format.

Each $S(\alpha, \beta, T)$ table can contain the following:

- Thermal inelastic scattering cross section;
- Thermal elastic scattering cross section; and

- Correlated energy-angle distributions for thermal inelastic and elastic scattering.

Note that when we refer to “inelastic” and “elastic” scattering now, we are actually using these terms with respect to the *scattering system*. Thermal inelastic scattering means that the scattering system is left in an excited state; no particular nucleus is left in an excited state as would be the case for inelastic level scattering (which only occurs at much higher incident neutron energies). In a crystalline material, the excitation of the scattering system could correspond to the production of phonons. In a molecule, it could correspond to the excitation of rotational or vibrational modes.

Both thermal elastic and thermal inelastic scattering are generally divided into incoherent and coherent parts. Coherent elastic scattering refers to scattering in crystalline solids like graphite or beryllium. These cross sections are characterized by the presence of *Bragg edges* that relate to the crystal structure of the scattering material. Incoherent elastic scattering refers to scattering in hydrogenous solids such as polyethylene. As it occurs in ACE data, thermal inelastic scattering includes both coherent and incoherent effects and is dominant for most other materials including hydrogen in water.

2.6.11.1 Calculating Integrated Cross Sections

The first aspect of using $S(\alpha, \beta, T)$ tables is calculating cross sections to replace the data that would normally appear on the incident neutron tables, which do not account for thermal binding effects. For incoherent elastic and inelastic scattering, the cross sections are stored as linearly interpolable functions on a specified energy grid. For coherent elastic data, the cross section can be expressed as

$$\sigma(E) = \frac{\sigma_c}{E} \sum_{E_i < E} f_i e^{-4WE_i} \quad (2.97)$$

where σ_c is the effective bound coherent scattering cross section, W is the effective Debye-Waller coefficient, E_i are the energies of the Bragg edges, and f_i are related to crystallographic structure factors. Since the functional form of the cross section is just $1/E$ and the proportionality constant changes only at Bragg edges, the proportionality constants are stored and then the cross section can be calculated analytically based on

(2.97).

2.6.11.2 Outgoing Angle for Coherent Elastic Scattering

Another aspect of using $S(\alpha, \beta, T)$ tables is determining the outgoing energy and angle of the neutron after scattering. For incoherent and coherent elastic scattering, the energy of the neutron does not actually change, but the angle does change. For coherent elastic scattering, the angle will depend on which Bragg edge scattered the neutron. The probability that edge i will scatter the neutron is given by

$$\frac{f_i e^{-4W E_i}}{\sum_j f_j e^{-4W E_j}}. \quad (2.98)$$

After a Bragg edge has been sampled, the cosine of the scattering angle is given analytically by

$$\mu = 1 - \frac{E_i}{E} \quad (2.99)$$

where E_i is the energy of the Bragg edge that scattered the neutron.

2.6.11.3 Outgoing Angle for Incoherent Elastic Scattering

For incoherent elastic scattering, the probability distribution for the cosine of the scattering angle is represented as a series of equally-likely discrete cosines $\mu_{i,j}$ for each incoming energy E_i on the thermal elastic energy grid. First the outgoing angle bin j is sampled. Then, if the incoming energy of the neutron satisfies $E_i < E < E_{i+1}$ the final cosine is

$$\mu = \mu_{i,j} + f(\mu_{i+1,j} - \mu_{i,j}) \quad (2.100)$$

where the interpolation factor is defined as

$$f = \frac{E - E_i}{E_{i+1} - E_i}. \quad (2.101)$$

2.6.11.4 Outgoing Energy and Angle for Inelastic Scattering

On each $S(\alpha, \beta, T)$ table, there is a correlated angle-energy secondary distribution for neutron thermal inelastic scattering. While the documentation for the ACE format [51] implies that there are a series of equiprobable outgoing energies, the outgoing energies may have non-uniform probability distribution. In particular, if the thermal data were processed with $iwt = 0$ in NJOY, then the first and last outgoing energies have a relative probability of 1, the second and second to last energies have a relative probability of 4, and all other energies have a relative probability of 10. The procedure to determine the outgoing energy and angle is as such. First, the interpolation factor is determined from (2.101). Then, an outgoing energy bin is sampled either from a uniform distribution or from the aforementioned skewed distribution. The outgoing energy is then interpolated between values corresponding to neighboring incoming energies:

$$E = E_{i,j} + f(E_{i+1,j} - E_{i,j}) \quad (2.102)$$

where $E_{i,j}$ is the j th outgoing energy corresponding to the i th incoming energy. For each combination of incoming and outgoing energies, there is a series of equiprobable outgoing cosines. An outgoing cosine bin is sampled uniformly and then the final cosine is interpolated on the incoming energy grid:

$$\mu = \mu_{i,j,k} + f(\mu_{i+1,j,k} - \mu_{i,j,k}) \quad (2.103)$$

where $\mu_{i,j,k}$ is the k th outgoing cosine corresponding to the j th outgoing energy and the i th incoming energy.

2.6.12 Unresolved Resonance Region Probability Tables

In the unresolved resonance energy range, resonances may be so closely spaced that it is not possible for experimental measurements to resolve all resonances. To properly account for self-shielding in this energy range, OpenMC uses the probability table method [69]. For most thermal reactors, the use of probability tables will not significantly affect

results. However, for some fast reactors and other problems with an appreciable flux spectrum in the unresolved resonance range, lack of probability tables may lead to incorrect results.

Probability tables in the ACE format are generated from the UNRESR module in NJOY [70] following the method of Levitt [69]. A similar method employed for the RACER and MC21 Monte Carlo codes is described in a paper by Sutton and Brown [71]. For the discussion here, we will focus only on use of the probability table as it appears in the ACE format.

Each probability table for a nuclide contains the following information at a number of incoming energies within the unresolved resonance range:

- Cumulative probabilities for cross section bands;
- Total cross section (or factor) in each band;
- Elastic scattering cross section (or factor) in each band;
- Fission cross section (or factor) in each band;
- (n, γ) cross section (or factor) in each band; and
- Neutron heating number (or factor) in each band.

It should be noted that unresolved resonance probability tables affect only integrated cross sections and no extra data need be given for secondary angle/energy distributions. Secondary distributions for elastic and inelastic scattering would be specified whether or not probability tables were present.

The procedure for determining cross sections in the unresolved range using probability tables is as follows. First, the bounding incoming energies are determined, i.e. find i such that $E_i < E < E_{i+1}$. We then sample a cross section band j using the cumulative probabilities for table i . This allows us to then calculate the elastic, fission, and capture cross sections from the probability tables interpolating between neighboring incoming energies. If linear interpolation is specified, then the cross sections are calculated as

$$\sigma = \sigma_{i,j} + f(\sigma_{i+1,j} - \sigma_{i,j}) \quad (2.104)$$

where $\sigma_{i,j}$ is the j th-band cross section corresponding to the i th incoming neutron energy and f is the interpolation factor defined in the same manner as (2.101). If logarithmic interpolation is specified, the cross sections are calculated as

$$\sigma = \exp\left(\log \sigma_{i,j} + f \log \frac{\sigma_{i+1,j}}{\sigma_{i,j}}\right) \quad (2.105)$$

where the interpolation factor is now defined as

$$f = \frac{\log \frac{E}{E_i}}{\log \frac{E_{i+1}}{E_i}}. \quad (2.106)$$

A flag is also present in the probability table that specifies whether an inelastic cross section should be calculated. If so, this is done from a normal reaction cross section (either MT=51 or a special MT). Finally, if the cross sections defined above are specified to be factors and not true cross sections, they are multiplied by the underlying smooth cross section in the unresolved range to get the actual cross sections. Lastly, the total cross section is calculated as the sum of the elastic, fission, capture, and inelastic cross sections.

2.6.13 Variance Reduction Techniques

2.6.13.1 Survival Biasing

In problems with highly absorbing materials, a large fraction of neutrons may be killed through absorption reactions, thus leading to tallies with very few scoring events. To remedy this situation, an algorithm known as *survival biasing* or *implicit absorption* (or sometimes *implicit capture*, even though this is a misnomer) is commonly used.

In survival biasing, absorption reactions are prohibited from occurring and instead, at every collision, the weight of neutron is reduced by the probability of absorption occurring, i.e.

$$w' = w \left(1 - \frac{\sigma_a(E)}{\sigma_t(E)}\right) \quad (2.107)$$

where w' is the weight of the neutron after adjustment and w is the weight of the neutron

before adjustment. A few other things need to be handled differently if survival biasing is turned on. Although fission reactions never actually occur with survival biasing, we still need to create fission sites to serve as source sites for the next generation in the method of successive generations. The algorithm for sampling fission sites is the same as that described in subsection 2.6.6. The only difference is in (2.28). We now need to produce

$$\nu = \frac{w}{k} \frac{\nu_t \sigma_f(E)}{\sigma_t(E)} \quad (2.108)$$

fission sites, where w is the weight of the neutron before being adjusted. One should note this is just the expected number of neutrons produced *per collision* rather than the expected number of neutrons produced given that fission has already occurred.

Additionally, since survival biasing can reduce the weight of the neutron to very low values, it is always used in conjunction with a weight cutoff and Russian roulette. Two user adjustable parameters w_c and w_s are given, which are the weight below which neutrons should undergo Russian roulette and the weight assigned if they survive Russian roulette, respectively. The algorithm for Russian roulette is as follows. After a collision, if $w < w_c$, then the neutron is killed with probability $1 - w/w_s$. If it survives, the weight is set equal to w_s . One can confirm that the average weight following Russian roulette is simply w , so the game can be considered “fair”. By default, the cutoff weight in OpenMC is $w_c = 0.25$ and the survival weight is $w_s = 1.0$. These parameters vary from one Monte Carlo code to another.

2.7 Tallies

2.7.1 Filters and Scores

The tally capability in OpenMC takes a similar philosophy as that employed in the MC21 Monte Carlo code [16] to give maximum flexibility in specifying tallies while still maintaining scalability. Any tally in a Monte Carlo simulation can be written in the

following form:

$$X = \underbrace{\int d\mathbf{r} \int d\mathbf{\Omega}}_{\text{filters}} \int dE \underbrace{f(\mathbf{r}, \mathbf{\Omega}, E)}_{\text{scores}} \psi(\mathbf{r}, \mathbf{\Omega}, E) \quad (2.109)$$

A user can specify one or more filters which identify which regions of phase space should score to a given tally (the limits of integration as shown in (2.109)) as well as the scoring function (f in (2.109)). For example, if the desired tally was the (n, γ) reaction rate in a fuel pin, the filter would specify the cell which contains the fuel pin and the scoring function would be the radiative capture macroscopic cross section. The following quantities can be scored in OpenMC: flux, total reaction rate, scattering reaction rate, neutron production from scattering, higher scattering moments, (n, xn) reaction rates, absorption reaction rate, fission reaction rate, neutron production rate from fission, and surface currents. The following variables can be used as filters: universe, material, cell, birth cell, surface, mesh, pre-collision energy, and post-collision energy.

With filters for pre- and post-collision energy and scoring functions for scattering and fission production, it is possible to use OpenMC to generate cross sections with user-defined group structures. These multigroup cross sections can subsequently be used in deterministic solvers such as coarse mesh finite difference (CMFD) diffusion [28].

2.7.2 Using Maps for Filter-Matching

Some Monte Carlo codes suffer severe performance penalties when tallying a large number of quantities. Care must be taken to ensure that a tally system scales well with the total number of tally bins. In OpenMC, a mapping technique is used that allows for a fast determination of what tally/bin combinations need to be scored to a given particle's phase space coordinates. For each discrete filter variable, a list is stored that contains the tally/bin combinations that could be scored to for each value of the filter variable. If a particle is in cell n , the mapping would identify what tally/bin combinations specify cell n for the cell filter variable. In this manner, it is not necessary to check the phase space variables against each tally. Note that this technique only applies to discrete filter variables and cannot be applied to energy bins. For energy filters, it is necessary to

perform a binary search on the specified energy grid.

2.7.3 Volume-Integrated Flux and Reaction Rates

One quantity we may wish to compute during the course of a Monte Carlo simulation is the flux or a reaction rate integrated over a finite volume. The volume may be a particular cell, a collection of cells, or the entire geometry. There are various methods by which we can estimate reaction rates

2.7.3.1 Analog Estimator

The analog estimator is the simplest type of estimator for reaction rates. The basic idea is that we simply count the number of actual reactions that take place and use that as our estimate for the reaction rate. This can be written mathematically as

$$R_x = \frac{1}{W} \sum_{i \in A} w_i \quad (2.110)$$

where R_x is the reaction rate for reaction x , i denotes an index for each event, A is the set of all events resulting in reaction x , and W is the total starting weight of the particles, and w_i is the pre-collision weight of the particle as it enters event i . One should note that (2.110) is volume-integrated so if we want a volume-averaged quantity, we need to divide it by the volume of the region of integration. If survival biasing is employed, the analog estimator cannot be used for any reactions with zero neutrons in the exit channel.

2.7.3.2 Collision Estimator

While the analog estimator is conceptually very simple and easy to implement, it can suffer higher variance due to the fact low probability events will not occur often enough to get good statistics if they are being tallied. Thus, it is desirable to use a different estimator that allows us to score the tally more often. One such estimator is the collision estimator. Instead of tallying a reaction only when it happens, the idea is to

make a contribution to the tally at every collision.

We can start by writing a formula for the collision estimate of the flux. Since $R = \Sigma_t \phi$ where R is the total reaction rate, Σ_t is the total macroscopic cross section, and ϕ is the scalar flux, it stands to reason that we can estimate the flux by taking an estimate of the total reaction rate and dividing it by the total macroscopic cross section. This gives us the following formula:

$$\phi = \frac{1}{W} \sum_{i \in C} \frac{w_i}{\Sigma_t(E_i)} \quad (2.111)$$

where W is again the total starting weight of the particles, C is the set of all events resulting in a collision with a nucleus, and $\Sigma_t(E)$ is the total macroscopic cross section of the target material at the incoming energy of the particle E_i .

If we multiply both sides of (2.111) by the macroscopic cross section for some reaction x , then we get the collision estimate for the reaction rate for that reaction:

$$R_x = \frac{1}{W} \sum_{i \in C} \frac{w_i \Sigma_x(E_i)}{\Sigma_t(E_i)} \quad (2.112)$$

where $\Sigma_x(E_i)$ is the macroscopic cross section for reaction x at the incoming energy of the particle E_i . In comparison to (2.110), we see that the collision estimate will result in a tally with a larger number of events that score to it with smaller contributions (since we have multiplied it by Σ_x/Σ_t).

2.7.3.3 Track-length Estimator

One other method we can use to increase the number of events that score to tallies is to use an estimator that contributes to a tally at every track for the particle rather than every collision. This is known as a track-length estimator, sometimes also called a path-length estimator. We first start with an expression for the volume integrated flux, which can be written as

$$V \phi = \int d\mathbf{r} \int dE \int d\Omega \int dt \psi(\mathbf{r}, \hat{\Omega}, E, t) \quad (2.113)$$

where V is the volume, ψ is the angular flux, \mathbf{r} is the position of the particle, $\hat{\Omega}$ is the direction of the particle, E is the energy of the particle, and t is the time. By noting that $\psi(\mathbf{r}, \hat{\Omega}, E, t) = v n(\mathbf{r}, \hat{\Omega}, E, t)$ where n is the angular neutron density, we can rewrite (2.113) as

$$V\phi = \int d\mathbf{r} \int dE \int dt v \int d\Omega n(\mathbf{r}, \hat{\Omega}, E, t). \quad (2.114)$$

Using the relations $N(\mathbf{r}, E, t) = \int d\Omega n(\mathbf{r}, \hat{\Omega}, E, t)$ and $d\ell = v dt$ where $d\ell$ is the differential unit of track length, we then obtain

$$V\phi = \int d\mathbf{r} \int dE \int d\ell N(\mathbf{r}, E, t). \quad (2.115)$$

Equation (2.115) indicates that we can use the length of a particle's trajectory as an estimate for the flux, i.e. the track-length estimator of the flux would be

$$\phi = \frac{1}{W} \sum_{i \in T} w_i \ell_i \quad (2.116)$$

where T is the set of all the particle's trajectories within the desired volume and ℓ_i is the length of the i th trajectory. In the same vein as (2.112), the track-length estimate of a reaction rate is found by multiplying (2.116) by a macroscopic reaction cross section:

$$R_x = \frac{1}{W} \sum_{i \in T} w_i \ell_i \Sigma_x(E_i). \quad (2.117)$$

One important fact to take into consideration is that the use of a track-length estimator precludes us from using any filter that requires knowledge of the particle's state following a collision because by definition, it will not have had a collision at every event. Thus, for tallies with outgoing-energy filters (which require the post-collision energy) or for tallies of scattering moments (which require the scattering cosine), we must use an analog estimator.

2.7.4 Statistics

Any given tally result from a Monte Carlo calculation represents an estimate of the mean of some random variable of interest. This random variable typically corresponds to some physical quantity like a reaction rate, a net current across some surface, or the neutron flux in a region. Given that all tallies are produced by a stochastic process, there is an associated uncertainty with each value reported. It is important to understand how the uncertainty is calculated and what it tells us about our results. To that end, we will introduce a number of theorems and results from statistics that should shed some light on the interpretation of uncertainties.

2.7.4.1 Law of Large Numbers

The law of large numbers is an important statistical result that tells us that the average value of the result of a large number of repeated experiments should be close to the expected value. Let X_1, X_2, \dots, X_n be an infinite sequence of independent, identically-distributed random variables with expected values $E(X_1) = E(X_2) = \mu$. One form of the law of large numbers states that the sample mean $\bar{X}_n = \frac{X_1 + \dots + X_n}{n}$ converges in probability to the true mean, i.e. for all $\epsilon > 0$

$$\lim_{n \rightarrow \infty} P(|\bar{X}_n - \mu| \geq \epsilon) = 0. \quad (2.118)$$

2.7.4.2 Central Limit Theorem

The central limit theorem (CLT) is perhaps the most well-known and ubiquitous statistical theorem that has far-reaching implications across many disciplines. The CLT is similar to the law of large numbers in that it tells us the limiting behavior of the sample mean. Whereas the law of large numbers tells us only that the value of the sample mean will converge to the expected value of the distribution, the CLT says that the distribution of the sample mean will converge to a normal distribution. As before, let us define X_1, X_2, \dots, X_n to be an infinite sequence of independent, identically-distributed random variables with expected values $E(X_i) = \mu$ and variances $\text{Var}(X_i) = \sigma^2 < \infty$. Note

that we don't require that these random variables take on any particular distribution — they can be normal, log-normal, Weibull, etc. The central limit theorem states that as $n \rightarrow \infty$, the random variable $\sqrt{n}(\bar{X}_n - \mu)$ converges in distribution to the standard normal distribution:

$$\sqrt{n} \left(\frac{1}{n} \sum_{i=1}^n X_i - \mu \right) \xrightarrow{d} \mathcal{N}(0, \sigma^2). \quad (2.119)$$

2.7.4.3 Estimating Statistics of a Random Variable

2.7.4.3.1 Mean Given independent samples drawn from a random variable, the sample mean is simply an estimate of the average value of the random variable. In a Monte Carlo simulation, the random variable represents physical quantities that we want tallied. If X is the random variable with N observations x_1, x_2, \dots, x_N , then an unbiased estimator for the population mean is the sample mean, defined as

$$\bar{x} = \frac{1}{N} \sum_{i=1}^N x_i. \quad (2.120)$$

2.7.4.3.2 Variance The variance of a population indicates how spread out different members of the population are. For a Monte Carlo simulation, the variance of a tally is a measure of how precisely we know the tally value, with a lower variance indicating a higher precision. There are a few different estimators for the population variance. One of these is the second central moment of the distribution also known as the biased sample variance:

$$s_N^2 = \frac{1}{N} \sum_{i=1}^N (x_i - \bar{x})^2 = \left(\frac{1}{N} \sum_{i=1}^N x_i^2 \right) - \bar{x}^2. \quad (2.121)$$

This estimator is biased because its expected value is actually not equal to the population variance:

$$E[s_N^2] = \frac{N-1}{N} \sigma^2 \quad (2.122)$$

where σ^2 is the actual population variance. As a result, this estimator should not be used in practice. Instead, one can use Bessel's correction to come up with an unbiased

sample variance estimator:

$$s^2 = \frac{1}{N-1} \sum_{i=1}^N (x_i - \bar{x})^2 = \frac{1}{N-1} \left(\sum_{i=1}^N x_i^2 - N\bar{x}^2 \right). \quad (2.123)$$

This is the estimator normally used to calculate sample variance. The final form in (2.123) is especially suitable for computation since we do not need to store the values at every realization of the random variable as the simulation proceeds. Instead, we can simply keep a running sum and sum of squares of the values at each realization of the random variable and use that to calculate the variance.

2.7.4.3.3 Variance of the Mean The previous sections discussed how to estimate the mean and variance of a random variable using statistics on a finite sample. However, we are generally not interested in the *variance of the random variable* itself; we are more interested in the *variance of the estimated mean*. The sample mean is the result of our simulation, and the variance of the sample mean will tell us how confident we should be in that result.

Fortunately, it is quite easy to estimate the variance of the mean if we are able to estimate the variance of the random variable. We start with the observation that if we have a series of uncorrelated random variables, we can write the variance of their sum as the sum of their variances:

$$\text{Var} \left(\sum_{i=1}^N X_i \right) = \sum_{i=1}^N \text{Var}(X_i). \quad (2.124)$$

This result is known as the Bienaymé formula. We can use this result to determine a formula for the variance of the sample mean. Assuming that the realizations of our random variable are again identical, independently-distributed samples, then we have that

$$\text{Var}(\bar{X}) = \text{Var} \left(\frac{1}{N} \sum_{i=1}^N X_i \right) = \frac{1}{N^2} \sum_{i=1}^N \text{Var}(X_i) = \frac{1}{N^2} (N\sigma^2) = \frac{\sigma^2}{N}. \quad (2.125)$$

We can combine this result with (2.123) to come up with an unbiased estimator for the

variance of the sample mean:

$$s_{\bar{x}}^2 = \frac{1}{N-1} \left(\frac{1}{N} \sum_{i=1}^N x_i^2 - \bar{x}^2 \right). \quad (2.126)$$

At this point, an important distinction should be made between the estimator for the variance of the population and the estimator for the variance of the mean. As the number of realizations increases, the estimated variance of the population based on (2.123) will tend to the true population variance. On the other hand, the estimated variance of the mean will tend to zero as the number of realizations increases. A practical interpretation of this is that the longer you run a simulation, the better you know your results. Therefore, by running a simulation long enough, it is possible to reduce the stochastic uncertainty to arbitrarily low levels.

2.7.4.3.4 Confidence Intervals While the sample variance and standard deviation give us some idea about the variability of the estimate of the mean of whatever quantities we've tallied, it does not help us interpret how confident we should be in the results. To quantify the reliability of our estimates, we can use confidence intervals based on the calculated sample variance.

A $1 - \alpha$ confidence interval for a population parameter is defined as such: if we repeat the same experiment many times and calculate the confidence interval for each experiment, then $1 - \alpha$ percent of the calculated intervals would encompass the true population parameter. Let x_1, x_2, \dots, x_N be samples from a set of independent, identically-distributed random variables each with population mean μ and variance σ^2 . The t -statistic is defined as

$$t = \frac{\bar{x} - \mu}{s/\sqrt{N}} \quad (2.127)$$

where \bar{x} is the sample mean from (2.120) and s is the standard deviation based on (2.123). If the random variables X_i are normally-distributed, then the t -statistic has a Student's t -distribution with $N - 1$ degrees of freedom. This implies that

$$Pr \left(-t_{1-\alpha/2, N-1} \leq \frac{\bar{x} - \mu}{s/\sqrt{N}} \leq t_{1-\alpha/2, N-1} \right) = 1 - \alpha \quad (2.128)$$

where $t_{1-\alpha/2, N-1}$ is the $1 - \alpha/2$ percentile of a t -distribution with $N - 1$ degrees of freedom. Thus, the $1 - \alpha$ two sided confidence interval for the sample mean is

$$\bar{x} \pm t_{1-\alpha/2, N-1} \frac{s}{\sqrt{N}}. \quad (2.129)$$

One should be cautioned that (2.129) only applies if the *underlying random variables* are normally-distributed. In general, this may not be true for a tally random variable — the central limit theorem guarantees only that the sample mean is normally distributed, not the underlying random variable. If batching is used, then the underlying random variable, which would then be the averages from each batch, will be normally distributed as long as the conditions of the central limit theorem are met.

Let us now outline the method used in OpenMC to calculate the percentile of the Student's t -distribution. For one or two degrees of freedom, the percentile can be written analytically. For one degree of freedom, the t -distribution becomes a standard Cauchy distribution whose cumulative distribution function is

$$c(x) = \frac{1}{\pi} \arctan x + \frac{1}{2}. \quad (2.130)$$

Thus, inverting the cumulative distribution function, we find the x percentile of the standard Cauchy distribution to be

$$t_{x,1} = \tan\left(\pi\left(x - \frac{1}{2}\right)\right). \quad (2.131)$$

For two degrees of freedom, the cumulative distribution function is the second-degree polynomial

$$c(x) = \frac{1}{2} + \frac{x}{2\sqrt{x^2 + 2}}. \quad (2.132)$$

Solving for x , we find the x percentile to be

$$t_{x,2} = \frac{2\sqrt{2}(x - 1/2)}{\sqrt{1 - 4(x - 1/2)^2}} \quad (2.133)$$

For degrees of freedom greater than two, it is not possible to obtain an analytical formula

for the inverse of the cumulative distribution function. We must either solve for the inverse numerically or resort to an approximation. Approximations for percentiles of the t -distribution have been found with high levels of accuracy. OpenMC uses the following approximation [72]:

$$t_{x,n} = \sqrt{\frac{n}{n-2}} \left(z_x + \frac{1}{4} \frac{z_x^3 - 3z_x}{n-2} + \frac{1}{96} \frac{5z_x^5 - 56z_x^3 + 75z_x}{(n-2)^2} + \frac{1}{384} \frac{3z_x^7 - 81z_x^5 + 417z_x^3 - 315z_x}{(n-2)^3} \right) \quad (2.134)$$

where z_x is the x percentile of the standard normal distribution. In order to determine an arbitrary percentile of the standard normal distribution, we use an unpublished rational approximation [73]. After using the rational approximation, one iteration of Newton's method is applied to improve the estimate of the percentile.

2.8 Eigenvalue Calculations

An eigenvalue calculation, also referred to as a criticality calculation, is a transport simulation wherein the source of neutrons includes fission neutrons. Unlike a fixed source calculation where the source of neutrons is known *a priori*, the neutron source distribution in an eigenvalue calculation has to be determined on-the-fly during the calculation.

2.8.1 Method of Successive Generations

The method used to converge on the fission source distribution in an eigenvalue calculation, known as the method of successive generations, was first introduced by Lieberoth [74]. In this method, a finite number of neutron histories, N , are tracked through their lifetime iteratively. If fission occurs, rather than tracking the resulting fission neutrons, the spatial coordinates of the fission site, the sampled outgoing energy and direction of the fission neutron, and the weight of the neutron are stored for use in the subsequent generation. As we discussed briefly in chapter 1, the array used for storing the fission

site information is called the fission bank. At the end of each fission generation, N source sites for the next generation must be randomly sampled from the M fission sites that were stored to ensure that the neutron population does not grow exponentially. The sampled source sites are stored in a separate array called the *source bank* and can be retrieved during the subsequent generation.

Since the neutron source distribution is not known at the start of the calculation, the user must supply an assumption regarding how the fission source sites are distributed. This assumption could be a uniform distribution over some region of the geometry or simply a point source. Regardless of the choice of initial source distribution, the method is guaranteed to converge to the true source distribution. Until the source distribution converges, tallies should not be scored to since they will otherwise include contributions from an unconverged source distribution. It is important to have a means for determining when the source distribution has converged in order to know when to start accumulating tallies

2.8.2 Shannon Entropy

It can be shown that the convergence rate of the source distribution is in general slower than that of global eigenvalue, k [20]. One should thus examine not only the convergence of k but also the convergence of the source distribution in order to make decisions on when to start active batches.

That being said, the representation of the source distribution makes it a bit more difficult to analyze its convergence. Since k is a scalar quantity, one can simply look at a line plot of k versus the number of batches and ascertain whether it has converged. On the other hand, the source distribution at any given batch is a finite set of coordinates in Euclidean space. In order to analyze the convergence, we would either need to use a method for assessing convergence of an N -dimensional quantity or transform our set of coordinates into a scalar metric. The latter approach has been developed considerably over the last decade and a method now commonly used in Monte Carlo eigenvalue calculations is to use a metric called the Shannon entropy [75], a concept borrowed

from information theory.

To compute the Shannon entropy of the source distribution, we first need to discretize the source distribution rather than having a set of coordinates in Euclidean space. This can be done by superimposing a structured mesh over the geometry (containing at least all fissionable materials). Then, the fraction of source sites that are present in each mesh element is counted:

$$S_i = \frac{\text{Source sites in } i\text{th mesh element}}{\text{Total number of source sites}} \quad (2.135)$$

The Shannon entropy is then computed as

$$H = - \sum_{i=1}^N S_i \log_2 S_i \quad (2.136)$$

where N is the number of mesh elements. With (2.136), we now have a scalar metric that we can use to assess the convergence of the source distribution by observing line plots of the Shannon entropy versus the number of batches.

In recent years, researchers have started looking at ways of automatically assessing source convergence to relieve the burden on the user of having to look at plots of k and the Shannon entropy. A number of methods have been proposed (see e.g. [76, 77]), but each of these is not without problems.

Chapter 3

Fission Bank Algorithms

3.1 Introduction

We began discussing in chapter 1 several aspects of Monte Carlo simulations that may inhibit them from scaling to large numbers of processors. One of these aspects is the parallelization of the fission source iterations that are necessary in an eigenvalue calculation. Traditional parallel implementations of the fission source iterations have been shown to degrade parallel efficiency with just tens or hundreds of processors [45]. Thus, in order to scale Monte Carlo eigenvalue calculations to thousands or millions of processors, a new approach is needed for parallelizing fission source iterations.

Within each fission source iteration, N source neutrons are simulated and create M fission sites¹ that are stored in the fission bank. To ensure that the neutron population does not grow or shrink exponentially, N source sites for the next generation are randomly sampled from the M fission bank sites that were stored.

A common requirement in Monte Carlo particle transport codes is that identical runs should produce identical results — this also applies to parallel calculations, i.e. a parallel calculation should reproduce the same answers as a serial calculation. Without reproducibility, it would be difficult to debug or otherwise verify that modifications to the code do not cause errors. Thus, the process by which the N source sites are sampled

¹The production of fission sites is weighted such that expected value of M is N . However, in any given generation, it is unlikely that $M = N$ exactly.

from the M fission bank sites has to be done in a reproducible manner. Similarly the order of the source bank sites from one generation to the next should be the same as in a serial calculation. When an eigenvalue calculation is run in parallel, each process has its own source bank and fission bank and thus coordination is required between processes. The use of work scheduling algorithms wherein the mapping of source sites to processes is non-deterministic make maintaining reproducibility in a parallel calculation even more challenging.

In section 3.2, we present an analysis of a master-slave parallel algorithm for fission source site sampling and redistribution and elucidate its limitations. In section 3.3, we introduce a novel algorithm with a nearest-neighbor communication pattern and present a theoretical analysis that confirms our intuition that it should scale better than the master-slave algorithm. Measurements taken within OpenMC to validate the theoretical analysis are reported in section 3.4. Both algorithms were implemented in OpenMC to compare their performance and demonstrate scalability of the nearest-neighbor algorithm on contemporary supercomputers, the results of which are discussed in section 3.5. Finally, miscellaneous considerations such as load balancing and fault tolerance are briefly discussed in section 3.6.

The material in this chapter largely follows from a paper published in *Nuclear Science and Engineering* [78].

3.2 Master-Slave Algorithm

Monte Carlo particle transport codes commonly implement an SPMD model by having one master process that controls the scheduling of work while the remaining processes wait to receive work from the master, process the work, and then send their results to the master at the end of the simulation. This idea is illustrated in Figure 3-1. The most common parallel algorithm for fission source site sampling and redistribution also relies on the master process for coordination — doing so makes it is easier to achieve reproducibility. In order to guarantee that the process by which fission sites are randomly sampled does not depend on the number of processors, the master-slave algorithm is

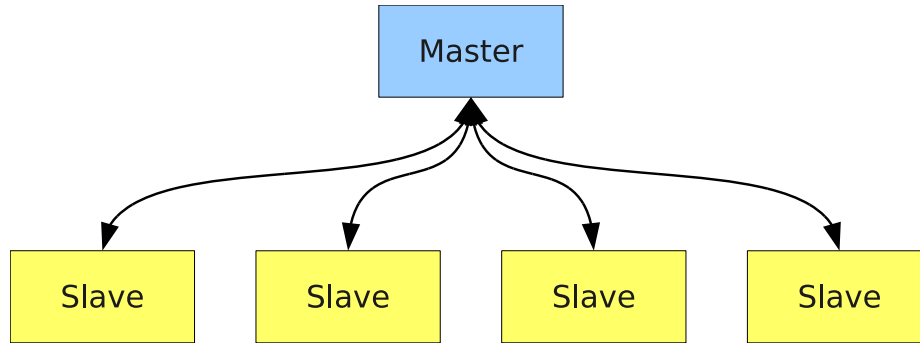


Figure 3-1: Typical master-slave algorithm.

typically implemented in the following manner [48]:

1. Each slave process *sends* its fission bank sites to the master process. With M fission sites in total distributed across the slave processes, this step can be completed in $O(M)$ time. Since $E[M] = N$, this implies that this step is $O(N)$.
2. The master process sorts or orders the fission sites based on a unique identifier. While a naïve sort would require $O(N \log N)$ steps on average, Brown outlines a reordering algorithm in [79] that can reduce this to $O(N)$.
3. The master process samples N fission sites from the ordered array of M sites. This requires a loop over all fission sites and thus, by the same logic as before, is $O(N)$.
4. The master process *broadcasts* all the fission sites to the slave processes. Since each slave process does not need to keep every source site in memory, one could modify the algorithm from a broadcast to a *scatter*. However, for practical reasons (e.g. work self-scheduling [20]), this is normally not done in production Monte Carlo codes. This step is also, at best, $O(N)$ as we will see later.

The first and last steps of this algorithm involve communication between the master and slave processes, whereas the second and third steps require computation only on the master process. However, each of these steps is $O(N)$ at best. In practice, it is the network communication that becomes prohibitive and prevents scalability, so we will thus focus our efforts on analyzing the communication cost.

To estimate the communication cost of the master-slave algorithm, we will introduce a simple latency-bandwidth model. In this model, we assume that the time that it takes to send a message between two processes is given by $\alpha + (dN)\beta$, where α is the time it takes to initiate the communication (latency), β is the transfer time per unit of data (inverse bandwidth), N is the number of fission sites, and d is the size in bytes of each fission site.

The first step of the master-slave algorithm is to send p messages to the master process, each of size dN/p on average. Thus, the total time to send these messages is

$$t_{\text{send}} = p\alpha + dN\beta. \quad (3.1)$$

Estimating the time of the broadcast is complicated by the fact that different MPI implementations may use different algorithms to perform collective communications. Worse yet, a single implementation may use a different algorithm depending on how many processes are communicating and the size of the message. Using multiple algorithms allows one to minimize latency for small messages and minimize bandwidth for long messages.

We will focus here on the implementation of broadcast in the MPICH2 implementation [80]. For short messages, MPICH2 uses a binomial tree algorithm. In this algorithm, the root process sends the data to one process in the first step, and then in the subsequent step, both the root and the other process can send the data to other processes. Thus, it takes a total of $\lceil \log_2 p \rceil$ steps to complete the communication where $\lceil x \rceil$ is the smallest integer not less than x . The time to complete the communication is

$$t_{\text{short}} = \lceil \log_2 p \rceil (\alpha + dN\beta). \quad (3.2)$$

This algorithm works well for short messages since the latency term scales logarithmically with the number of processes. However, for long messages, an algorithm that has lower bandwidth has been proposed by Barnett et al. [81] and implemented in MPICH2. Rather than using a binomial tree, the broadcast is divided into a scatter and an *allgather*. The time to complete the scatter is $\log_2 p \alpha + \frac{p-1}{p} N\beta$ using a binomial tree algorithm.

The allgather is performed using a ring algorithm that completes in $(p - 1)\alpha + \frac{p-1}{p}N\beta$. Thus, together the time to complete the broadcast is

$$t_{\text{long}} = (\log_2 p + p - 1)\alpha + 2\frac{p-1}{p}dN\beta. \quad (3.3)$$

The fission bank data will generally exceed the threshold for switching from short to long messages (typically 8 kilobytes), and thus we will use the equation for long messages. Adding (3.1) and (3.3), we find the total cost of communication for the master-slave algorithm to be

$$t_{\text{master-slave}} = (\log_2 p + 2p - 1)\alpha + \frac{3p-2}{p}dN\beta. \quad (3.4)$$

For large N , it stands to reason that the communication will be bandwidth-dominated. Based on the bandwidth term in (3.4), we see that the combined communication requires $O(N)$ time.

3.3 Nearest-Neighbor Algorithm

To reduce the amount of communication required in a fission bank synchronization algorithm, it is desirable to move away from the master-slave algorithm to a nearest-neighbor algorithm whereby each process communicates only with other processes that are logically adjacent in the network topology. This concept is illustrated in Figure 3-2.

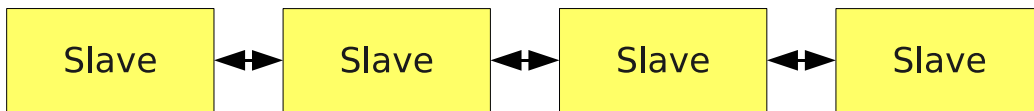


Figure 3-2: Nearest-neighbor communication pattern.

Since the source sites for each fission generation are sampled from the fission sites banked from the previous generation, it is common in the master-slave algorithm for a fission site to be banked on one process, sent back to the master, and finally sent back to the same process as a source site. As a result, much of the communication inherent in the master-slave algorithm is entirely unnecessary. By allowing each process to store and sample fission sites locally and sending sites between processes only as needed, one

can cut down on most of the communication. The proposed algorithm to achieve this works as follows:

1. An exclusive scan is performed on the number of sites banked, and the total number of fission bank sites is broadcasted to all processes. By picturing the fission bank as one large array distributed across multiple processes, one can see that this step enables each process to determine the starting index of fission bank sites in this array. Let us call the starting and ending indices on the i th process a_i and b_i , respectively;
2. Each process samples sites at random from the fission bank using the same starting seed. A separate array on each process is created that consists of sites that were sampled local to that process, i.e. if the index of the sampled site is between a_i and b_i , it is set aside;
3. If a_i is less than iN/p where N is the total number of particles per generation and p is the number of processors, then send $iN/p - a_i$ sites to the left adjacent process. Similarly, if a_i is greater than iN/p , then receive $a_i - iN/p$ from the left adjacent process. This idea is applied to the fission bank sites at the end of each process' array as well. If b_i is less than $(i + 1)N/p$, then receive $(i + 1)N/p - b_i$ sites from the right adjacent process. If b_i is greater than $(i + 1)N/p$, then send $b_i - (i + 1)N/p$ sites to the right adjacent process. Thus, each process sends/receives only two messages under normal circumstances.

The following example illustrates how this algorithm works. Let us suppose we are simulating $N = 1,000$ particles distributed over four processes. For this example, it is instructive to look at the state of the fission bank and source bank at several points in the algorithm:

1. The beginning of a fission generation where each process has N/p source sites;
2. The end of a fission generation where each process has accumulated fission sites;
3. After sampling, where each process has some amount of source sites usually not equal to N/p ;

4. After redistribution, where each process again has N/p source sites for the next generation.

At the end of each fission generation, each process needs $N/p = 250$ fission bank sites to continue on the next generation. Suppose that process p_0 produces 270 fission bank sites, p_1 produces 230, p_2 produces 290, and p_3 produces 250. After each process samples from its fission bank sites, let's assume that p_0 has 260 source sites, p_1 has 215, p_2 has 280, and p_3 has 245. For each process to have the same number of source sites, p_0 needs to send its right-most 10 sites to p_1 , and p_2 needs to send its left-most 25 sites to p_1 and its right-most 5 sites to p_3 . A schematic of this example is shown in Figure 3-3. The data local to each process is given a different hatching, and the cross-hatched regions represent source sites that are communicated between logically adjacent process.

Determining the expected communication cost of the nearest-neighbor algorithm is not trivial due to the fact that the cost will be a function of how many fission sites are sampled on each process. If each process samples exactly N/p sites, it would not be necessary to communicate any fission bank sites. However, if any one process samples more or less than N/p sites, the deviation will result in communication between logically adjacent processes. To determine the expected deviation, let us analyze the algorithm based on the fundamentals of the Monte Carlo process.

The steady-state neutron transport equation for a multiplying medium can be written in the form of an eigenvalue problem [74],

$$S(\mathbf{r}) = \frac{1}{k} \int F(\mathbf{r}' \rightarrow \mathbf{r}) S(\mathbf{r}') d\mathbf{r}, \quad (3.5)$$

where \mathbf{r} is the spatial coordinates of phase space, $S(\mathbf{r})$ is the source distribution defined as the expected number of neutrons born from fission per unit phase-space volume at \mathbf{r} , $F(\mathbf{r}' \rightarrow \mathbf{r})$ is the expected number of neutrons born from fission per unit phase space volume at \mathbf{r} caused by a neutron at \mathbf{r}' , and k is the fundamental mode eigenvalue.

In a Monte Carlo eigenvalue calculation, the power iteration method is applied iteratively to obtain stochastic realizations of the source distribution and estimates of the k -eigenvalue. Let us define $\hat{S}^{(m)}$ to be the realization of the source distribution at fission

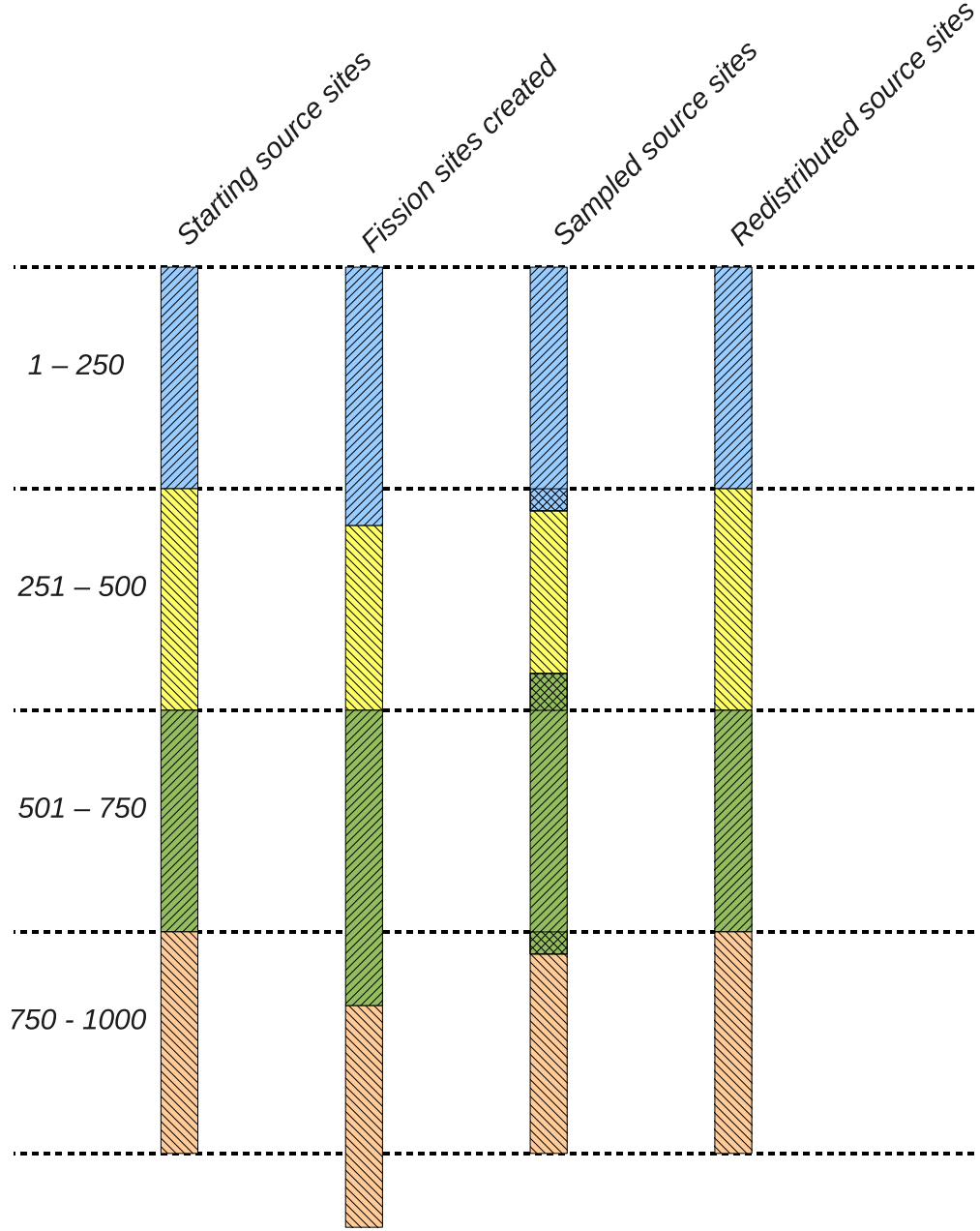


Figure 3-3: Example illustrating nearest-neighbor fission bank algorithm.

generation m and $\hat{\epsilon}^{(m)}$ to be the deviation from the deterministic solution arising from the stochastic nature of the tracking process. We can write the stochastic realization in terms of the fundamental source distribution and the fluctuating component as [82]

$$\hat{S}^{(m)}(\mathbf{r}) = NS(\mathbf{r}) + \sqrt{N}\hat{\epsilon}^{(m)}(\mathbf{r}), \quad (3.6)$$

where N is the number of particle histories per generation. Without loss of generality, we shall drop the superscript notation indicating the generation as it is understood that the stochastic realization is at a particular generation. The expected value of the stochastic source distribution is simply

$$E[\hat{S}(\mathbf{r})] = NS(\mathbf{r}) \quad (3.7)$$

since $E[\hat{\epsilon}(\mathbf{r})] = 0$. The noise in the source distribution is due only to $\hat{\epsilon}(\mathbf{r})$ and thus the variance of the source distribution will be

$$\text{Var}[\hat{S}(\mathbf{r})] = N\text{Var}[\hat{\epsilon}(\mathbf{r})]. \quad (3.8)$$

Lastly, the stochastic and true eigenvalues can be written as integrals over all phase space of the stochastic and true source distributions, respectively, as

$$\hat{k} = \frac{1}{N} \int \hat{S}(\mathbf{r}) d\mathbf{r} \quad \text{and} \quad k = \int S(\mathbf{r}) d\mathbf{r}, \quad (3.9)$$

noting that $S(\mathbf{r})$ is $O(1)$ since the true source distribution is not a function of N (see Nease et al. [83] for a thorough discussion). One should note that the expected value k calculated by Monte Carlo power iteration (i.e. the method of successive generations) will be biased from the true fundamental eigenvalue of (3.5) by $O(1/N)$ [82], but we will assume henceforth that the number of particle histories per generation is sufficiently large to neglect this bias.

With this formalism, we now have a framework within which we can determine the properties of the distribution of expected number of fission sites. The explicit form of the source distribution can be written as

$$\hat{S}(\mathbf{r}) = \sum_{i=1}^M w_i \delta(\mathbf{r} - \mathbf{r}_i) \quad (3.10)$$

where \mathbf{r}_i is the spatial location of the i th fission site, w_i is the statistical weight of the fission site at \mathbf{r}_i (i.e. the weight of the neutron entering into a fission reaction), and M is the total number of fission sites. It is clear that the total weight of the fission sites is

simply the integral of the source distribution. Integrating (3.6) over all space, we obtain

$$\int \hat{S}(\mathbf{r}) d\mathbf{r} = N \int S(\mathbf{r}) d\mathbf{r} + \sqrt{N} \int \hat{\epsilon}(\mathbf{r}) d\mathbf{r}. \quad (3.11)$$

Substituting the expressions for the stochastic and true eigenvalues from (3.9), we can relate the stochastic eigenvalue to the integral of the noise component of the source distribution as

$$N\hat{k} = Nk + \sqrt{N} \int \hat{\epsilon}(\mathbf{r}) d\mathbf{r}. \quad (3.12)$$

Since the expected value of $\hat{\epsilon}$ is zero, the expected value of its integral will also be zero. We thus see that the variance of the integral of the source distribution, i.e. the variance of the total weight of fission sites produced, is directly proportional to the variance of the integral of the noise component. Let us call this term σ^2 for simplicity:

$$\text{Var} \left[\int \hat{S}(\mathbf{r}) d\mathbf{r} \right] = N\sigma^2. \quad (3.13)$$

The actual value of σ^2 will depend on the physical nature of the problem, whether variance reduction techniques are employed, etc. For instance, one could surmise that for a highly scattering problem, σ^2 would be smaller than for a highly absorbing problem since more collisions will lead to a more precise estimate of the source distribution. Similarly, using survival biasing should in theory reduce the value of σ^2 .

Let us now consider the case where the N total histories are divided up evenly across p processes. Since each process simulates N/p histories, we can write the source distribution as

$$\hat{S}_i(\mathbf{r}) = \frac{N}{p} S(\mathbf{r}) + \sqrt{\frac{N}{p}} \hat{\epsilon}_i(\mathbf{r}) \quad \text{for } i = 1, \dots, p \quad (3.14)$$

Integrating over all space and simplifying, we can obtain an expression for the eigenvalue on the i th process:

$$\hat{k}_i = k + \sqrt{\frac{p}{N}} \int \hat{\epsilon}_i(\mathbf{r}) d\mathbf{r}. \quad (3.15)$$

It is easy to show from this expression that the stochastic realization of the global

eigenvalue is merely the average of these local eigenvalues:

$$\hat{k} = \frac{1}{p} \sum_{i=1}^p \hat{k}_i. \quad (3.16)$$

As was mentioned earlier, at the end of each generation one must sample N sites from the M sites that were created. Thus, the source for the next generation can be seen as the fission source from the current generation divided by the stochastic realization of the eigenvalue since it is clear from (3.9) that $\hat{k} = M/N$. Similarly, the number of sites sampled on each process that will be used for the next generation is

$$M_i = \frac{1}{\hat{k}} \int \hat{S}_i(\mathbf{r}) d\mathbf{r} = \frac{N}{p} \frac{\hat{k}_i}{\hat{k}}. \quad (3.17)$$

While we know conceptually that each process will under normal circumstances send two messages, many of these messages will overlap. Rather than trying to determine the actual communication cost, we will instead attempt to determine the maximum amount of data being communicated from one process to another. At any given generation, the number of fission sites that the j th process will send or receive, Λ_j , is

$$\Lambda_j = \left| \sum_{i=1}^j M_i - \frac{jN}{p} \right|. \quad (3.18)$$

Noting that jN/p is the expected value of the summation, we can write the expected value of Λ_j as the mean absolute deviation of the summation:

$$E[\Lambda_j] = E \left[\left| \sum_{i=1}^j M_i - \frac{jN}{p} \right| \right] = \text{MD} \left[\sum_{i=1}^j M_i \right] \quad (3.19)$$

where MD indicates the mean absolute deviation of a random variable. The mean absolute deviation is an alternative measure of variability.

In order to ascertain any information about the mean deviation of M_i , we need to know the nature of its distribution. Thus far, we have said nothing of the distributions of the random variables in question. The total number of fission sites resulting from the

tracking of N neutrons can be shown to be normally distributed via the Central Limit Theorem (provided that N is sufficiently large) since the fission sites resulting from each neutron are “sampled” from independent, identically-distributed random variables. Thus, \hat{k} and $\int \hat{S}(\mathbf{r}) d\mathbf{r}$ will be normally distributed as will the individual estimates of these on each process.

Next, we need to know what the distribution of M_i in (3.17) is or, equivalently, how \hat{k}_i/\hat{k} is distributed. The distribution of a ratio of random variables is not easy to calculate analytically, and it is not guaranteed that the ratio distribution is normal if the numerator and denominator are normally distributed. For example, if X is a standard normal distribution and Y is also standard normal distribution, then the ratio X/Y has the standard Cauchy distribution. The reader should be reminded that the Cauchy distribution has no defined mean or variance. That being said, Geary [84] has shown that, for the case of two normal distributions, if the denominator is unlikely to assume values less than zero, then the ratio distribution is indeed approximately normal. In our case, \hat{k} absolutely cannot assume a value less than zero, so we can be reasonably assured that the distribution of M_i will be normal.

For a normal distribution with mean μ and distribution function $f(x)$, it can be shown that

$$\int_{-\infty}^{\infty} f(x) |x - \mu| dx = \sqrt{\frac{2}{\pi}} \int_{-\infty}^{\infty} f(x) (x - \mu)^2 dx \quad (3.20)$$

by substituting the probability distribution function of a normal distribution for $f(x)$, making a change of variables, and integrating both sides. Thus the mean absolute deviation is $\sqrt{2/\pi}$ times the standard deviation. Therefore, to evaluate the mean absolute deviation of M_i , we need to first determine its variance. Substituting (3.16) in (3.17), we can rewrite M_i solely in terms of $\hat{k}_1, \dots, \hat{k}_p$:

$$M_i = \frac{N \hat{k}_i}{\sum_{j=1}^p \hat{k}_j}. \quad (3.21)$$

Since we know the variance of \hat{k}_i , we can use the error propagation law to determine

the variance of M_i :

$$\text{Var}[M_i] = \sum_{j=1}^p \left(\frac{\partial M_i}{\partial \hat{k}_j} \right)^2 \text{Var}[\hat{k}_j] + \sum_{j \neq m} \sum_{m=1}^p \left(\frac{\partial M_i}{\partial \hat{k}_j} \right) \left(\frac{\partial M_i}{\partial \hat{k}_m} \right) \text{Cov}[\hat{k}_j, \hat{k}_m] \quad (3.22)$$

where the partial derivatives are evaluated at $\hat{k}_j = k$. Since \hat{k}_j and \hat{k}_m are independent if $j \neq m$, their covariance is zero and thus the second term cancels out. Evaluating the partial derivatives, we obtain

$$\text{Var}[M_i] = \left(\frac{N(p-1)}{kp^2} \right)^2 \frac{p\sigma^2}{N} + \sum_{j \neq i} \left(\frac{-N}{kp^2} \right)^2 \frac{p\sigma^2}{N} = \frac{N(p-1)}{k^2 p^2} \sigma^2. \quad (3.23)$$

Through a similar analysis, one can show that the variance of $\sum_{i=1}^j M_i$ is

$$\text{Var} \left[\sum_{i=1}^j M_i \right] = \frac{Nj(p-j)}{k^2 p^2} \sigma^2 \quad (3.24)$$

Thus, the expected amount of communication on process j , i.e. the mean absolute deviation of $\sum_{i=1}^j M_i$, is proportional to

$$E[\Lambda_j] = \sqrt{\frac{2Nj(p-j)\sigma^2}{\pi k^2 p^2}}. \quad (3.25)$$

Equation (3.25) has all the properties that one would expect based on intuition:

- As the number of particle histories increases, the communication cost on each process increases as well;
- If $p = 1$, i.e. if the problem is run on only one process, the variance will be zero. This reflects the fact that exactly N sites will be sampled if there is only one process.
- For $j = p$, the variance will be zero. Again, this says that when you sum the number of sites from each process, you will get exactly N sites.

We can determine the process that has the highest communication cost by differentiating (3.25) with respect to j , setting it equal to zero, and solving for j . Doing so yields

$j_{\max} = p/2$. Interestingly, substituting $j = p/2$ in (3.25) indicates that the maximum communication cost is actually independent of the number of processes:

$$E[\Lambda_{j_{\max}}] = \sqrt{\frac{N\sigma^2}{2\pi k^2}}. \quad (3.26)$$

We can now proceed as before and estimate the communication time using the latency-bandwidth model. As discussed earlier, each process should send or receive only two messages, one to each of its neighbors. Since the largest message will occur on process $j_{\max} = p/2$, we can use (3.26) and (3.1) to estimate the communication time for the nearest-neighbor algorithm as

$$t_{\text{nearest-neighbor}} = 2\alpha + d\sqrt{\frac{2N\sigma^2}{\pi k^2}}\beta \quad (3.27)$$

To compare the communication time of the two algorithms, we can assume that the message size is large enough that the communication will be bandwidth dominated. Dividing (3.4) by (3.27), we find that

$$\frac{t_{\text{master-slave}}}{t_{\text{nearest-neighbor}}} = \frac{(\log_2 p + 2p - 1)\alpha + \frac{3p-2}{p}dN\beta}{2\alpha + d\sqrt{\frac{2N\sigma^2}{\pi k^2}}\beta} \approx \frac{(3p-2)k\sqrt{N\pi/2}}{p\sigma}. \quad (3.28)$$

In the limit of large p , this ratio becomes

$$\lim_{p \rightarrow \infty} \frac{t_{\text{master-slave}}}{t_{\text{nearest-neighbor}}} = \sqrt{\frac{N\pi}{2}} \cdot \frac{3k}{\sigma}. \quad (3.29)$$

We can see from (3.27) that the nearest-neighbor algorithm requires $O(\sqrt{N})$ time instead of $O(N)$ as for the master-slave algorithm. This should allow the the algorithm to scale to very large numbers of total processes or particles per generation. In fact, we can show that arbitrarily good scaling can be achieved. Let t be the time to simulate N particles on p processors. Expressing the network communication time as a fraction of

the time to simulate the particles, we find that:

$$\frac{t_{\text{nearest-neighbor}}}{t} \propto \frac{\sqrt{N}}{N/p} \propto \frac{p}{\sqrt{N}} \quad (3.30)$$

Thus, if we keep p constant and increase N , the relative time to complete network communication will be reduced since the simulation time is proportional to N and the communication is proportional to \sqrt{N} .

3.4 Validation of Theoretical Analysis

To ensure that any assumptions made in the foregoing analysis are sound, several test cases using an implementation of the nearest-neighbor fission bank algorithm in OpenMC were run to provide results that can be compared with the theoretical analysis. The number of processes and particle histories for each case are shown in Table 3.1. Each

Table 3.1: Test cases for nearest-neighbor fission bank algorithm.

| Case | Processes (p) | Histories (N) |
|------|-------------------|-------------------|
| 1 | 8 | 80,000 |
| 2 | 8 | 160,000 |
| 3 | 16 | 80,000 |
| 4 | 16 | 160,000 |

case was run for 10,000 generations and at the end of each run, the standard deviation of the number of fission bank sites sent to logically adjacent processes was determined for each process as a proxy for the communication cost. For Case 1, the data were fit to the following function (with the same dependence on j and p as in (3.25)) using a least squares regression:

$$f(j, p, \beta) = \frac{\beta}{p} \sqrt{j(p-j)}. \quad (3.31)$$

The fitting coefficient β was then used to predict the expected amount of communication for the other three cases. Figure 3-4 shows the expected number of fission bank sites sent or received from neighboring processes, $E[\Lambda_j]$, for Cases 1 and 2 along with the least squares regression fit based on (3.31) for Case 1 and the prediction for Case 2. Figure 3-

5 shows the expected number of fission bank sites sent or received from neighboring processes for Cases 3 and 4 along with the predicted fits. A few observations can be

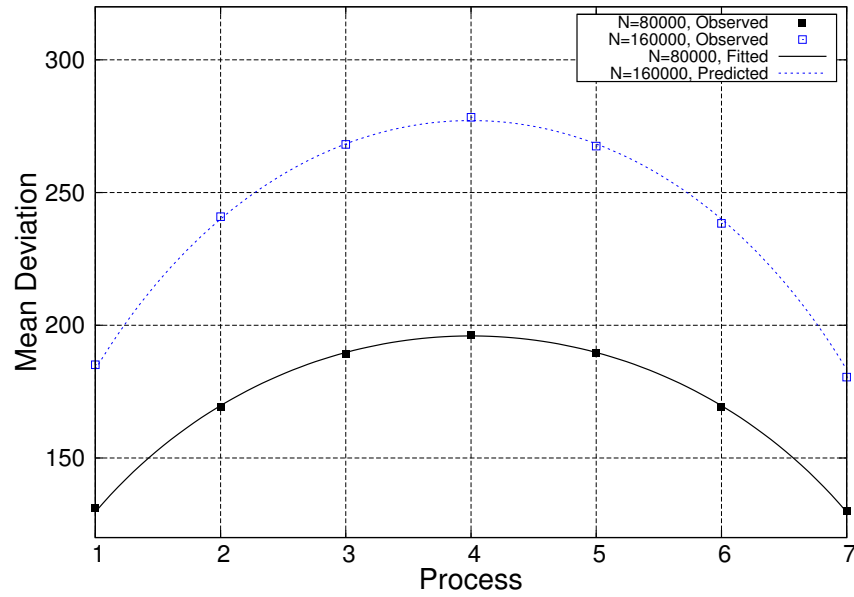


Figure 3-4: Expected number of fission bank sites sent to neighboring processes using 8 processes.

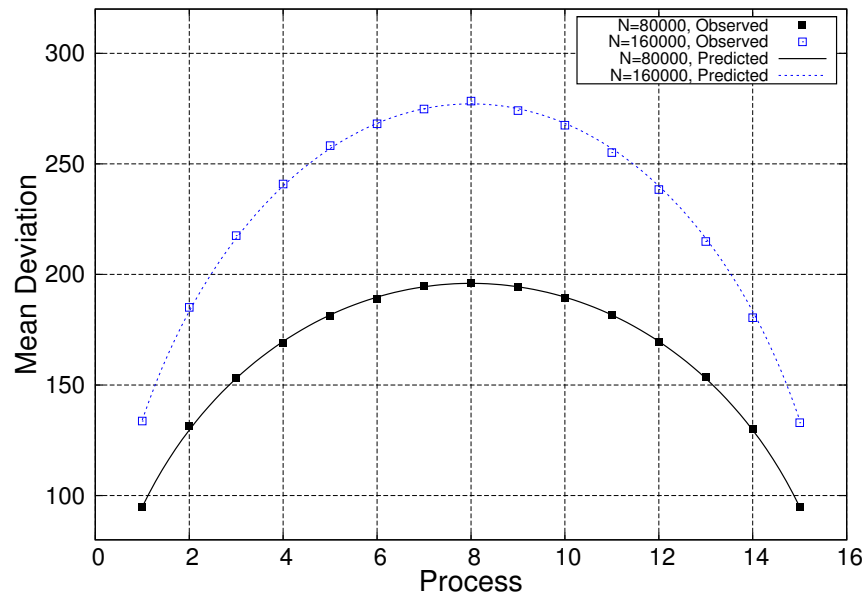


Figure 3-5: Expected number of fission bank sites sent to neighboring processes using 16 processes.

made from these figures. Firstly, the data from the four test cases demonstrates that

the foregoing theoretical analysis is indeed correct. Furthermore, one can observe from these two figures that the maximum communication does occur for process $j_{\max} = p/2$ and that this maximum is independent of p as predicted.

It is also instructive to check our assumption that $\sum_{i=1}^j M_i$ is normally distributed. One way of doing this is through a quantile-quantile (Q-Q) plot, comparing the observed quantiles of the data with the theoretical quantiles of the normal distribution. If the data are normally distributed, the points on the Q-Q plot should lie along a line. Figure 3-6 shows a Q-Q plot for the number of fission bank sites sent or received on the first process for Case 1. The data clearly lie along a straight line and thus the data are normally

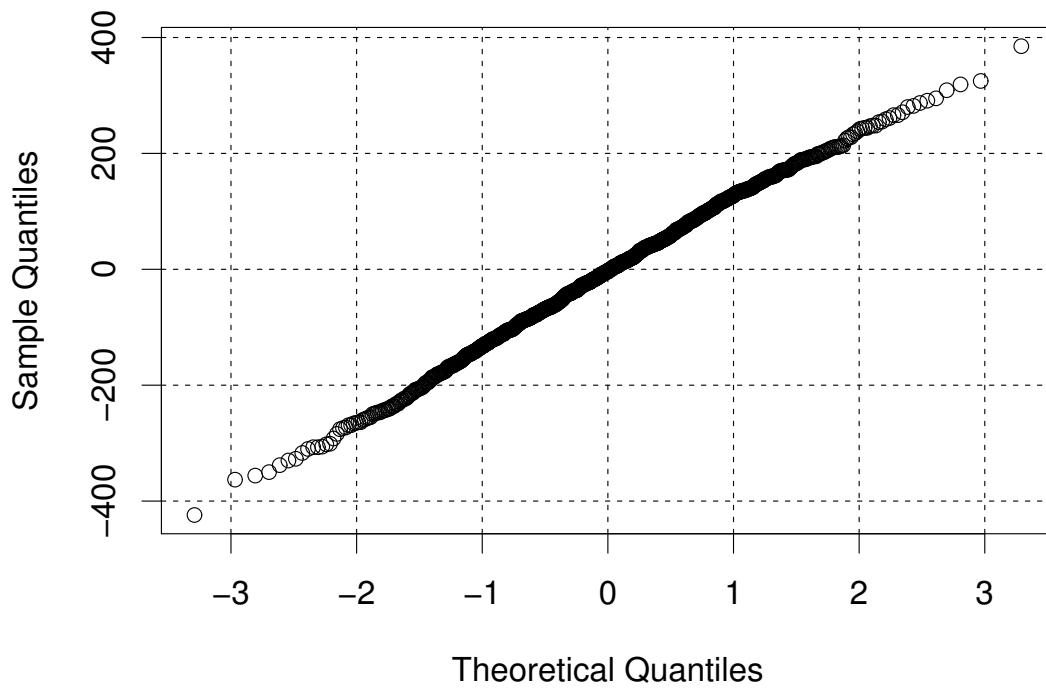


Figure 3-6: Q-Q plot of M_1 for Case 1

distributed. This conclusion was also confirmed using the Shapiro-Wilk test for normality [85].

3.5 Results

3.5.1 Communication Time

In section 3.3, it was shown that the communication cost of nearest-neighbor algorithm will depend on a parameter σ representing the variance in the number of sites sent between adjacent processes. Thus, while we can conclude from (3.29) that the nearest-neighbor algorithm will certainly outperform the master-slave algorithm in the limit of large p and N , it is more difficult to make inferences regarding the performance of the two algorithms for smaller cases.

In order to compare the two algorithms, both were implemented in OpenMC. A separate simulation using each of the algorithms was run from a single process up to 88 processes in parallel on a small cluster with an Ethernet network interconnect. In each case, the number of histories was 40,000 times the number of processes so that each process simulates the same number of histories. Each simulation was run for 20 fission generations. Figure 3-7 shows the total time spent on fission bank synchronization for the two algorithms. We see that the nearest-neighbor algorithm performs nearly

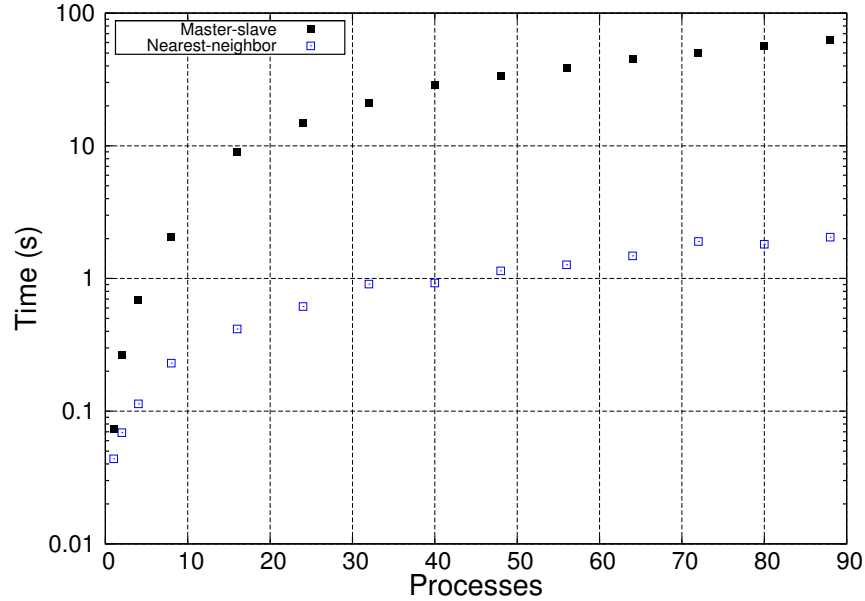


Figure 3-7: Execution time for fission bank algorithms.

two orders of magnitude faster than the master-slave algorithm for large p and large

N . In these simulations, we have ignored the time spent sampling fission sites and copying data in memory which may become non-negligible for large N . Thus, to truly demonstrate scalability, simulations with much larger N and p are needed.

3.5.2 Parallel Scaling

To test parallel scaling, an OpenMC model of the Monte Carlo Performance Benchmark was simulated on both the Blue Gene/P at the Argonne Leadership Computing Facility (Intrepid) and the Cray XK6 at the Oak Ridge Leadership Computing Facility (Jaguar) using the nearest-neighbor fission bank algorithm. On the Blue Gene/P, up to 163,840 cores were used with 4000 particles per processor core per generation. On the Cray XK6, up to 131,072 cores were used with 20,000 particles per processor core per generation. For this study, the total work per processor was kept constant (weak scaling) rather than the total amount of work over all processors (strong scaling). Figure 3-8 shows the effective number of particles simulated per second as a function of the number of processors in comparison to the ideal calculation rate (assuming no communication between fission source iterations). Excellent parallel efficiency is achieved even above 100,000 processors.

A few notes should be made regarding the achieved scaling shown in Figure 3-8. First, it was necessary to use non-blocking communication semantics rather than blocking communication; when blocking communication was attempted, the scaling behavior was observed to be much worse. Additionally, it was necessary to turn off the calculation of Shannon entropy during the simulations. In OpenMC, the number of mesh cells used for the Shannon entropy mesh grows linearly with the number of particles per generation. At the end of the fission generation, the number of source sites in each mesh cell has to be reduced from all processes before being used in (2.136). As such, in a series of weak scaling runs, the communication associated with calculating Shannon entropy would grow linearly with the number of processors — turning off the calculation of Shannon entropy circumvents this. Another simple solution would be to fix the size of the Shannon entropy mesh irrespective of the number of particles per generation.

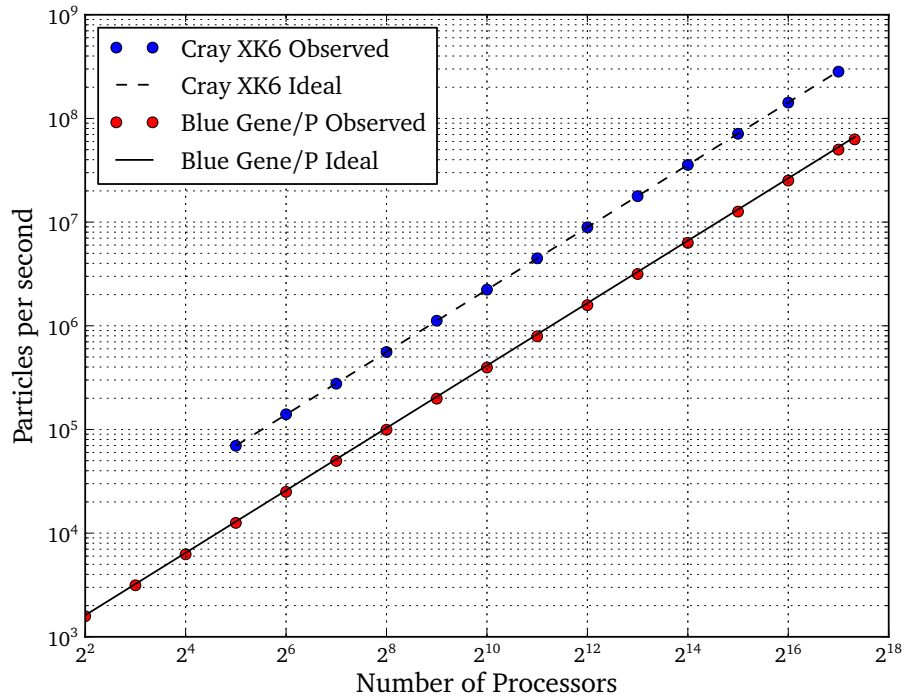


Figure 3-8: Parallel scaling for the Monte Carlo Performance Benchmark on the Cray XK6 (Jaguar) and Blue Gene/P (Intrepid) supercomputers.

3.6 Other Considerations

3.6.1 Load Balancing

One important requirement for a parallel Monte Carlo calculation is proper load-balancing, i.e. it is undesirable to have a process sitting idle with no work to do while other processes are still busy working. This is especially the case when the hardware architecture is heterogeneous (having different types of processors in a single cluster). In the master-slave algorithm, work self-scheduling is achieved by having each slave process request small batches of work from the master, and as each batch is completed, the slave may request more work. By breaking up the problem into smaller batches, this ensures that in a single source iteration, a processor that is twice as fast as another processor will also be assigned twice as many histories to compute, and thus all processors should finish their work at approximately the same time.

The nearest-neighbor algorithm unfortunately precludes the use of the aforementioned self-scheduling algorithm since an important aspect of the algorithm is to assign particle histories sequentially to the processes to preserve their order. It should be noted that if one did not care to preserve reproducibility in a calculation, the self-scheduling scheme could easily be applied for load-balancing with the nearest-neighbor fission bank algorithm.

The results in Figure 3-8 demonstrate that the lack of a load balancing mechanism does not degrade parallel efficiency when used on a homogeneous cluster. Previous studies using MCNP on a homogeneous Linux cluster have shown a 5-10% loss in parallel efficiency when not using load balancing [20].

It is also possible to employ a basic means of load balancing for heterogeneous architectures using in the nearest-neighbor algorithm by “tuning” the algorithm to the specific characteristics of the cluster. If one were to measure the performance of each type of processor on the cluster in terms of particles processed per second, the number of histories on each processor could be adjusted accordingly instead of merely distributing particles uniformly (N/p on each processor).

3.6.2 Fault Tolerance

For petascale and future exascale architectures, it is desirable to have some means of fault tolerance to ensure that not all results are lost in the event of a hardware failure. In current Monte Carlo codes, this can be achieved by having all processes periodically rendezvous and collectively dump data to a file that can be used to restart the run. While providing insurance against lost simulation time, performing fault tolerance this way unfortunately degrades parallel performance since it entails collective communication between all processors. Notwithstanding, the algorithm we have presented here does not inhibit the use of fault tolerance in this manner.

3.7 Conclusions

In this chapter, we presented a new algorithm for parallelizing the source iterations in a Monte Carlo criticality calculation. This algorithm takes advantage of the fact that many of the fission sites produced on one processor can be used as source sites on that same processor — in doing so, it avoids unnecessary communication between processors.

Analysis of the algorithm shows that it should outperform existing algorithms for fission bank synchronization and furthermore, the performance gap increases for an increasing number of histories or processors. Test results on the OpenMC Monte Carlo code confirm this finding. The analysis also shows that the maximum amount of communication in the algorithm is independent of the number of processors and instead will depend on the number of histories per generation and the physical characteristics of the problem at hand. Again, testing within OpenMC confirms this prediction. Finally, a scaling study was performed on the Titan and Intrepid supercomputers and demonstrated perfect scaling with over 100,000 processor cores using the nearest-neighbor algorithm.

The reader should keep in mind that while the algorithm presented here will significantly improve the time necessary to sample and distribute fission sites between generations, it has no effect on the actual transport simulation of particles moving through a material medium. Thus, it will not improve smaller simulations that would typically run on a workstation. However, for large simulations that necessitate the use of a large cluster or supercomputer to complete in a reasonable amount of time, this novel algorithm improves the parallel efficiency and is an important step in achieving scalability up to thousands or millions of processors.

One potential shortcoming of the present algorithm is that it precludes the use of load balancing via existing algorithms for heterogeneous computer architectures. A basic method to provide load balancing in such situations based on “tuning” the algorithm was suggested, although it has not yet been tested.

Chapter 4

Tally Reduction Algorithms

In chapter 3, a nearest-neighbor fission bank algorithm was proposed, implemented in OpenMC, and demonstrated to enable parallel scaling in Monte Carlo k -eigenvalue calculations with over 100,000 processors. While this algorithm is an important and necessary component in being able to perform realistic LWR analysis with Monte Carlo methods, it is only one piece of the puzzle. We had also identified in chapter 1 that large tallies can become problematic in large-scale parallel simulations due to excessive communication requirements. In fact, in the scaling study in section 3.5, no tallies were included in the runs, and hence the necessary network communication from collecting tallies was obviated.

In this chapter, we propose a method that would greatly reduce network communication when performing parallel simulations with large tally data by using statistical batching across fission generations. In section 4.1, we first review batch statistics and their current utility in Monte Carlo simulations. A modified batching algorithm is then proposed and analyzed in section 4.2. The Monte Carlo performance benchmark was simulated using an implementation of the algorithm in OpenMC; the results of these tests are reported in section 4.3.

The algorithm being presented in this chapter was published in an article in *Transactions of the American Nuclear Society* [86].

4.1 Batch Statistics

To construct an estimate for the sample mean and its variance for any tally in a Monte Carlo simulation, the following formulas are generally used:

$$\bar{x} = \frac{1}{N} \sum_{i=1}^N x_i \quad (4.1)$$

$$s_{\bar{x}}^2 = \frac{1}{N-1} \left[\frac{\sum_{i=1}^N x_i^2}{N} - \left(\frac{\sum_{i=1}^N x_i}{N} \right)^2 \right] \quad (4.2)$$

where x_i is a single realization of the random variable, \bar{x} is the sample mean, $s_{\bar{x}}^2$ is the variance of the sample mean, and N is the number of realizations. A single realization may be the accumulated score from a single particle history in a fixed-source calculation or from a single fission generation in a criticality calculation. A few assumptions have been made in the use of (4.2); it is assumed that N is large enough for the law of large numbers and the central limit theorem (CLT) to apply, and it is assumed that the realizations were drawn from independent and identically distributed random variables, again to satisfy conditions of the CLT.

In the method of successive generations used for Monte Carlo eigenvalue calculations, the locations of source sites in one generation may be correlated with the locations of source sites in a subsequent generation. This is especially true in problems where the overall dimensions of the problem are large relative to the mean free path of neutrons. The correlation between fission sites also results in a correlation between realizations of tally random variables. Unfortunately, this correlation is not accounted for in (4.2). As a result, in problems where there is significant correlation between successive generations (equivalently, in problems with high dominance ratios), using (4.2) to calculate the variance of the sample mean can result in underprediction of the true variance, and hence underprediction of confidence interval width for tallies.

Various solutions to the underprediction of true variance have been studied in the literature. One of the simpler solutions proposed is to simply treat the accumulated

scores from multiple fission generations, referred to as a *batch*¹, as a single realization of a tally random variable [87]. Mathematically, grouping M successive realizations, $x_i, i = 1, \dots, M$, of a random variable yields a separate estimate of a new random variable:

$$y_j = \sum_{i=(j-1)M+1}^{jM} x_i. \quad (4.3)$$

We note that M must be sufficiently large for the central limit theorem to apply to the distribution of y_j , i.e. the batch must be large enough to sufficiently reduce correlation between successive batches. The sample mean and its variance for the new random variable are then

$$\bar{y} = \frac{1}{N'} \sum_{j=1}^{N'} y_j \quad (4.4)$$

$$s_{\bar{y}}^2 = \frac{1}{N' - 1} \left[\frac{\sum_{j=1}^{N'} y_j^2}{N'} - \left(\frac{\sum_{j=1}^{N'} y_j}{N'} \right)^2 \right] \quad (4.5)$$

where $N' = N/M$. It is obvious by inspection that the sample mean \bar{x} and \bar{y} will have the same value regardless of the batching strategy. Furthermore, while the variances will in general be different, it can be shown that the expected value of the variances $s_{\bar{x}}^2$ and $s_{\bar{y}}^2$ are the same. The use of batches provides two main benefits:

1. If M is large enough, the random variables that result from the batching process are guaranteed to be normally distributed as per the central limit theorem.
2. With a large enough batch size, the correlation between successive realizations of the tally random variables becomes negligible, thus ensuring that the true variance is not underestimated.

This method has been implemented and successfully utilized in the MC21 Monte Carlo code [19].

¹Many people use the terms “batch”, “generation”, and “cycle” interchangeably. In this paper, the term “batch” specifically refers to the grouping of multiple realizations and is generally not the same as a “generation” or “cycle” in a criticality calculation.

4.2 Reduction of Tally Scores

Now let us focus our attention on a situation whereby we are performing a Monte Carlo simulation on p processors with the entire geometry of the problem replicated on each processor. After each realization, every processor has its own accumulated score for the tally variable $x_{i,k}$ where k denotes the k th processor. Traditionally, to obtain the same answer as would be obtained in a serial calculation, we would need to take the summation of the tallies across all processors at the end of the realization, i.e. $x_i = \sum_{k=1}^p x_{i,k}$. This is depicted in Figure 4-1 where scores inside each box are summed into a single realization. Algorithm 4-1 shows a pseudocode for the tallying process when applied to an eigenvalue calculation. In terms of network communication, we will

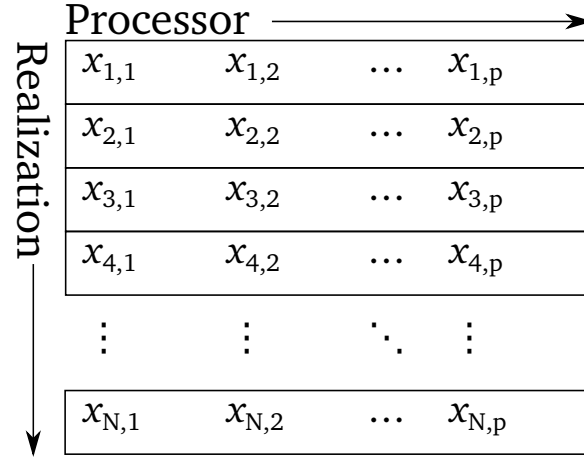


Figure 4-1: Summation of tally scores across processors when doing statistics based on a single particle history or single generation.

need to send at a minimum 8 bytes for each of the ℓ tally bins on $p - 1$ processors to the master process. Thus, the total amount of data that must be communicated during the simulation is $8\ell N(p - 1)$ bytes since the summation must be done at every realization. For a simulation with large ℓ and/or large p , the time to perform this communication can become prohibitive. An example of such a scenario is the calculation of the global power distribution in a large reactor model using a cluster or supercomputer, a calculation easily requiring millions of tally bins, if not more.

Performing statistics over a batch consisting of multiple realizations somewhat alleviates the communication requirements while providing other aforementioned benefits.

Algorithm 4-1: Pseudocode for reducing tally scores across multiple processors when doing statistics based on a single fission generation.

```

for  $i = 1 \rightarrow N$  do                                ▷ Loop over generations
     $x_{i,\ell} \leftarrow 0$ 
    for  $j = 1 \rightarrow N_p$  do                                ▷ Loop over particles
        while alive do
            Move to next collision
             $x_{i,\ell} \leftarrow x_{i,\ell} + \text{score}$ 
        end while
    end for
    MPI_Reduce( $x_{i,\ell}, x_i, \dots$ )                                ▷ Communication
     $s_1 \leftarrow s_1 + x_i$                                 ▷ Accumulate running sums
     $s_2 \leftarrow s_2 + x_i^2$ 
end for
 $\bar{x} \leftarrow \frac{s_1}{N}$                                 ▷ Use running sums to calculate statistics
 $s_{\bar{x}}^2 \leftarrow \frac{1}{N-1} \left[ \frac{s_2}{N} - \left( \frac{s_1}{N} \right)^2 \right]$ 

```

The summation of tally scores for this scenario is depicted in Figure 4-2, and pseudocode for the tallying process is shown in Algorithm 4-2. Since the reduction now need only be performed at the end of a batch, the data requirement is then $8\ell N'(p-1)$.

Rather than considering the batch to be the accumulation of scores from many realizations across many processors, there is no reason that one cannot reproduce the same sample mean, within floating point precision, by considering a batch to be the accumulation of scores from many realizations on a single processor. This idea is shown in Figure 4-3. Pseudocode for the tallying process as applied in an eigenvalue calculation is shown in Algorithm 4-3. Expressed mathematically, our new random variable is

$$z_{j,k} = \sum_{i=(j-1)M+1}^{jM} x_{i,k}. \quad (4.6)$$

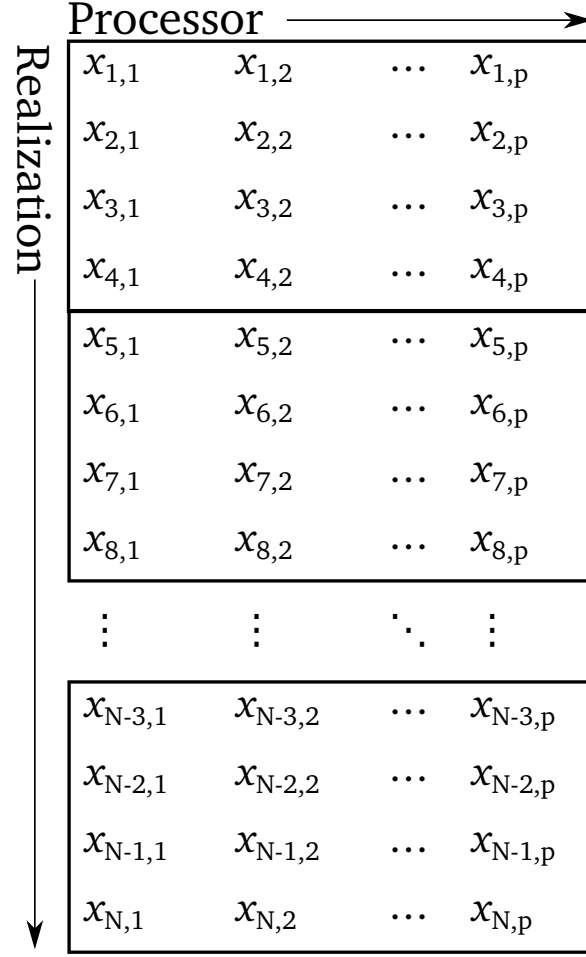


Figure 4-2: Summation of tally scores across processors when doing statistics based on a single batch with $M = 4$.

The sample mean and its variance for this random variable would then be

$$\bar{z} = \frac{1}{N'p} \sum_{j=1}^{N'} \sum_{k=1}^p z_{j,k} \quad (4.7)$$

$$s_z^2 = \frac{1}{N'p - 1} \left[\frac{\sum_{j=1}^{N'} \sum_{k=1}^p z_{j,k}^2}{N'p} - \left(\frac{\sum_{j=1}^{N'} \sum_{k=1}^p z_{j,k}}{N'p} \right)^2 \right] \quad (4.8)$$

with N' defined the same as before. In this scheme, only one reduction needs to be performed at the very end of the simulation. The data requirement is then $16\ell(p-1)$ bytes since we need to take the summation of the accumulated score and accumulated squares of scores for each tally bin. Thus, the total data that we need to communicate

Algorithm 4-2: Pseudocode for reducing tally scores across multiple processors when doing statistics based on batches consisting of multiple fission generations.

```

for  $i = 1 \rightarrow N'$  do                                ▷ Loop over batches
   $x_{i,\ell} \leftarrow 0$ 
  for  $j = 1 \rightarrow M$  do                                ▷ Loop over generations
    for  $k = 1 \rightarrow N_p$  do                                ▷ Loop over particles
      while alive do
        Move to next collision
         $x_{i,\ell} \leftarrow x_{i,\ell} + \text{score}$ 
      end while
    end for
  end for
  MPI_Reduce( $x_{i,\ell}, x_i, \dots$ )                                ▷ Communication
   $s_1 \leftarrow s_1 + x_i$                                 ▷ Accumulate running sums
   $s_2 \leftarrow s_2 + x_i^2$ 
end for
 $\bar{x} \leftarrow \frac{s_1}{N'}$                                 ▷ Use running sums to calculate statistics
 $s_{\bar{x}}^2 \leftarrow \frac{1}{N'-1} \left[ \frac{s_2}{N'} - \left( \frac{s_1}{N'} \right)^2 \right]$ 

```

has been reduced by a factor of

$$\frac{8\ell N(p-1)}{16\ell(p-1)} = \frac{N}{2} \quad (4.9)$$

For large N , as is typical in a Monte Carlo calculation, the reduction in data communication requirements may significantly improve the parallel efficiency.

4.3 Results

To test the efficacy of the proposed method, the ability to perform statistics based on batches, either across processors or on individual processors, was implemented in the OpenMC Monte Carlo code. A model of the Monte Carlo Performance Benchmark [14] was then simulated without (Case 1) and with (Case 2) the proposed method on a Linux cluster using eight nodes, each with two quad-core Intel Xeon E5620 processors for a total of 64 cores. In both cases, the neutron production rate was tallied over a 289 x 289 x 100 mesh for a total of 8,352,100 tally bins. Each case was run with 640,000 particles

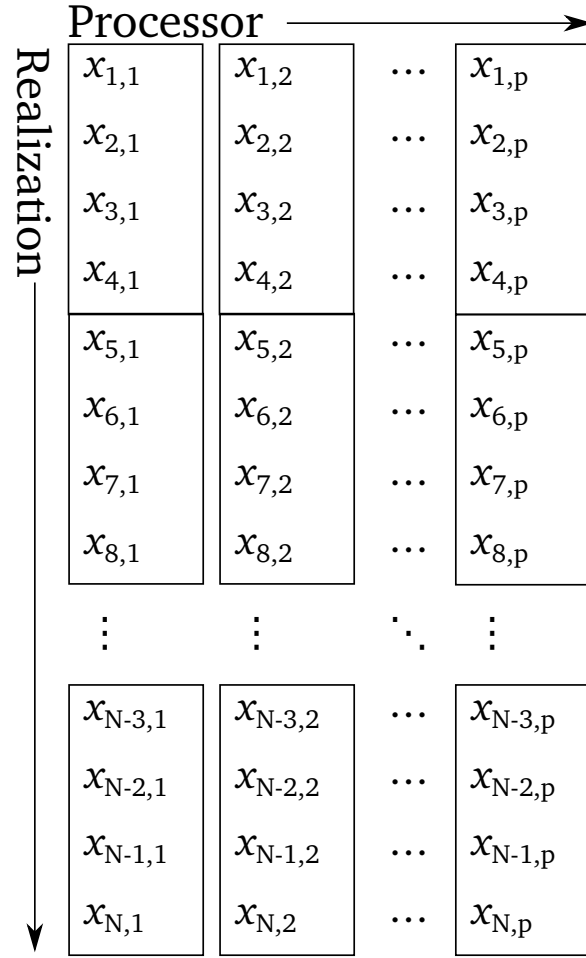


Figure 4-3: Summation of tally scores across processors when doing statistics based on a batch combining realizations from a single processor with $M = 4$.

per generation with 150 inactive batches and 150 active batches². For the neutron cross sections and $S(\alpha, \beta)$ tables, ENDF/B-VII.0 data was used. Table 4.1 shows the elapsed wall-clock times for these two cases. We see that not taking the summation of the tallies across processors at every generation results in a significant reduction in elapsed time. Most importantly, the time spent accumulating tallies was reduced by over 90%. The gross reduction in simulation time will depend on many factors including simulation parameters (e.g. how many particles are run per generation) as well as the specific hardware for the system being used (e.g. network latency and bandwidth).

Figure 4-4 and Figure 4-5 show the CPU usage and network communication, respectively, as reported by the Ganglia Monitoring System. On Figure 4-4, no pause is

²One generation per batch was used for both cases.

Algorithm 4-3: Pseudocode for reducing tally scores across multiple processors when doing statistics based on batches combining realizations from a single processor.

```

for  $i = 1 \rightarrow N'$  do                                ▷ Loop over batches
   $x_{i,\ell} \leftarrow 0$ 
  for  $j = 1 \rightarrow M$  do                                ▷ Loop over generations
    for  $k = 1 \rightarrow N_p$  do                                ▷ Loop over particles
      while alive do
        Move to next collision
         $x_{i,\ell} \leftarrow x_{i,\ell} + \text{score}$ 
      end while
    end for
  end for
   $s_{1,\ell} \leftarrow s_{1,\ell} + x_{i,\ell}$                                 ▷ Accumulate running sums
   $s_{2,\ell} \leftarrow s_{2,\ell} + x_{i,\ell}^2$ 
end for
MPI_Reduce( $s_{1,\ell}, s_1, \dots$ )                                ▷ Communication
MPI_Reduce( $s_{2,\ell}, s_2, \dots$ )                                ▷ Communication
 $\bar{x} \leftarrow \frac{s_1}{N'}$                                 ▷ Use running sums to calculate statistics
 $s_{\bar{x}}^2 \leftarrow \frac{1}{N'-1} \left[ \frac{s_2}{N'} - \left( \frac{s_1}{N'} \right)^2 \right]$ 

```

Table 4.1: Elapsed wall-clock time for Monte Carlo Performance Benchmark with 8,352,100 tally bins.

| Variable | Case 1 | Case 2 |
|---------------------------|----------|---------|
| Total simulation time | 1268.7 s | 953.8 s |
| Time in inactive batches | 425.3 s | 426.2 s |
| Time in active batches | 843.4 s | 527.6 s |
| Time accumulating tallies | 348.8 s | 30.4 s |

observed between cases 1 and 2 as they were run back-to-back. The case 2 run began at 9:29.

One can see from these figures that during the second simulation, where reductions on tallies were not performed until the end of the simulation, the network usage was drastically lower than when reductions were performed at every generation. Lastly, we remark that all reported sample means of the tally variables were identical and nearly all variances were within two standard deviations of one another.

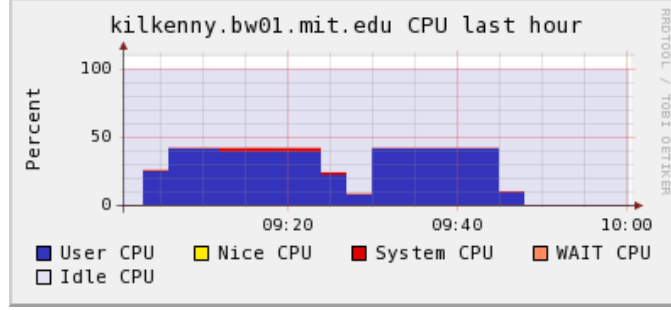


Figure 4-4: Percentage CPU usage of entire cluster during two simulations of the Monte Carlo Performance Benchmark.

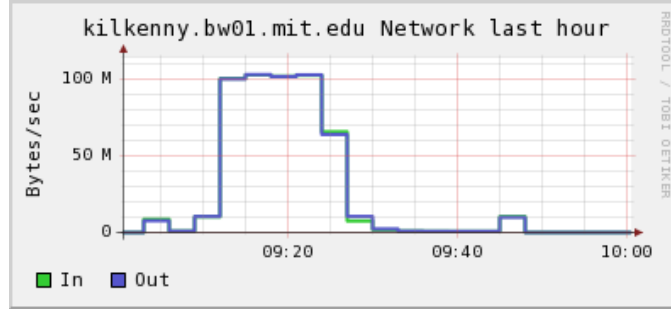


Figure 4-5: Network bandwidth during two simulations of the Monte Carlo Performance Benchmark.

4.4 Conclusions

A novel scheme for reducing data communication requirements in parallel Monte Carlo calculations has been introduced here primarily aimed at criticality calculations. In a large-scale simulation with thousands of processors, it is natural to consider the batch to be the accumulation of scores from one processor over the entire run ($M = N$). Provided each processor did a sufficient amount of work to obtain reasonable statistics, the estimate of the variance of the sample mean will be reliable since one would have p realizations of the random variable.

One concern that might arise from the use of this technique is that the variance of the sample mean will not be reproducible when running in parallel, i.e. the variance of the sample mean will not be the same as if one had run the exact same calculation in serial. However, the *expected value* of the sample variance will be the same and the sample mean will be reproduced to within floating point error. For users who are willing to sacrifice reproducibility of tally variances, this detriment is far outweighed by the

overwhelming benefit of drastically reduced network communication and improved parallel efficiency.

It should be noted that this method does require that the sum and sum of squares over realizations for each tally bin be stored in memory on each processor. Strictly speaking, the traditional methods only require storing a temporary variable on each slave processor to accumulate scores that would be sent to the master, i.e. the sum and sum of squares for each tally bin need to be stored only on the master process. However, some, if not many, Monte Carlo codes do not take advantage of this fact and simply replicate all tally data in the memory of each process.

As a final note, even when this method is used, it may still be desirable to perform a reduction over some global tallies such as the eigenvalue. If the eigenvalue is not reduced at each generation, each process would have a different estimate of the eigenvalue; therefore the average number of fission sites produced at each collision would differ from a serial run. To preserve reproducibility of the sample means of local tallies, it is thus necessary to reduce the eigenvalue at each generation. The parallel communication necessary to perform a parallel reduction of global tallies such as the eigenvalue will be very small since it is generally limited to only a few quantities.

Chapter 5

Domain Decomposition

5.1 Background

To this point, we have described methods which will drastically improve scalability for calculations utilizing thousands or millions of processors. With these methods, it is possible to effectively utilize leadership class supercomputers for Monte Carlo calculations — but there is one caveat. The simulations would still be forced to rely on parallelism over particles, meaning that all problem data such as cross sections, tallies, and material compositions must be replicated on every process. As we began discussing in chapter 1, data for temperature-dependent cross sections in LWR simulations may reach upwards of hundreds of gigabytes, and tallies can easily exceed terabytes of memory. In order to reduce per-node memory requirements, two strategies have been proposed: domain decomposition and data decomposition. In this chapter, we will focus on the analysis of domain decomposition for LWR analysis using Monte Carlo.

In many, if not most, areas of computational physics, spatial domain decomposition is the most natural and desirable method for achieving parallelism. Each subdomain is assigned to a different processor, and thus each processor needs only to work on its subdomain. This makes sense when the work in the problem is proportional to, and evenly distributed over, the size of the problem. This is true of most mesh-based methods such as finite difference, finite element, etc. Monte Carlo particle transport, on the other hand, does not possess this characteristic. The computational effort in a Monte Carlo

simulation is in transporting the particles; as a result, the work is unpredictable and not guaranteed to be evenly distributed across a problem. Moreover, fast-streaming particles can cross the entire problem. Thus, the use of spatial domain decomposition for Monte Carlo particle transport can suffer from poor load balancing and overhead from network communication required for transferring particles between subdomains.

5.1.1 Review of Prior Work

The use of domain decomposition to reduce per-node memory in Monte Carlo particle transport simulations was first proposed by Alme et al. in 2001 [88]. A slight variation on normal domain decomposition was also suggested — instead of just decomposing the geometry, subdomains could also be replicated. The motivation for this is so that areas of the problem that have a higher particle density, and hence more work, have proportionally more processors dedicated to them.

Domain decomposition was subsequently implemented in a production Monte Carlo code, Mercury, being developed by Lawrence Livermore National Laboratory [89]. A load balancing scheme similar to that proposed by Alme et al. was also implemented in Mercury whereby the assignment of processors to domains is periodically adjusted based on the actual work distribution [90]. The initial implementation worked only with mesh-bashed geometries where the connectivity between regions could be readily determined. This was later expanded to constructive solid geometries; the algorithms used for this were described in [91].

Domain decomposition has also been applied to Monte Carlo simulation of thermal radiation transport [92]. In that work, Brunner et al. focused on message-passing semantics for domain decomposition schemes, i.e. how to best communicate particles between processors. This work was later expanded to include situations where the number of particles in a given transport sweep was not known *a priori* [93]. However, in both of those papers, it is explicitly assumed that the problem is perfectly load balanced, and no solutions are presented for problems that exhibit poor load balancing.

Finally, domain decomposition is also being implemented in a new Monte Carlo

code, Shift, under development at Oak Ridge National Laboratory [94]. The domain decomposition algorithm described by Brunner [93] was chosen with the added ability to have overlapping domains to reduce the incidence of particles crossing subdomain boundaries and hence reduce the overall network communication.

5.1.2 Recent Developments

While the study and application of domain decomposition to Monte Carlo particle transport simulations now has a ten year history, including the implementation in two major Monte Carlo codes, there is surprisingly little theoretical analysis of domain decomposition schemes. In all the papers we've reviewed thus far [88, 90, 91, 92, 93], arguments about the efficacy of domain decomposition were made based on measurements in either simple or actual codes. This is good from the perspective that no assumptions are needed to draw conclusions; however, the downside is that it is hard to gain an understanding of why or why not domain decomposition would work in a given problem. In particular, the prior work does not reveal whether domain decomposed Monte Carlo simulations could be successfully employed for realistic LWR analysis because the test problems were not LWR models.

Recognizing the lack of a theoretical foundation with which domain decomposition algorithms could be analyzed, Siegel et al. published a study in 2012 [95] where they attempted to quantify the communication costs in order to assess the feasibility of carrying out efficient domain decomposition in a parameter regime relevant to LWR analysis. Key scaling regimes were identified and performance estimates were carried out over a range of characteristic parameters. The results demonstrated that for their chosen model problem, good performance could be attained for reasonable effective latency and bandwidth values with partition particle densities as low as 10^4 per node¹. This analysis represents an important step toward quantifying the key theoretical issues and helped to establish the feasibility of carrying out robust LWR calculations with Monte Carlo methods.

¹The testing platform in [95] was the Blue Gene/P supercomputer at Argonne National Laboratory.

That being said, the analysis in [95] does not address the impact of initial particle imbalances and small variations in local leakage rates on evolving particle distributions. If particle communication costs are potentially manageable in light of typical machine bandwidths and latencies, to what extent will load imbalances negatively impact performance to the point where such an approach is no longer a practical alternative? Establishing a quantitative foundation for this performance penalty will greatly facilitate weighing tradeoffs in deciding the best path forward among various approaches for next-generation Monte Carlo codes. In this chapter, this issue is addressed directly by attempting to quantify the effect of particle load imbalances on the performance of domain decomposed Monte Carlo algorithms.

In section 5.2, an expression for the communication penalty from load imbalances is derived from theoretical considerations. However, the starting assumption is that leakage rates are spatially constant and therefore the expression only accounts for load imbalances due to the initial particle distribution. In a Monte Carlo simulation, the stochastic nature of the solution will result in spatially varying leakage rates. This is explicitly accounted for in section 5.3; the resulting expression appears similar to that derived in section 5.2 but with an extra factor accounting for the variable leakage rates. Finally, in section 5.4, measured data from simulations of the Monte Carlo performance benchmark using OpenMC are used to evaluate the load imbalance penalty for various domain sizes.

The analysis and results from this chapter are derived from a paper accepted for publication in *Journal of Computational Physics* [96].

5.2 Analysis

5.2.1 Problem definition

To fully define the problem, let us begin with a domain X segmented into N non-overlapping partitions $X = \cup x_j, j = 1, \dots, N$. In a light-water reactor, these partitions might be chosen for convenience to be a full fuel assembly or some part of an assembly.

If we denote the initial number of particles on partition x_j as $p_{0,j}$, then the initial global particle count P_0 is given by:

$$P_0 = \sum_{j=1}^N p_{0,j}. \quad (5.1)$$

For simplicity, assume that each partition is mapped to a single process in a three-dimensional virtual Cartesian topology of N processes. As in chapter 3, we are assuming a one-to-one mapping of processes to processors, and thus we use the terms *processor*, *partition*, and *process* interchangeably.

On a given partition, particles local to that partition are advanced through a sequence of interactions until they are either 1) absorbed² or 2) reach a processor boundary. For optimal performance particles that reach the boundary are buffered locally until all particle trajectories are computed, and are subsequently exchanged with neighboring processors. We refer to the particle exchange phase of this process as a *stage*, and to a complete set of stages (i.e. until all particles are absorbed) as a *generation*. At the end of each generation, the fission source is updated and the next generation begins.

Define the particle *local leakage* λ on each x_j for a given stage i as

$$\lambda_{i,j} = \frac{\text{number of particles leaving } x_j \text{ at stage } i}{\text{number of particles starting in } x_j \text{ at stage } i}.$$

The goal of this analysis is to estimate the impact of initial particle load imbalances and spatially varying local leakage values on previous performance estimates of domain-decomposed LWR simulations. We refer to the perfectly load balanced, constant leakage scenario as the *ideal* case. This was explored in depth in [95], where it was shown that communication costs imposed a reasonable penalty on overall simulation time for a broad range of relevant parameter values.

Following [97] we first define the *load balance* Γ_i at each stage i as

$$\Gamma_i = \frac{\bar{P}_i}{P_i^{max}}, \quad (5.2)$$

²In a non-analog simulation, particles can also be killed from Russian roulette or other variance reduction techniques.

where

$$\bar{p}_i = \frac{1}{N} \sum_{j=1}^N p_{i,j}$$

and p_i^{max} denotes the maximum particle count on a partition at stage i . The amount the load balance Γ_i differs from the ideal case $\Gamma = 1$ measures the relative difference between the highest particle and average particle counts:

$$1 - \Gamma_i = \frac{p_i^{max} - \bar{p}_i}{p_i^{max}}. \quad (5.3)$$

Note that unlike [97] we express the load imbalance in terms of particle densities rather than execution time. Their equivalence will be argued in the following section.

We seek to estimate a related but distinct quantity — an upper bound for the relative difference between the total simulation time per generation of the non-ideal case and the ideal case. We define this relative difference as the *load imbalance penalty* Δ :

$$\Delta = \frac{\tau' - \tau}{\tau} = \frac{\tau'}{\tau} - 1, \quad (5.4)$$

where τ denotes the total simulation time per generation in the ideal case, and τ' for the non-ideal case. Note that an expression for Δ must include both the particle tracking as well as the communication costs across all stages of a given generation. While related to the per-stage particle load balance, the load imbalance penalty is a distinct quantity.

5.2.2 Basic properties

Given this simple problem definition above, and assuming that leakage at the problem boundary is negligible (a good approximation for power reactors), the *global* number of particles at any *stage* is given by

$$P_{i+1} = \sum_{j=1}^N p_{i+1,j} = \sum_{j=1}^N \lambda_{i,j} p_{i,j} \quad i = 0, 1, \dots, M-1 \quad (5.5)$$

where M denotes the final stage in the generation — i.e. when all particles are absorbed and none remain. We emphasize again that P_i denotes the global particle count at stage i while $p_{i,j}$ denotes the local particle count on partition j at stage i .

To estimate τ' , the per-generation simulation time in the non-ideal case, we seek an expression for the *local* particle distribution — i.e. the number of particles on each partition x_j at stage i . Assuming the leakage is equal on all surfaces, the neutron count on a partition is given by:

$$p_{i+1,j} = \frac{1}{6} (\lambda_{i,j1} p_{i,j1} + \lambda_{i,j2} p_{i,j2} + \cdots + \lambda_{i,j6} p_{i,j6}) \quad (5.6)$$

where $j1, j2, \dots, j6$ denote the six immediate neighbors of partition j on a Cartesian lattice. Equation (5.6) simply states that, in advancing stages, a given partition receives 1/6th of the leaked particles from each of its six neighbors on a Cartesian grid.

Equation (5.6) shows that the evolution of the local particle distribution depends on the detailed alignment of the local particle counts and the local leakage rates. To reduce it further requires additional assumptions. We start by noting that, in an LWR, the neutron spectrum and material heterogeneities are roughly constant from partition to partition (this property is demonstrated using simulation data in section 5.4). This observation makes the case of approximately spatially uniform local leakages of great practical interest in the present context, and thus we initially consider the case of $\lambda_{i,j} = \lambda_i$. Note that we still expect non-trivial per-stage variation in leakages as neutron energies will shift toward the thermal range with increasing stages. Important model corrections for small spatial variations in λ will be considered in section 5.3.

For spatially constant λ , (5.5) then becomes

$$\begin{aligned} P_i &= \sum_{j=1}^N \lambda_{i-1} p_{i-1,j} = \lambda_{i-1} \sum_{j=1}^N p_{i-1,j} = \lambda_{i-1} P_{i-1} \\ &= \lambda_{i-1} \lambda_{i-2} \cdots \lambda_0 P_0 \\ &\approx \langle \lambda \rangle^i P_0 \quad i = 1, 2, \dots, M \end{aligned} \quad (5.7)$$

where $\langle \lambda \rangle$ is defined as the geometric mean of the leakage rate,

$$\langle \lambda \rangle = \sqrt[M]{\lambda_{M-1} \lambda_{M-2} \cdots \lambda_0}. \quad (5.8)$$

Equation (5.6) then simplifies to

$$p_{i+i,j} = \frac{\lambda_i}{6} (p_{i,j1} + p_{i,j2} + \cdots + p_{i,j6}) \quad (5.9)$$

Equation (5.9) shows that, for spatially constant λ , at each subsequent stage each partition has the average value of the total leaked particles from the neighboring partitions in the previous stage. Equation (5.7) shows that, in the case of constant λ , the particle load imbalance does not affect the number of stages required to complete a generation, which can be estimated by setting $P_i = 1$ in (5.7):

$$\langle \lambda \rangle^M P_0 = 1 \implies M \approx -\frac{\log P_0}{\log \langle \lambda \rangle}. \quad (5.10)$$

Both properties are used in the analysis that follows.

5.2.3 Expression for τ

Given these basic properties, we first seek an estimate of the total per-generation cost in the idealized case of an initial even distribution of particles and spatially constant λ . This is accomplished by decomposing τ into a local work τ_l and inter-process communication τ_c component as

$$\tau = \tau_l + \tau_c. \quad (5.11)$$

In the case of perfect load balancing and assuming a roughly equal distribution of track length and neutron spectra across partitions (i.e. our earlier assumption of constant λ), the local work τ_l should be roughly proportional to the total number of particles tracked on a partition in a given generation,

$$\tau_l \approx \mu \sum_{i=0}^M \bar{P}_i, \quad (5.12)$$

where the constant μ is a measure of the tracking time per particle, and where it is understood that the particle count $p_{i,j}$ is the same on any given partition, since all partitions are equivalent in the ideal case.

The communication time τ_c can be further decomposed into a latency and bandwidth component [95]. For each generation, a total of M messages need to be sent to each processor's six neighbors, so in general the total time per generation due to message latency can be modeled as proportional to $6\alpha M$, where α is some measure of the effective application-level latency for a single send.

If we ignore the dependence of λ on stage, by definition $\lambda\bar{P}_i$ particles are sent from each processor at stage i , and the total number of particles sent in a generation from any processor is $\lambda\sum_i\bar{P}_i$. Thus, the bandwidth term can be roughly modeled as $\beta\lambda\sum_i\bar{P}_i$, where β denotes the effective inverse bandwidth for nearest-neighbor exchanges (expressed in time per particle).

When we account for stage dependence λ is replaced by $\|\lambda\|$, defined as the solution to the M th order polynomial:

$$\sum_{i=1}^M \|\lambda\|^i = \lambda_0 + \lambda_1\lambda_0 + \cdots + \lambda_{M-1}\lambda_{M-2}\cdots\lambda_0. \quad (5.13)$$

The bandwidth term can then be written as:

$$\begin{aligned} \beta \sum_{i=0}^{M-1} \lambda_i \bar{P}_i &= \beta(\lambda_0 \bar{P}_0 + \lambda_1 \bar{P}_1 + \cdots + \lambda_{M-1} \bar{P}_{M-1}) \\ &= \beta(\lambda_0 \bar{P}_0 + \lambda_1 \lambda_0 \bar{P}_0 + \cdots + \lambda_{M-1} \lambda_{M-2} \cdots \lambda_0 \bar{P}_0) \\ &= \beta \bar{P}_0 (\lambda_0 + \lambda_1 \lambda_0 + \cdots + \lambda_{M-1} \lambda_{M-2} \cdots \lambda_0) \\ &= \beta \bar{P}_0 \sum_{i=1}^M \|\lambda\|^i. \end{aligned} \quad (5.14)$$

Using these relations together with (5.10) then yields the following expression for the total communication time:

$$\tau_c = -6\alpha \frac{\log P_0}{\log \langle \lambda \rangle} + \beta \bar{P}_0 \sum_{i=1}^M \|\lambda\|^i. \quad (5.15)$$

Using the same approach on (5.12) and combining with (5.15) gives the final expression for total simulation time in the idealized case:

$$\begin{aligned}\tau &= -6\alpha \frac{\log P_0}{\log \langle \lambda \rangle} + \mu \bar{P}_0 \sum_{i=0}^M \|\lambda\|^i + \beta \bar{P}_0 \sum_{i=1}^M \|\lambda\|^i \\ &= -6\alpha \frac{\log P_0}{\log \langle \lambda \rangle} + \left(\mu \sum_{i=0}^M \|\lambda\|^i + \beta \sum_{i=1}^M \|\lambda\|^i \right) \bar{P}_0.\end{aligned}\quad (5.16)$$

5.2.4 Expression for τ'

We now seek an estimate for the total simulation time τ' in the presence of an initial load imbalance. For convenience we first express $p_{i,j}$ as a combination of partition mean and fluctuating parts. That is,

$$\delta p_{i,j} = p_{i,j} - \bar{P}_i. \quad (5.17)$$

When a load imbalance is present the partition with the largest particle count controls the total performance cost. If we denote the particle count on this process as $p_i^{max} = \bar{P}_i + \delta p_i^{max}$, then by the same logic as in the previous section, the load-imbalanced performance is:

$$\tau' = -6\alpha \frac{\log P_0}{\log \langle \lambda \rangle} + \mu \sum_{i=0}^M p_i^{max} + \beta \sum_{i=0}^{M-1} \lambda_i p_i^{max}. \quad (5.18)$$

While we cannot directly evaluate the sum of p_i^{max} , a simple upper bound can be derived by recognizing that, assuming roughly equal leakage to each neighbor, the largest possible value of p at stage $i+1$ occurs if all six neighbors of a partition contain p_i^{max} particles. Thus,

$$p_{i+1}^{max} \leq \lambda_i p_i^{max}. \quad (5.19)$$

This implies that

$$\begin{aligned}\sum_{i=0}^M p_i^{max} &\leq \mu (p_0^{max} + \lambda_0 p_0^{max} + \lambda_1 \lambda_0 p_0^{max} + \cdots + \lambda_{M-1} \lambda_{M-2} \cdots \lambda_0 p_0^{max}) \\ &= \mu p_0^{max} (1 + \lambda_0 + \lambda_1 \lambda_0 + \cdots + \lambda_{M-1} \lambda_{M-2} \cdots \lambda_0) \\ &= \mu p_0^{max} \sum_{i=0}^M \|\lambda\|^i\end{aligned}\quad (5.20)$$

and

$$\begin{aligned}
\sum_{i=0}^{M-1} \lambda_i p_i^{max} &\leq \mu (\lambda_0 p_0^{max} + \lambda_1 p_1^{max} + \cdots + \lambda_{M-1} p_{M-1}^{max}) \\
&= \mu (\lambda_0 p_0^{max} + \lambda_1 \lambda_0 p_0^{max} + \cdots + \lambda_{M-1} \lambda_{M-2} \cdots \lambda_0 p_0^{max}) \\
&= \mu p_0^{max} (\lambda_0 + \lambda_1 \lambda_0 + \cdots + \lambda_{M-1} \lambda_{M-2} \cdots \lambda_0) \\
&= \mu p_0^{max} \sum_{i=1}^M \|\lambda\|^i.
\end{aligned} \tag{5.21}$$

Substituting (5.20) and (5.21) into (5.18), we obtain

$$\begin{aligned}
\tau' &= -6\alpha \frac{\log P_0}{\log \langle \lambda \rangle} + \mu p_0^{max} \sum_{i=0}^M \|\lambda\|^i + \beta p_0^{max} \sum_{i=1}^M \|\lambda\|^i \\
&= -6\alpha \frac{\log P_0}{\log \langle \lambda \rangle} + \left(\mu \sum_{i=0}^M \|\lambda\|^i + \beta \sum_{i=1}^M \|\lambda\|^i \right) p_0^{max}.
\end{aligned} \tag{5.22}$$

With expressions for τ and τ' , we can now proceed to estimate the load imbalance penalty.

5.2.5 Expression for Δ

Using (5.4), (5.16), and (5.22) and noting that $p_0^{max} = \bar{P}_0 + \delta p_0^{max}$, we get the following expression for Δ :

$$\Delta = \frac{\left(\mu \sum_{i=0}^M \|\lambda\|^i + \beta \sum_{i=1}^M \|\lambda\|^i \right) \delta p_0^{max}}{-6\alpha \frac{\log P_0}{\log \langle \lambda \rangle} + \left(\mu \sum_{i=0}^M \|\lambda\|^i + \beta \sum_{i=1}^M \|\lambda\|^i \right) \bar{P}_0}. \tag{5.23}$$

We can simplify (5.23) slightly by dividing each term by the expression in parentheses, i.e.

$$\Delta = \frac{\delta p_0^{max}}{-6\alpha \frac{\log P_0}{\log \langle \lambda \rangle} \left(\mu \sum_{i=0}^M \|\lambda\|^i + \beta \sum_{i=1}^M \|\lambda\|^i \right)^{-1} + \bar{P}_0}. \tag{5.24}$$

The first term in the denominator of (5.24) measures the importance of latency relative to bandwidth and tracking timescales, which is presumed to be small for typical problem sizes and parameter regimes (e.g. see [95]) but which is retained here for the sake of generality. Note that (5.24) implies that

$$\Delta \leq \frac{\delta p_0^{max}}{\overline{p_0}} = \frac{1}{\Gamma_0} - 1, \quad (5.25)$$

which should be a good approximation for applications where the latency term is much smaller than the bandwidth and tracking terms. We see, then, that assuming spatially constant λ and given isotropic neutron local leakage and constant mean tracking rates per partition, we can establish an upper bound for Δ entirely in terms of the initial particle configuration.

5.3 Variable leakage rates

Equation (5.24) should give a reasonable estimate for reactor applications across a range of parameter values, where material inhomogeneities are roughly equally distributed and thus local leakage rates show very little variation. However, it fails to capture a critical effect that emerges as we move to smaller partition sizes, and which sets an important limit on the utility of the domain-decomposed approach. To see this we explicitly account for spatially variant, non-constant leakage in the formulation of the model.

Consider a distribution of leakage rates across partitions at a given stage with a maximum value defined as:

$$\lambda_i^{max} = \max \{ \lambda_{i,j} : 1 \leq j \leq N \}. \quad (5.26)$$

In estimating the computation time for this scenario compared to the ideal case (i.e. calculating Δ), the question arises of what corresponding spatially constant value of λ should be used for the ideal case. Several options are reasonable, but here we choose a mean value that preserves stages. Specifically, if we define a particle-weighted mean

leakage as:

$$\bar{\lambda}_i = \frac{\sum_{j=1}^N p_{i,j} \lambda_{i,j}}{P_i} \quad (5.27)$$

then the ideal and non-ideal cases are guaranteed to have the same number of global particles at successive stages:

$$\frac{P_{i+1}}{P_i} = \frac{1}{P_i} \sum_{j=1}^N \lambda_{i,j} p_{i,j} = \bar{\lambda}_i.$$

Thus, the performance for the ideal case with variable leakage rates is now

$$\begin{aligned} \tau &= -6\alpha \frac{\log P_0}{\log \langle \bar{\lambda} \rangle} + \mu \sum_{i=0}^M \bar{P}_i + \beta \sum_{i=0}^{M-1} \bar{\lambda}_i \bar{P}_i \\ &= -6\alpha \frac{\log P_0}{\log \langle \bar{\lambda} \rangle} + \left(\mu \sum_{i=0}^M \|\bar{\lambda}\|^i + \beta \sum_{i=1}^M \|\bar{\lambda}\|^i \right) \bar{P}_0 \end{aligned} \quad (5.28)$$

where $\langle \bar{\lambda} \rangle$ is the geometric mean (over stages) of the particle-weighted mean leakage at each stage, i.e.

$$\langle \bar{\lambda} \rangle = \sqrt[M]{\bar{\lambda}_{M-1} \bar{\lambda}_{M-2} \cdots \bar{\lambda}_0}.$$

and $\|\bar{\lambda}\|$ is defined analogous to (5.13):

$$\sum_{i=1}^M \|\bar{\lambda}\|^i = \bar{\lambda}_0 + \bar{\lambda}_1 \bar{\lambda}_0 + \cdots + \bar{\lambda}_{M-1} \bar{\lambda}_{M-2} \cdots \bar{\lambda}_0.$$

Following (5.19), then, the largest possible particle count at stage i occurs on partition x_j if on its six neighbors p_i^{max} coincides with λ_i^{max} . That is,

$$p_{i+1}^{max} \leq \lambda_i^{max} p_i^{max}. \quad (5.29)$$

This implies that

$$\tau' \leq -6\alpha \frac{\log P_0}{\log \langle \bar{\lambda} \rangle} + \mu \sum_{i=0}^M p_i^{max} + \beta \sum_{i=0}^M \lambda_i^{max} p_i^{max}.$$

Following the same logic as in (5.20), (5.21), and (5.22) we can derive an upper bound

for τ' in the case of variable λ :

$$\tau' \leq -6\alpha \frac{\log P_0}{\log \langle \bar{\lambda} \rangle} + \left(\mu \sum_{i=0}^M \|\lambda^{max}\|^i + \beta \sum_{i=1}^M \|\lambda^{max}\|^i \right) P_0^{max} \quad (5.30)$$

where $\|\lambda^{max}\|$ is defined as

$$\sum_{i=1}^M \|\lambda^{max}\|^i = \lambda_0^{max} + \lambda_1^{max} \lambda_0^{max} + \dots + \lambda_{M-1}^{max} \lambda_{M-2}^{max} \dots \lambda_0^{max}.$$

We can then use (5.28) and (5.30) to obtain the following upper bound for the load imbalance:

$$\Delta \leq \frac{-6\alpha \frac{\log P_0}{\log \langle \bar{\lambda} \rangle} + \left(\mu \sum_{i=0}^M \|\lambda^{max}\|^i + \beta \sum_{i=1}^M \|\lambda^{max}\|^i \right) P_0^{max}}{-6\alpha \frac{\log P_0}{\log \langle \bar{\lambda} \rangle} + \left(\mu \sum_{i=0}^M \|\bar{\lambda}\|^i + \beta \sum_{i=1}^M \|\bar{\lambda}\|^i \right) \bar{P}_0} - 1. \quad (5.31)$$

Again, taking the very reasonable assumption (see e.g. [95]) that the latency term is small relative to the sum of the bandwidth and tracking terms, we can establish a more intuitive upper bound:

$$\Delta \leq \frac{C}{\Gamma_0} - 1. \quad (5.32)$$

where we have defined the factor C as

$$C = \frac{\mu \sum_{i=0}^M \|\lambda^{max}\|^i + \beta \sum_{i=1}^M \|\lambda^{max}\|^i}{\mu \sum_{i=0}^M \|\bar{\lambda}\|^i + \beta \sum_{i=1}^M \|\bar{\lambda}\|^i}. \quad (5.33)$$

One can interpret this as follows — accounting for variable leakage rates has introduced a “correction factor” relative to (5.25); clearly, when $\|\bar{\lambda}\| = \|\lambda^{max}\|$, (5.32) reduces to

(5.25). Further simplification can be made to (5.33) by writing

$$C = \frac{\mu + \beta \frac{\sum_{i=1}^M \|\lambda^{max}\|^i}{\sum_{i=0}^M \|\lambda^{max}\|^i}}{\mu + \beta \frac{\sum_{i=1}^M \|\bar{\lambda}\|^i}{\sum_{i=0}^M \|\bar{\lambda}\|^i}} \frac{\sum_{i=0}^M \|\lambda^{max}\|^i}{\sum_{i=0}^M \|\bar{\lambda}\|^i} \quad (5.34)$$

and subsequently using the approximation

$$\sum_{i=1}^M x^i \approx x \sum_{i=0}^M x_i \quad (5.35)$$

which should hold for large M . Applying (5.35) to $\|\lambda^{max}\|$ and $\|\bar{\lambda}\|$ in (5.34) yields

$$C \approx \frac{\mu + \beta \|\lambda^{max}\|}{\mu + \beta \|\bar{\lambda}\|} \frac{\sum_{i=0}^M \|\lambda^{max}\|^i}{\sum_{i=0}^M \|\bar{\lambda}\|^i}. \quad (5.36)$$

The greater the spatial variation in leakage rates the more the system bandwidth and neutron tracking rates factor into the performance. The implications of these formulas are explained in the simple tests below, where we aim to estimate C as a function of the main problem parameters.

5.4 Evaluation of model

For a given initial particle configuration, evaluation of the model equation (5.31) requires estimates for the particle tracking rate μ , the application-level inverse bandwidth β and latency α , and the local leakage rate estimates from which to compute $\|\lambda^{max}\|$ and $\|\bar{\lambda}\|$. These parameters vary widely by both machine and specific code application. Here we evaluate these terms in a parameter regime relevant to LWR physics on modern supercomputers. Other applications and machine architectures can be evaluated with appropriate values of these parameters.

5.4.1 Leakage rates

While best-estimate application-level bandwidth and latency terms can be estimated from standard benchmarks (e.g. [98]), the leakage rate terms in (5.31) are more difficult to approximate. Simplified models, such as the Wigner rational approximation [99] provide rough estimates of expected domain-dependent leakage rates, but do a poor job at estimating stage dependence. Thus, to be as precise as possible we measure these values directly using an existing Monte Carlo particle transport code — OpenMC [21]. Note that, though parallel, OpenMC does not employ domain decomposition. To model partitions and stages, we overlay within OpenMC an imaginary grid decomposition and effectively measure the behavior of particles between fictional stages during a generation. The resulting particle loads and number of stages should be identical to a truly domain decomposed code using an identical computational grid.

The specific test executed was based on the Monte Carlo Performance benchmark [14] using 0.5 billion active particle histories. Leakage rates at each stage and within each partition were measured for three cases: a single assembly, quarter-assembly, and ninth-assembly partition overlay using 20, 40, and 60 axial levels, respectively. In each case, the benchmark model was simulated on a 19-node Intel Xeon dual core cluster with 1 million neutrons per generation for 150 inactive and 500 active generations. For neutron cross sections, data from ENDF/B-VII.0 was used.

Figure 5-1 illustrates the scale and level of variation in local leakage rates for the full, quarter, and one-ninth assembly cases. The plots shown are for the axial level nearest the middle of the core at stage zero. They represent “typical” leakage rate distributions and are intended to graphically illustrate their relative lack of spatial coherency and small range of values. Also, it is evident from the figure that, as expected, leakage rates increase non-trivially with decreasing partition size. To see this more clearly, Figure 5-2 shows the stage-dependent mean and standard deviation (error bar overlay) of λ for each simulation. In each case, we see the clear trend that as neutrons thermalize (undergo successive collisions), the leakage rates decrease corresponding to a shorter mean free path. Furthermore, the superposed standard deviations indicate extremely

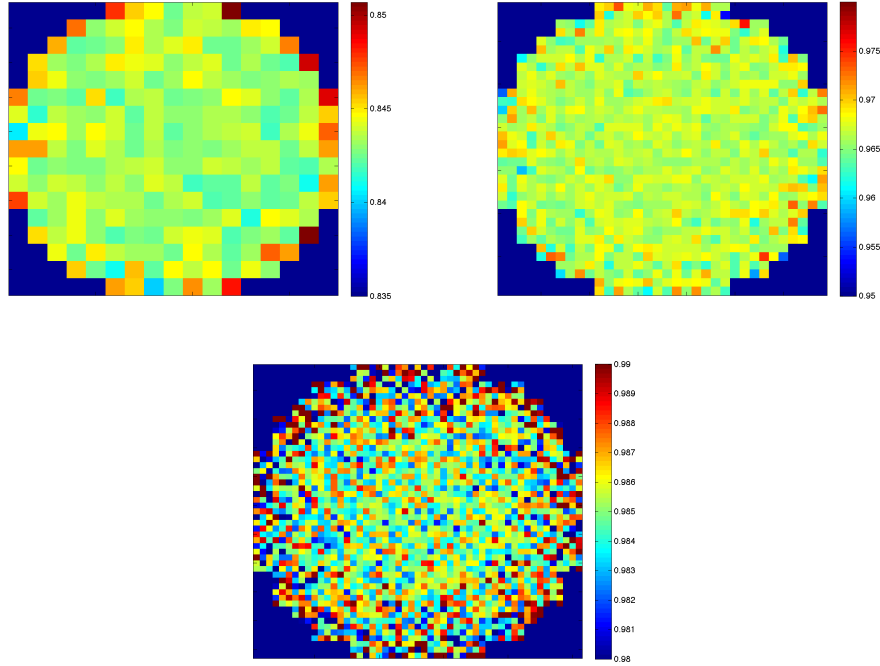


Figure 5-1: Leakage rate distributions for the full, quarter, and ninth assembly experiments.

small spatial variation in the first several stages, which accounts for the majority of data movement and performance cost. When particle counts are small in later stages statistical variations result in larger standard deviation values, but their impact on total performance is expected to be small. We note that this very small spatial variation hints that the correction factor for variable λ in (5.33) may be small. This is evaluated in the next section.

We next test the predictions for total number of stages M per generation given by (5.10), i.e.

$$M = -\frac{\log P_0}{\log \langle \bar{\lambda} \rangle}. \quad (5.37)$$

The values of the $\langle \bar{\lambda} \rangle$ were calculated for each of the three experiments and inserted into (5.37). Table 5.1 compares these results with those obtained directly from the simulation. The model formula behaves as expected, differing by only several percent from the measured data. Exact correspondence is not expected — statistical fluctuations, slight anisotropies and other minor effects are likely to yield small variations. For

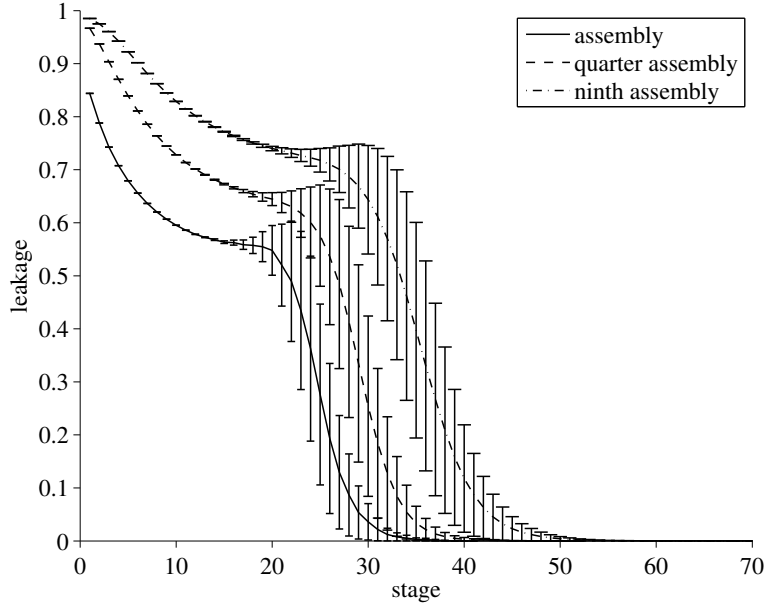


Figure 5-2: Average values of leakage rate λ at each stage for the full, quarter, and ninth assembly experiments.

practical purposes though the current estimate is more than adequate.

Table 5.1: The number of stages M for the three numerical experiments vs. the value predicted by (5.37).

| Experiment | M (data) | M (model) |
|------------------|------------|-------------|
| Full assembly | 41 | 39 |
| Quarter assembly | 52 | 51 |
| Ninth assembly | 71 | 70 |

It is furthermore instructive to test the fidelity of (5.29) to the true measure maximum particle counts at each stage. While (5.29) is a true statement, in a practical sense it is of questionable value if it over-predicts p_i^{max} by too significant a margin. Figure 5-3 shows the computed value of p_i^{max} for each stage versus the value predicted by (5.29). Given that leakage rate variation is very small spatially, it is not surprising to see that (5.29) works extremely well as an upper bound, over-predicting the measured value by less than 1.0% for the initial stages (which account for the bulk of the particle transfers).

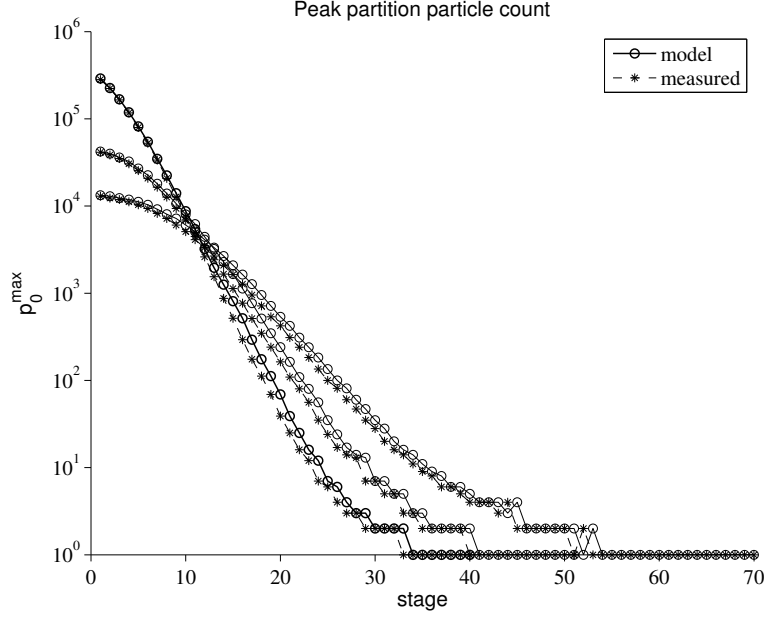


Figure 5-3: Computed values of p^{max} for each stage versus the value predicted by (5.29).

5.4.2 Evaluation of correction factor C and penalty Δ

Given an initial particle configuration and reasonable estimates for leakage, it remains to evaluate C in (5.33). To reiterate, under the assumption of spatially constant leakage C is unity and the load imbalance penalty can be upper bounded by the initial particle configuration as $\frac{p_0^{max}}{p_0}$. When leakage rates vary spatially C measures the amplification of the performance penalty. We estimate C in two steps, first evaluating the contribution of the bandwidth and tracking times, given by the first term in (5.36):

$$\frac{\mu + \beta ||\lambda^{max}||}{\mu + \beta ||\bar{\lambda}||} = \frac{1 + \frac{\beta}{\mu} ||\lambda^{max}||}{1 + \frac{\beta}{\mu} ||\bar{\lambda}||}. \quad (5.38)$$

Note that for any conventional machine $\beta \ll \mu$, reflecting that tracking rates are much slower than inter-processor communication, and since $||\bar{\lambda}|| \sim ||\lambda^{max}||$, (5.38) remains very close to unity and contributes negligibly to the overall load imbalance. This demonstrates the important fact that for all practical purposes the system bandwidth and latency have very little effect on the load imbalance penalty, which is determined almost entirely by the physics of neutron transport as expressed by the local leakage

rates.

The second contribution of C is the second term in (5.36):

$$\frac{\sum_{i=0}^M \|\lambda^{max}\|^i}{\sum_{i=0}^M \|\bar{\lambda}\|^i}.$$

Note that unlike (5.38) this term becomes problematic as the processor grid is refined, since we intuitively expect maximum leakage rates of unity for sufficiently small domains. Assuming that this is the case, the numerator is upper bounded by $1 + M$. If the average value does not approach unity, the Taylor series approximation should be a good approximation and we can rewrite this expression as:

$$\frac{\sum_{i=0}^M \|\lambda^{max}\|^i}{\sum_{i=0}^M \|\bar{\lambda}\|^i} \leq (1 + M)(1 - \|\bar{\lambda}\|).$$

While this term is likely a modest fraction of the total number of stages, we must recall that M , the number of stages itself, increases rapidly with decreasing partition size, and even a small fraction could easily significantly amplify the load imbalance.

To explore this in greater depth requires use of the OpenMC simulation results. Table 5.2 shows the results, including the model predictions for the load imbalance penalty for the full, quarter, and ninth assembly experiments. In the evaluation of the various terms, we used the values $\beta = 10^{-8}$ s/particle and tracking time $\mu = 5 \times 10^{-4}$ s/particle. Note that, within the precision presented, the bandwidth term (second column) is identical in all cases, a manifestation of the fact that bandwidths are much higher than tracking rates. In all cases, the initial particle configuration and thus $\frac{p_0^{max}}{P_0}$ is shown to be roughly independent of partition size as one would expect.

Equation (5.32) states that, with no load rebalancing, a simulation with this initial particle distribution is expected to take at most $C \frac{p_0^{max}}{P_0}$ as long as a perfectly load balanced simulation. For the full assembly simulation $C = 1.13$ and the total penalty is 3.67, which could in many contexts be considered reasonable compared to, for example, the cost and complexity of implementing repartitioning algorithms. Moreover, this is expected to be increasingly true as we move toward HPC architectures where off-chip

Table 5.2: Values of Δ and the various terms which contribute to it for each of the three numerical experiments using the Monte Carlo performance benchmark.

| Experiment | $\frac{\mu + \beta \ \lambda^{max}\ }{\mu + \beta \ \bar{\lambda}\ }$ | $\frac{\sum_{i=0}^M \ \lambda^{max}\ ^i}{\sum_{i=0}^M \ \bar{\lambda}\ ^i}$ | C | $\frac{p_0^{max}}{\bar{p}_0}$ | Δ |
|------------------|---|---|------|-------------------------------|----------|
| Full assembly | 1.00 | 1.13 | 1.13 | 3.24 | 3.67 |
| Quarter assembly | 1.00 | 2.58 | 2.58 | 3.28 | 8.47 |
| Ninth assembly | 1.00 | 6.98 | 6.98 | 3.45 | 24.15 |

data movement becomes much more expensive than local operations. However, it is clear that the situation rapidly deteriorates for decreasing partition size, with a value of $C = 6.98$ for the ninth assembly experiments. This corresponds to a load imbalance penalty of 24.15, which for most contexts is likely unacceptably high. It is clear what has happened both in the model and the physics — in the one-ninth assembly case the peak leakage is unity for all but the final stage, and thus the summation in the numerator of C approaches M . Note that we expect the performance to degenerate even further with decreasing partition size since M is expected to increase according to (5.10).

5.5 Conclusions

We have developed simple relationships to quantitatively analyze the impact of load imbalances on the performance of non-overlapping domain decomposed Monte Carlo methods in the context of reactor analysis. These techniques provide a quantitative framework to estimate the additional performance costs incurred by typical load imbalances in reactor applications. While the methodologies presented here are generalizable to a broader range of problems, many of the conclusions are intended to apply specifically to the case of steady state analysis of power reactors.

Our analyses showed that, perhaps contrary to initial intuition, over reasonable parameter ranges the machine characteristics (bandwidth and latency) had very little impact on resulting load imbalances. The dominant effect was expressed as an amplification factor whose value grew rapidly with decreasing partition size, and which we could roughly estimate using results from a non-domain-decomposed code.

Preliminary results of these analyses were presented for a classic reactor benchmark, indicating that load imbalances were modest for assembly-size partitions, but increased dramatically as partition sizes were decreased beyond that point. This indicates that domain decomposition is likely a reasonable strategy for modest-size parallelism but that it is inherently limited when we consider the massive levels of concurrency on the path to exascale computing (at least without significant repartitioning, which is likely to be increasingly expensive on future architectures).

For the reactor benchmark analyzed, the lack of enrichment zoning across the core led to a factor of about three penalty due to non-uniform particle densities. This penalty would be lower for an actual reactor configuration wherein the natural power distribution (and hence the particle distribution) is flatter. At any rate, the load imbalance due to non-uniform particle densities, i.e. $\frac{P_0^{max}}{P_0}$, can largely be eliminated by a method that forces the particle distribution to be approximately uniform such as the uniform fission site method [19]. However, the load imbalance due to non-uniform leakage cannot easily be circumvented; the use of overlapping domains may reduce C somewhat, but at the expense of further algorithmic complexity in scoring tallies.

To get a sense of how large C might be for an actual reactor simulation, we must determine the minimum number of domains necessary based on memory constraints. In subsection 1.5.3, it was estimated that a high-fidelity simulation of the MIT PWR benchmark would require 11 TB of tallies. If we assume that on a large supercomputer, we have 2 GB of memory available per core, then the tally memory must be divided over at least 5500 domains. This corresponds to a domain size somewhere between the full-assembly and quarter-assembly cases discussed, and hence C should be smaller than 2.5. Based on these considerations alone, domain-decomposed simulations of full core reactor problems may be feasible with acceptable load imbalance penalties.

In addition to judging whether these penalties are large or small in an absolute sense, the techniques presented allow one to weigh tradeoffs between domain decomposition and more sophisticated data decomposition strategies for their specific needs, or perhaps to estimate the cost of carrying out load re-balancing or other re-tracking techniques within an operational production code. When processing power is cheap and memory is

at a premium, performance penalties less than an order of magnitude are not necessarily large. Performance models that go beyond the purely speculative are a critical component of assessing the best path forward.

Chapter 6

Data Decomposition

6.1 Background

It has been mentioned several times already in this thesis, but it bears reminding the reader once again — one of the imminent challenges for Monte Carlo, as well as deterministic, methods is coping with limited amounts of memory. While the availability of great amounts of processing power might otherwise enable us to perform simulations with remarkable fidelity, the memory requirements for such simulations will often exceed that available. For a high-fidelity realistic LWR simulation, tally data alone will likely require terabytes of memory (see discussion in subsection 1.5.3). This problem is exacerbated by the fact that current parallel methods still generally rely on each program instance storing the full geometry, interaction cross sections, and tally data in memory.

There is of course good reason to use full memory replication — each process can simulate particles independently¹ of one another and the tally results can be collected at the end of the simulations. However, it is clear that some method for avoiding replication of cross section and tally data must be an essential component in any strategy to simulate reactor models with Monte Carlo. Two algorithms have been proposed in the literature that do offer the potential to avoid replication and furthermore decompose tally data across many processors: domain decomposition and data decomposition.

¹This is strictly only true in a fixed source calculation. In an eigenvalue calculation, there is a dependency between fission source iterations.

In chapter 5, we presented a theoretical analysis of domain decomposed Monte Carlo particle transport simulations looking at the effect of load imbalances on the total simulation time. The analysis demonstrated that load imbalances in domain decomposed simulations arise from two different phenomena: non-uniform particle densities and non-uniform spatial leakage. It's important to draw attention to the fact that even if we assumed zero latency and zero inverse bandwidth (i.e. an infinitely fast network), the load imbalance penalty does not disappear — it is a physical artifact. In this chapter, we now draw our attention to an algorithm which avoids load balancing issues by keeping individual particles local to a single process while explicitly decomposing the tally data.

6.1.1 Data decomposition

While a considerable amount of work and analysis has been carried out on domain decomposition, very little work has focused on data decomposition to-date. The basic concept of data decomposition is that a disjoint subset of the processes in a simulation act as *servers*, sending and/or receiving data to *compute processes* as needed². In its most general form, the data could be geometry, cross sections, and/or tallies. The compute processes handle the actual transport of particles from birth to death and communicate with the servers as needed. Thus, we see that data decomposition does have some similarities to domain decomposition in the sense that the compute processes are still tracking particles independently of one another. However, particles are never transferred from one process to another.

The potential for data decomposition to alleviate per-node memory restrictions had been identified by Brown and Martin as early as 2004 [100], but to-date it appears not to have been demonstrated or even analyzed. Some early scoping work was done to investigate whether remote memory access would be suitable for data decomposition algorithms [101]. However, these preliminary works focused more on decomposing geometry and cross section data. In this paper, we take a first look at an algorithm designed not to decompose geometry or cross section data but rather to decompose

²It is not absolutely necessary to have the servers and compute processes be mutually exclusive, but for the sake of simplicity we will consider them to be disjoint in the current work.

large tally data.

We note that the data decomposition method can generally be considered to be a partitioned global address space (PGAS) programming model. While PGAS models have been discussed widely within the computer science community, there have not yet been many practical applications using PGAS techniques or languages. A paper being presented at the IEEE International Conference on High Performance Computing, however, looks at the use of a partitioned global address space model for quantum Monte Carlo simulations [102].

The analysis and results in this chapter are included in a paper submitted for publication in *Journal of Computational Physics* [103].

6.1.2 Tally Server Algorithm

During a Monte Carlo simulation, estimates of physical parameters are made by keeping running sums of scores from events such as collisions or particle tracks. These running sums are referred to as *tallies*. The theory and implementation of tallies was discussed at length in section 2.7. The simplicity of tally incrementing makes it amenable to an atomic fetch-and-add operation (whether this be a CPU instruction or a remote direct memory access operation). Normally, tallies are stored in local memory. Synchronization between processors is typically performed only after simulating a predetermined number of particles, referred to as a *batch*. However, since tally data is not needed for determining the random walk of a particle, it can be stored remotely. For the sake of simplicity, we will look at an algorithm where the tally data is stored in the address space of a process whose sole purpose is to receive scores from other processes and increment the tallies accordingly. These processes are called *tally servers* by analog to a classic client-server architecture.

In the tally server data decomposition algorithm, we start with a set of p processes that are divided into c compute processes and s tally servers. Each of the compute processes is assigned a set of particles that it will track, one at a time. Within a single particle history, some events will cause scores to be tallied. However, instead of determining a

local memory location to increment for each score, a list of scores of size d bytes is sent to a tally server. Since all tally accumulation is performed on the server, the compute processes do not need to store the tallies in memory (other than meta-data describing the tally).

To be more explicit on the data requirements, it helps to recall the notion of *filters* and *scoring functions*, which were discussed in subsection 2.7.1. To summarize, a filter refers to a criterion that limits what events can score to a given tally. The filter criteria generally concern the properties of a particle. For example, a filter criterion could be that a particle has a collision within a defined mesh cell, or that a particle's energy is within a defined range. The scoring functions are the actual physical quantities to be tallied, such as flux, reaction rates, currents, etc. If an event satisfies all filter criteria for a tally, a *tally bin* for each scoring function would be incremented by an estimate of the scoring function. Thus, a single event can increment more than just a single location in memory. As an example, a tally could specify that the reaction rate for each of 300 nuclides should be determined. In such a case, each scoring event would have to increment 300 tally bins. We see that we will have d bytes where $d \geq 8$ (the size of one double-precision float) since a single scoring event may need to score to hundreds of scoring functions. The message sent to a server at a scoring event consists of the scores for each scoring function.

Each process that has been designated as a server does not track any particles but instead continuously receives data from the compute processes and increments the appropriate tally bins. The server implementation could use one-sided operations (remote memory access) or regular point-to-point communication by running a continuous receive loop. The entire tally data can be divided in any arbitrary manner. In practice, assigning sequential blocks of the tally data to each server should be sufficient. This could be equivalent to dividing the tallies by spatial region as in domain decomposition since the tally data itself can be arranged by spatial region. Note again that in this algorithm, the tally servers only need to store a subset of the tally data; they do not need to store geometry or cross section data since it is only needed for particle tracking and interactions.

6.2 Analysis

6.2.1 Derivation of performance model

Let us now develop a model for estimating the performance of a simulation using tally servers relative to a simulation where no tally servers are used. As defined earlier, p is the total number of processes, c is the number of compute processes, and s is the number of servers. It is assumed that there is a one-to-one correspondence between processes and processor cores, so we may interchangeably refer to compute processes or compute processors. We shall also define t_0 and t as the expected amount of time to simulate N particles on p processes without and with tally servers respectively. The goal of the following analysis will be to relate t to t_0 through a number of representative parameters. We will treat two cases separately: using blocking point-to-point communication and using non-blocking point-to-point communication.

6.2.1.1 Blocking Communication

When sending data to tally servers using blocking communication, we can divide t into two components: the time to simulate particles, t_c , and the time to send messages to servers, t_s . Note that for the purposes of this analysis, we shall ignore all other communication including synchronization of global tallies and the fission bank. The amount of communication associated with these aspects of the algorithm will not differ appreciably whether or not tally servers are used.

The actual time to simulate any given particle will vary widely based on the random walk of each particle; some particles will have many more collisions and tracks than others. We can assume that the time to simulate a particle is given by a distribution with a known mean μ . This parameter will be influenced by hardware and software characteristics such as the processor, the cache and memory hierarchy, compiler optimizations, etc. While it is generally difficult to predict μ *a priori*, it is straightforward to measure it with an actual simulation. Once μ is known, the expected time to complete a batch of N particles is $N\mu$. Without tally servers, we can assume perfect parallel scaling within a

single batch [21] such that

$$t_0 = \frac{N\mu}{p}. \quad (6.1)$$

The time to simulate N particles using the tally server algorithm is generally expected to be larger than that without tally servers for two reasons: 1) there are fewer processors available to simulate particles (i.e. $c < p$), and 2) communicating tally data to the servers will incur overhead. The expected time to simulate the N particles over c compute processes is

$$t_c = \frac{N\mu}{c}. \quad (6.2)$$

The overhead of tally communication is strongly dependent on the performance of the network interconnect. Let us assume that the time to send a message with d bytes of data between a compute process and a server is given by $\alpha + d\beta$, where α is the communication latency and β is the inverse bandwidth. We are implicitly assuming that the latency and bandwidth are uniform regardless of which compute process and server are communicating. This is obviously not strictly true since the communication time will depend on the relative distance between processors in the network topology as well as network contention. However, for the sake of analysis we can assume some gross average application-level latency and bandwidth to develop an intuition for the performance of the tally server model. At the software level, the effective application-level latency can in general depend on the message size³. For our analysis, we assume no such dependency as it would be both software and platform dependent. As we will see later, the cases of most practical interest are naturally bandwidth-dominated and thus the assumptions regarding latency are of minimal consequence.

Having knowledge of the network latency and bandwidth allows us to determine the tally server communication per scoring event. We also need to know how many scoring events occur per particle in order to determine the tally server overhead. Let us call f

³For example, MPI implementations generally use different protocols for “small” messages and “large” messages.

the expected number of scoring events per particle. This parameter will depend mostly on what filter criteria are applied to a tally. By definition, $f(\alpha + d\beta)$ is the expected tally server communication time for one particle. If each compute process is simulating N/c particles, then the expected communication time is

$$t_s = \frac{fN}{c}(\alpha + d\beta). \quad (6.3)$$

Combining (6.2) and (6.3), the expected time to simulate N particles using the tally server algorithm can be expressed as

$$t = t_c + t_s = \frac{N\mu}{c} + \frac{fN}{c}(\alpha + d\beta). \quad (6.4)$$

We can now divide (6.4) by (6.1) to obtain a relationship between t and t_0 :

$$\frac{t}{t_0} = \frac{p}{c} + \frac{pf}{c\mu}(\alpha + d\beta). \quad (6.5)$$

The first term on the right hand side of (6.5) represents the loss in efficiency due to the fact that not all p processes are available to simulate particles. The second term in (6.5) represents the loss in efficiency due to the need to send messages at every scoring event. One can see that the performance of the tally server algorithm will depend on many parameters. Three of these parameters are constant for a given computer architecture: the number of particles simulated per second and the network latency and bandwidth. The other two parameters, d and f , are application dependent. A detailed discussion of the choice of d and f is given below.

It is desirable to further develop equation (6.5) to eliminate the dependence on p and c . Ideally, one would want as few servers as possible to maximize the number of compute processes available. However, we need to have at least enough servers to ensure that messages can be received continuously, i.e. that no single server is inundated with messages. This can be stated mathematically by saying that the amount of time each server spends receiving messages is less than or equal to the expected time for the compute processes to finishing simulating particles. Since the total time receiving messages is ct_s , we have that

$$\frac{ct_s}{s} \leq t_c + t_s. \quad (6.6)$$

Combining (6.2), (6.3), and (6.6) and solving for c/s , we can obtain a rough estimate for an upper bound on the number of compute processes that can be supported by one server, which we call the *support ratio*:

$$\frac{c}{s} \leq \frac{\mu}{f(\alpha + d\beta)} + 1 \quad (6.7)$$

By substituting $s = p - c$ in (6.7) and rearranging terms, we obtain an estimate for the minimum value of p/c :

$$\frac{p}{c} = \frac{1 + \frac{2f}{\mu}(\alpha + d\beta)}{1 + \frac{f}{\mu}(\alpha + d\beta)}. \quad (6.8)$$

Substituting (6.8) into (6.5), we see that

$$\frac{t}{t_0} = 1 + \frac{2f}{\mu}(\alpha + d\beta). \quad (6.9)$$

Finally, we can define the overhead due to tally servers, Δ as the difference in times relative to t_0 .

$$\Delta_{\text{blocking}} = \frac{t - t_0}{t_0} = \frac{2f}{\mu}(\alpha + d\beta). \quad (6.10)$$

6.2.1.2 Non-blocking communication

The derivation of an expression similar to (6.9) but for non-blocking communication follows the same general procedure. The expressions for t_c and t_s are the same as before but are applied slightly differently. On the compute processes, there is no longer any overhead from blocking communication. Thus, the time to complete a batch of N neutrons is the greater of the time to simulate the particles on the compute processes and the time to receive the messages on the servers, i.e.

$$t = \max\left(t_c, \frac{ct_c}{s}\right). \quad (6.11)$$

As noted earlier, the support ratio would be determined in such a manner that the time to receive messages on the servers does not exceed t_c . Thus, the time to complete the batch is simply $t = t_c$. Dividing (6.2) by (6.1), we can relate t to the expected time to complete a batch without tally servers using non-blocking communication:

$$\frac{t}{t_0} = \frac{p}{c}. \quad (6.12)$$

As opposed to blocking communication, the only loss of efficiency with non-blocking communication is due to using fewer compute processes. To relate (6.12) to the parameters in our model, we again impose the constraint that the amount of time each server spends receiving messages is less than or equal to the expected time for the compute processes to finishing simulating particles. This implies that

$$\frac{ct_s}{s} \leq t_c \quad (6.13)$$

Note the similarity of (6.13) to (6.6): the only difference is that the expected time to finish simulating the N particles does not include the time to send messages since non-blocking communication is used. Again, combining (6.2), (6.3), and (6.13) and solving for c/s , we obtain an upper bound on support ratio:

$$\frac{c}{s} \leq \frac{\mu}{f(\alpha + d\beta)}. \quad (6.14)$$

By substituting $s = p - c$ in (6.14) and rearranging terms, we obtain an estimate for the minimum value of p/c :

$$\frac{p}{c} = 1 + \frac{f}{\mu}(\alpha + d\beta). \quad (6.15)$$

Since $t/t_0 = p/c$, we have that

$$\frac{t}{t_0} = 1 + \frac{f}{\mu}(\alpha + d\beta). \quad (6.16)$$

Thus, the expected overhead from tally servers when using non-blocking communication is

$$\Delta_{\text{non-blocking}} = \frac{t - t_0}{t_0} = \frac{f}{\mu} (\alpha + d\beta). \quad (6.17)$$

It is interesting to note that $\Delta_{\text{blocking}} = 2\Delta_{\text{non-blocking}}$. This implies that while non-blocking communication is expected to reduce the overhead considerably, the behavior of the overhead with changes in the model parameters will still follow the same general trends whether blocking or non-blocking communication is used.

6.2.2 Performance predictions

In order to draw any further conclusions regarding the overhead based on (6.10) and (6.17), we must develop realistic estimates for the speed of the network interconnect (α and β), the calculational rate (μ), and the amount and frequency of data being tallied (d and f). For the network latency and bandwidth, our systems of interest are two modern supercomputers: the Blue Gene/P supercomputer (Intrepid) at Argonne National Laboratory (ANL) and the Cray XK7 supercomputer (Titan) at Oak Ridge National Laboratory (ORNL). For the purposes of estimating d and f , we will look at solving for reaction rate distributions within fuel pins in the Monte Carlo performance benchmark [14] using simulations with OpenMC. The calculational rate will depend both on the computer architecture as well as the specific model chosen.

The Intrepid supercomputer has 40 Blue Gene/P racks with 1024 nodes each. In turn, each node has a quad-core PowerPC 450 processor and 2 GB of memory. Results from the HPC Challenge benchmark have shown that the average ping-pong message latency on Blue Gene/P is about 3.53 microseconds and the average ping-pong bandwidth is 0.3852 GB/s [104]. Thus, we can infer that $\alpha = 3.53 \cdot 10^{-6} \text{ s}$ and $\beta = 2.60 \cdot 10^{-9} \text{ s/byte}$ for the Intrepid Blue Gene/P supercomputer. For the Monte Carlo Performance Benchmark modified to use 320 nuclides in the fuel, our tests using OpenMC show that Blue Gene/P can simulate about 76 particles per second on each processor, i.e. $\mu = 0.0132 \text{ s/particle}$. We have chosen to use 320 nuclides in the fuel as this is the maximum number of nuclides available in the ENDF/B-VII.0 cross section library used in the simulation.

The Titan supercomputer has 18,688 Cray XK7 compute nodes, each of which has a

16-core AMD Opteron 6274 processor with 32 GB of memory and a nVidia Tesla K20 GPU. The Cray XK7 uses the Cray Gemini interconnect which has lower latency and higher bandwidth than the interconnect on the Blue Gene/P. Unfortunately, reliable performance measurements for the Cray Gemini interconnect are hard to come by. Preliminary measurements indicate an MPI latency of about 1.5 microseconds and a peak user data injection bandwidth of about 6 GB/s [105]. We will conservatively estimate the latency as $\alpha = 2.0 \cdot 10^{-6}$ s and the inverse bandwidth as $\beta = 2.5 \cdot 10^{-10}$ s/byte. Performing a simulation of the Monte Carlo performance benchmark on the Cray XK7 as described before gives us a particle tracking rate of $1/\mu = 140$.

Let us briefly discuss what values are appropriate to use for f , the number of events per particle. For the purpose of LWR core analysis, we are mostly interested in integrated fluxes and reaction rates in the fuel and thus can ignore all events in the cladding, water, and elsewhere. For the Monte Carlo performance benchmark which has a fuel pin diameter of 0.82 cm, each particle has on average 5.7 collisions in fuel and 21.3 tracks in fuel⁴. As a point of reference, each particle has about 26 collisions and 132 tracks during its lifetime⁵. Thus, the cases of most practical interest would be using a collision estimator to accumulate scores only in the fuel ($f = 5.7$) and using a track-length estimator to accumulate scores only in the fuel ($f = 21.3$). To obtain an upper bound on d , a good reference point is a depletion calculation where six reaction rates are needed for each of the 320 nuclides in the fuel. In this bounding case, a compute process would need to send $6 \cdot 320 \cdot 8 \text{ bytes} = 15.36 \text{ kilobytes}$ at each event.

To summarize the preceding considerations, Table 6.1 shows the parameter space for both the Intrepid and Titan supercomputers. Using these parameters, we can evaluate the expected overhead incurred due to sending data to the tally servers based on (6.10) and (6.17). Figure 6-1 shows the estimated tally server overhead as a function of f and d for the Intrepid supercomputer. Based on our performance model, one can see that the communication will be latency-dominated for small d and bandwidth-dominated for large d . Our upper bound of 15.36 kilobytes is clearly in the bandwidth-dominated

⁴If a fuel pin is subdivided into multiple regions for performing depletion analysis, the number of tracks would increase. We will assume no subdivision in the present work.

⁵These figures were obtained using no survival biasing techniques.

region. Figure 6-2 shows the estimated overhead as a function of f and d for the Titan supercomputer. For $f = 21.3$ and $d = 15360$, the model predicts an overhead of 14.0 and 3.5 percent of the total running time for the Intrepid Blue Gene/P and Titan Cray XK7 supercomputers, respectively, when using blocking communication. If non-blocking communication is used, the overhead is expected to be less than 10 percent on Intrepid as well.

Table 6.1: Parameters used for tally server overhead models in (6.10) and (6.17).

| Parameter | Description | Intrepid | Titan |
|-----------|----------------------------|----------------------|---------------------|
| α | Network Latency (s) | $3.53 \cdot 10^{-6}$ | $1.5 \cdot 10^{-6}$ |
| β | Network Bandwidth (s/byte) | $2.60 \cdot 10^{-9}$ | $1.0 \cdot 10^{-9}$ |
| $1/\mu$ | Particles/second | 76 | 140 |
| d | Data/event (bytes) | 0 – 15,360 | 0 – 15,360 |
| f | Events/particle | 0 – 132 | 0 – 132 |

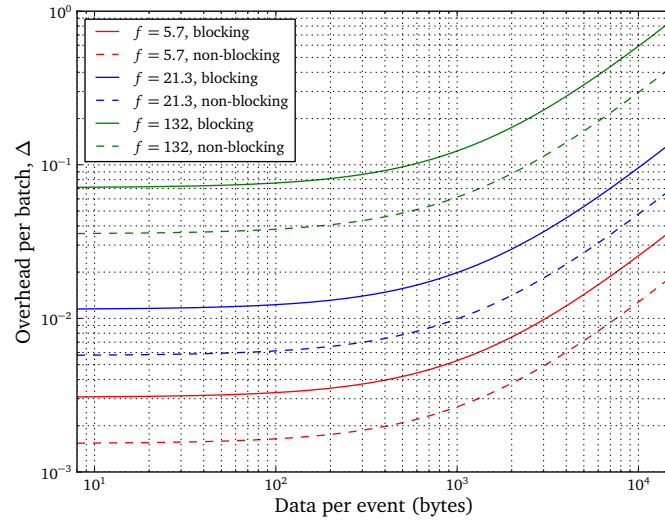


Figure 6-1: Estimated tally server overhead for Intrepid Blue Gene/P supercomputer based on (6.10) and (6.17).

We can also use equation (6.7) to identify the number of compute processors that can be supported by one server when using blocking communication. For our worst case of $f = 21.3$ and $d = 15360$, the constraint implies that on the Intrepid supercomputer we would need one server for every 15 compute processors. On the Titan supercomputer,

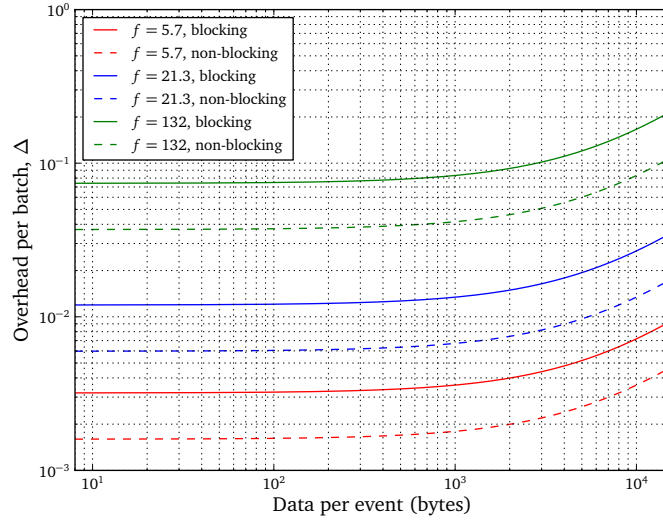


Figure 6-2: Estimated tally server overhead for Titan Cray XK7 supercomputer based on (6.10) and (6.17).

we would need one server for every 58 compute processors for the same values of f and d .

The predicted overhead due to tally servers based on the model in (6.10) and (6.17) is quite modest. In particular, over the range of parameter space that is of interest in LWR analysis, the overhead is generally less than 10% — a very small price to pay for the benefit of being able to have tallies of arbitrarily large size. The promising results based on the theory presented here warrant an actual implementation in a real Monte Carlo code. In section 6.3, we describe our implementation of this algorithm in the OpenMC Monte Carlo code. Actual test results using the implementation in OpenMC are presented in section 6.4. Before we discuss the implementation and results, however, we first discuss and analyze several considerations that may have an influence on the achievable performance.

6.2.3 Implications of total memory requirements

One may have noted in the derivation of the performance model that, even though the entire purpose of the algorithm is to allow for decomposition of the tally memory, nowhere was the total memory requirement for the tallies taken into account. In fact,

one of the alluring aspects of the tally server algorithm is that, in general, its performance does not depend on total amount of memory. However, we must be careful in interpreting such a statement too broadly as there are constraints on the memory.

The most obvious constraint is that the memory for each server must not exceed the available memory on a single node. Let M_t be the total memory required for tallies, M_s be the tally memory on each server, and M_n be the available memory on a node. This constraint implies that

$$M_s < M_n. \quad (6.18)$$

Another implicit assumption made in the course of the derivation was that the message being sent was small relative to the tally memory on each server. However, for a fixed tally size, the total tally memory on each server will be inversely proportional to the total number of processors (assuming a constant support ratio). Thus, as the total number of processors becomes very large, the total memory on each server could hypothetically become smaller than the message size for each scoring event. This situation would result in increased overhead as it would necessitate sending more messages. A reasonable constraint to impose is that the message size for each scoring event be smaller than the tally memory of each server:

$$d < M_s \quad (6.19)$$

In practice, even $d = M_s$ can cause problems since a single message can still overlap two servers. If we assume that the total memory required for tallies is divided evenly over the tally servers, then the constraints in (6.18) and (6.19) can be written in combined form as

$$d < \frac{M_t}{s} < M_n. \quad (6.20)$$

As we saw earlier, the upper limit on d for our cases of interest is 15,360. Let us suppose that the memory on a single node is $M_n = 32 \cdot 10^9$ bytes. If the total memory of the tallies is $M_t = 500 \cdot 10^9$ bytes, then (6.20) implies that

$$15.6 < s < 3.26 \cdot 10^6. \quad (6.21)$$

Thus, we must have at least 16 servers in order for the memory footprint of each to fit on a single node. This lower bound is quite easy to achieve even on a small cluster. For the upper bound, if we have more the 3.26 million servers, each server would have too little data compared to the size of a single message. At present, this limit puts no practical restrictions on our use of the algorithm.

The constraint in (6.20) can also tell us, given a total number of a tally servers, the range of total tally memory that can be reasonably accommodated. Let us suppose we wanted to perform a simulation using all nodes on the Mira Blue Gene/Q supercomputer at Argonne National Laboratory. This supercomputer has 48 racks each having 1024 nodes, each of which in turn has a 16 core processor for a total of 786,432 cores. Each node has $M_n = 16 \cdot 10^9$ bytes of memory. Assuming a support ratio of $c/s = 15$, we would need 49,152 servers. Thus, (6.20) implies that

$$755.0 \cdot 10^3 < M_t < 786.4 \cdot 10^{12}. \quad (6.22)$$

For any reasonable simulation, the total memory of the tallies will likely be somewhere between 755 kilobytes and 786 terabytes.

Admittedly, the foregoing analysis does not take into account the fact that tally servers will have to share the memory of a single node with compute processors. However, doing so would not change the overall conclusion that under normal circumstances, the memory requirements are not a formidable challenge to successfully employing the tally server algorithm.

6.2.4 Dependence of μ on d

To this point, we have assumed that μ is independent of all other parameters in our model. However, in most Monte Carlo transport codes, the rate at which particles are simulated depends on how much data needs to be tallied. Hence μ should really be a function of d , i.e. $\mu = \mu(d)$. In our case, d will vary according to how many nuclides

and scoring functions are being tallied. For every nuclide reaction rate that needs to be tallied, it is necessary to either calculate or look up a nuclide microscopic cross section at the time of tallying. As a result, μ will depend linearly on d . If μ_0 is the calculational rate with no tallies and μ_1 is the average time to process tally scores per byte, then we have that

$$\mu(d) = \mu_0 + d\mu_1 \quad (6.23)$$

Substituting $\mu(d)$ for μ in (6.16), the tally server overhead using non-blocking communication would then be

$$\Delta_{\text{non-blocking}} = \frac{f}{\mu_0 + d\mu_1} (\alpha + d\beta). \quad (6.24)$$

We see that the tendency would be to lessen the overhead as d is increased relative to the overhead in (6.17). In the actual performance measurements discussed in section 6.4, this effect is accounted for explicitly by measuring μ over a range of d .

6.3 Implementation

6.3.1 Description of algorithm

The algorithm described in subsection 6.1.2 was implemented in OpenMC; only modest changes were required to the source code to implement the tally server algorithm. At initialization time, processes are divided into compute processes and servers based on user input. If p total processes and s servers are specified, then the processes whose MPI rank satisfies $i + 1 \bmod s/p = 0$ are assigned as servers. Each user-defined tally has an array of score objects whose length is the product of the number of filter bins multiplied by the number of scoring functions. All scoring bins from user-defined tallies are concatenated into one “global” tally score array which is then divided equally over the servers. Finally, a look-up table is constructed that relates indices in the global tally scores array to indices within the scores array for each user-defined tally. The look-up

table enables the compute processes to determine which server they need to send scores to.

The necessary changes to the actual tallying subroutines that are used during particle tracking follow directly from the discussion in subsection 6.1.2. As a summary, Algorithm 6-1 shows a pseudocode outlining the salient points of the tally server algorithm as implemented in OpenMC. There are a few important points to note regarding this algorithm. Firstly, the array of scores created when a scoring event occurs contains the scores for all specified scoring functions. This means that the receiving server will increment multiple tally scores from a single message. Also note that the servers must be informed of when a batch of particles (or the simulation) has been completed as the servers are now responsible for computing sums and sums of squares of the tally score bins in order to calculate variances. At the end of the simulation, the servers must collectively write the tally results to disk. This can be done efficiently using parallel I/O techniques such as MPI-IO or parallel HDF5.

6.3.2 Potential optimizations

6.3.2.1 Explicit buffering

In Algorithm 6-1, an array of scores is sent to a server at every single scoring event. If f in (6.10) or (6.17) is very large, this would clearly create a large overhead regardless of whether the communication would be latency- or bandwidth-dominated. One potential workaround for this situation would be to explicitly buffer messages before sending. Rather than sending a message at every scoring event, we could create a buffer array on the compute process for each server that is some factor η larger than the total number of scoring functions for a tally. When the buffer array is full, it would then be sent to the corresponding server. In this case, we have decreased f by a factor of η and increased d by the same factor. The predicted overhead using non-blocking communication would then be

$$\Delta_{\text{non-blocking}} = \frac{f}{\eta\mu} (\alpha + d\eta\beta) = \frac{f}{\mu} \left(\frac{\alpha}{\eta} + d\beta \right). \quad (6.25)$$

We see in (6.25) that the latency term has been reduced by a factor of η , but the band-

Algorithm 6-1: Pseudocode for tally server algorithm

```
if compute process then
  for  $i \leftarrow 1$  to  $M$  do
    for  $j \leftarrow 1$  to  $N/p$  do
      while Particle  $j$  is alive do
        Process next event
        if Event satisfies filter criteria then
          Create array for scores
          for all Scoring functions do
            Calculate score
            Add score to array
          end for
          Determine server destination
          Send array to server
        end if
      end while
    end for
    Send 'finished' message to server
  end for
else if server then
  loop
    Receive message
    if End of batch then
      Accumulate tally scores
    else if End of simulation then
      Accumulate tally scores
    exit loop
  else
    for Score  $i \leftarrow 1$  to  $d$  do
      Determine memory location  $j$  to increment
      Increment tally  $j$  with score  $i$ 
    end for
  end if
end loop
Write tally results to state point file
end if
```

width term is unchanged. Since the main case of interest (depletion of an LWR model) was shown to be in the bandwidth-dominated region for contemporary supercomputers, the extra effort of implementing explicit buffering did not seem to justify the performance benefit for cases that are latency-dominated. This is especially true given that, as we will see in section 6.4, the overhead for latency-dominated cases is extremely small. Explicit buffering could also hypothetically limit network contention by reducing the total number of messages, but this effect is hard to quantify.

6.3.2.2 Combining successive scoring events

A small variation on the explicit buffering concept described in the previous section is to combine successive scores that match the same filter criteria. Let us suppose that for a tally with scoring bins $b_i, i = 1, \dots, k$, we have n consecutive scoring events that match the same filter criteria. Let $x_{i,j}$ be the i th score for the j th event. In the basic algorithm, we send a message containing the values $x_{1,j}, x_{2,j}, \dots, x_{k,j}$ to a server for each scoring event. Then the server adds each score to the appropriate scoring bin $b_i \leftarrow b_i + x_{i,j} \forall i$. Rather than sending n messages and having the server accumulate each array of scores, the compute processes can combine consecutive scores and subsequently send the sum to a server to be accumulated. Each compute process would calculate $x'_i = \sum_j x_{i,j}$, and the server would accumulate $b_i \leftarrow b_i + x'_i$. This scheme effectively reduces the number of scoring events per particle, f .

To obtain a simple estimate of the potential reduction in f , let us consider the case of track-length tallies in the fuel region. Any time a particle scatters within the fuel region, it will result in two separate tracks. The tally scores from these separate tracks could be combined and sent to a server in one message. This implies that the effective number of scoring events, f' , is then

$$f' = \left(1 - \frac{\Sigma_s \phi}{\Sigma_t \phi}\right) f \quad (6.26)$$

where $\Sigma_s \phi$ is the scattering reaction rate in the fuel and $\Sigma_t \phi$ is the total reaction rate in the fuel. For the Monte Carlo performance benchmark $\Sigma_s \phi / \Sigma_t \phi = 0.23$, so f would be reduced about 23%.

6.3.2.3 Topologically-aware layouts

To maximize network bandwidth and minimize latency, the mapping of processes to processor cores could hypothetically be optimized based on the topology of the particular machine the algorithm is implemented on. We chose a naïve implementation that is unaware of topology to ensure portability across different architectures and to demonstrate that successful use of the algorithm does not require such optimizations.

6.4 Results

The performance model developed in section 6.2 is dependent on a variety of parameters. On any given computer, α , β , and μ are effectively constant. The remaining parameters can be manipulated by varying the definition of the tallies and the job parameters. Thus, to fully test the performance of the tally server implementation, a parameter study should be carried out by running a series of simulations varying the parameters p , s , f , and d .

One could argue that based on (6.17), it should not be necessary to include p , c , or s in the parameter study since the overhead does not explicitly depend on those parameters. However, (6.17) was derived assuming that the support ratio attains its maximum based on the inequality in (6.14). In practice, it's not possible to know *a priori* what the maximum attainable support ratio is and thus it is instructive to test this directly. While the performance depends on f in general, our primary interest is tally events in the fuel region. As a result, we performed a parameter study using the modified version of OpenMC varying p , c/s , and d only.

First, a number of “baseline” simulations of the Monte Carlo performance benchmark were run to determine how μ varies with increasing d , and hence how t_0 varies with increasing d . The baseline simulations were run without tally servers to capture only the increase in simulation time due to cross section look-ups for tallies. On both the Titan supercomputer, the baseline simulations were run with 16 processors with a total of 32,000 particles per batch. Ten batches were run both without tallies (referred to as *inactive batches*) and with tallies (*active batches*). These values were found to be

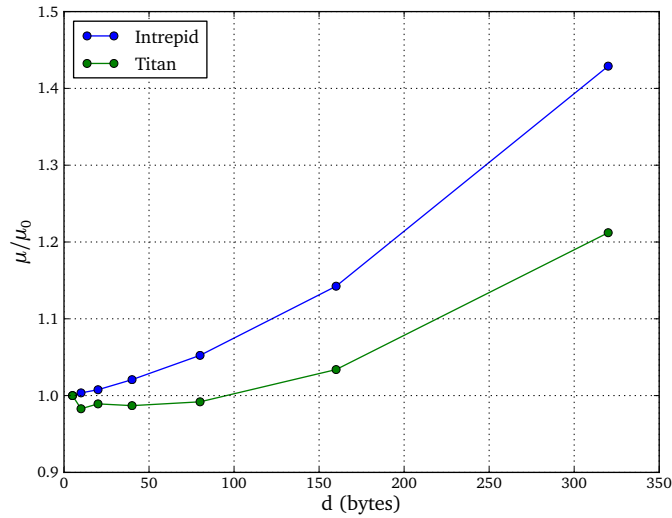


Figure 6-3: Observed dependence of μ on the amount of data tallied, d , on Intrepid and Titan.

adequate to accurately profile performance. On the Intrepid supercomputer, the baseline simulation was run with a single processor with 2000 particles per batch. Again, ten batches were run first without and then with tallies. For each case, a tally was set up with a mesh filter and a second filter to match only events within the fuel volume. The scoring functions requested were the flux, total reaction rate, scattering rate, absorption rate, fission rate, and neutron production rate for varying numbers of nuclides, starting with 5 nuclides and doubling the number of nuclides up to 320. Thus, the amount of data sent at each event varied from 240 bytes up to 15.36 kilobytes. Figure 6-3 shows the observed dependence of μ on d normalized to the $d = 5$ case.

The parameter study using tally servers on the Intrepid supercomputer consisted of 168 simulations with each combination of the following parameters: $p = 16, 32, 64, 128, 256, 512$, $c/s = 1, 3, 7, 15$, and $d = 240, 480, 960, 1920, 3840, 7680, 15360$. Like the baseline cases, the runs with tally servers had 10 inactive batches, 10 active batches, and $N/p = 500$. The effective overhead from tally servers was determined in the following manner. First, the expected overhead due to looking up cross sections during tallying was subtracted from the active batch time based on the results from the baseline cases. Then, the adjusted simulation time in active batches was divided by the inactive batch

time to determine the overhead in active batches. This essentially represents an estimate for the second term in (6.5), i.e. it does not account for the fact that we have fewer compute processors. However, if we know p and c , that source of overhead is trivial to calculate — it is really the extra overhead from message-passing that we are interested in. The overhead calculated in this manner for $c/s = 1$, $c/s = 3$, $c/s = 7$, and $c/s = 15$ is shown in Figure 6-4, Figure 6-5, Figure 6-6, and Figure 6-7, respectively.

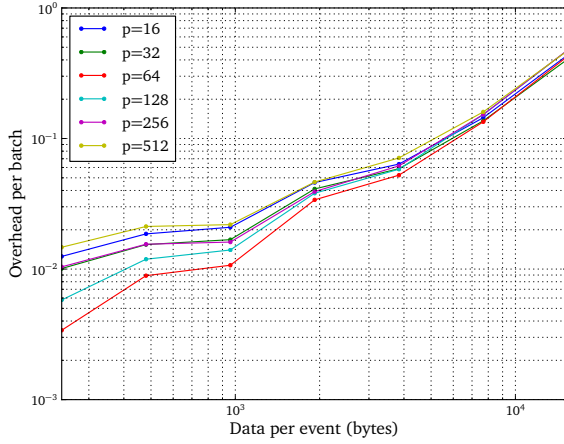


Figure 6-4: Tally server overhead on Intrepid Blue Gene/P as a function of data per event with $c/s = 1$.

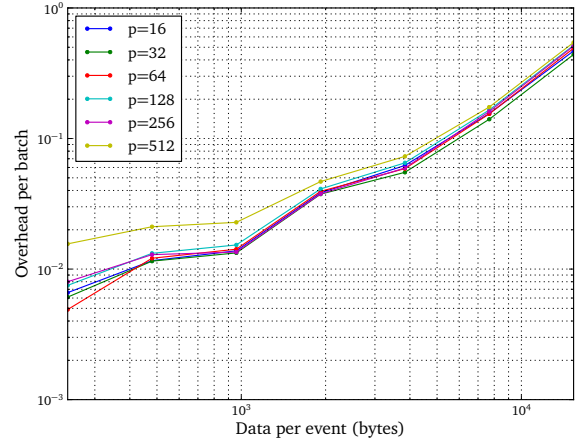


Figure 6-5: Tally server overhead on Intrepid Blue Gene/P as a function of data per event with $c/s = 3$.

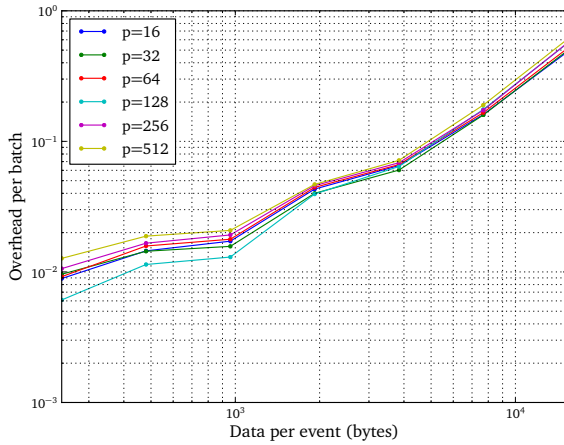


Figure 6-6: Tally server overhead on Intrepid Blue Gene/P as a function of data per event with $c/s = 7$.

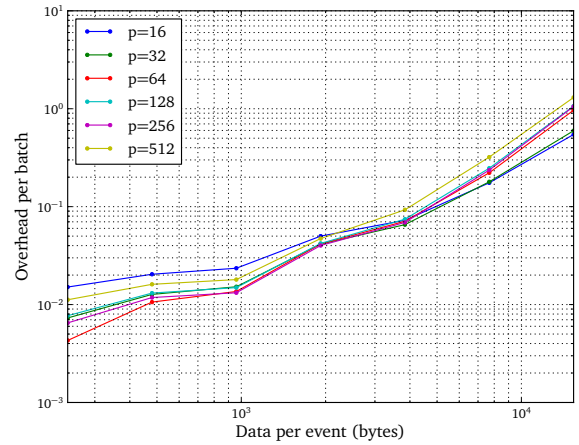


Figure 6-7: Tally server overhead on Intrepid Blue Gene/P as a function of data per event with $c/s = 15$.

It is also of interest to observe the behavior of the tally server overhead with increasing numbers of total processors. Recall that the performance model predicts that the

overhead should not depend on the number of processors used. Figure 6-8 shows the overhead plotted as a function of p for cases with $d = 15360$. We see that the overhead does not increase appreciably for $c/s = 1, 3, 7$. However, for $c/s = 15$ the performance begins to degrade. This may indicate that on Intrepid, this support ratio is not quite sufficient for all servers to keep up with the volume of messages. Since the model assumptions regarding achievable bandwidth do not account for contention, such deviation from the model is not unexpected.

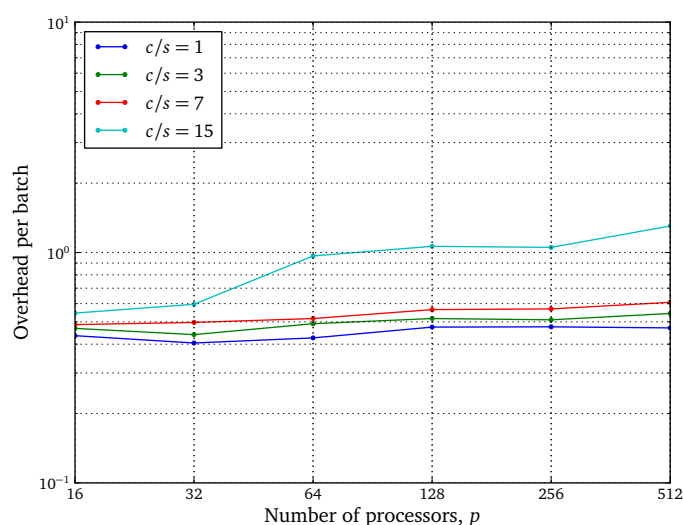


Figure 6-8: Tally server overhead on Intrepid Blue Gene/P as a function of p for $d = 15360$.

Another parameter study using tally servers on the Titan supercomputer consisted of 196 simulations with each combination of the following parameters: $p = 16, 32, 64, 128, 256, 512, 1024$, $c/s = 1, 3, 7, 15$, and $d = 240, 480, 960, 1920, 3840, 7680, 15360$. Again, the runs with tally servers had 10 inactive batches, 10 active batches, and $N/p = 1000$. The effective overhead from tally servers was determined as described for the study on Intrepid. The calculated overhead for $c/s = 1$, $c/s = 3$, $c/s = 7$, and $c/s = 15$ is shown in Figure 6-9, Figure 6-10, Figure 6-11, and Figure 6-12, respectively.

Similar to Figure 6-8, we can look at the behavior of the tally server overhead on Titan with increasing p . Figure 6-13 shows the overhead plotted as a function of p for cases with $d = 15360$. We see that the overhead is relatively stable with increasing p . However,

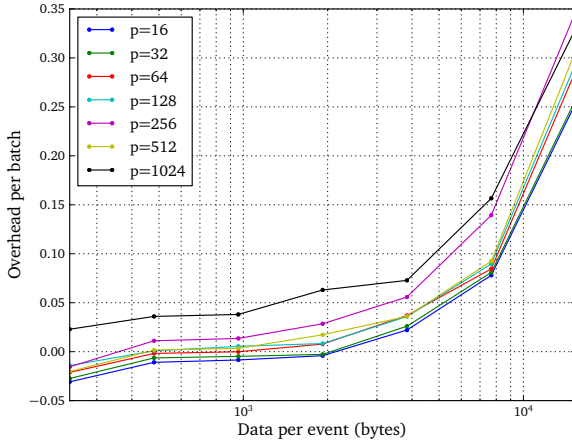


Figure 6-9: Tally server overhead on Titan Cray XK7 as a function of data per event with $c/s = 1$.

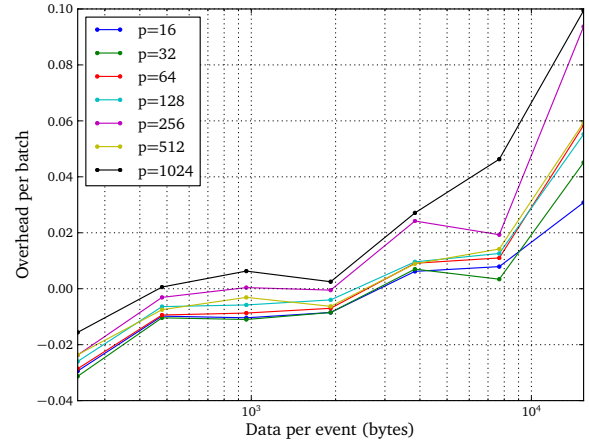


Figure 6-10: Tally server overhead on Titan Cray XK7 as a function of data per event with $c/s = 3$.

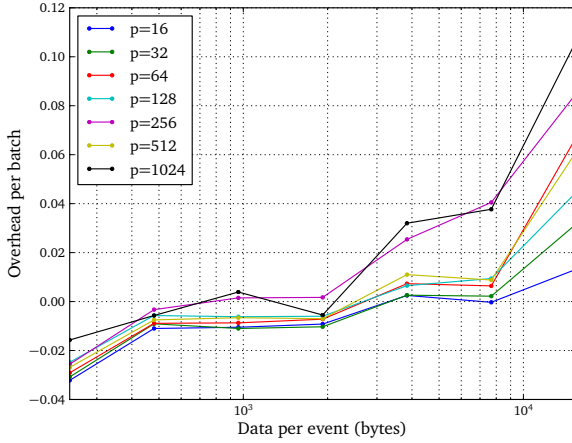


Figure 6-11: Tally server overhead on Titan Cray XK7 as a function of data per event with $c/s = 7$.

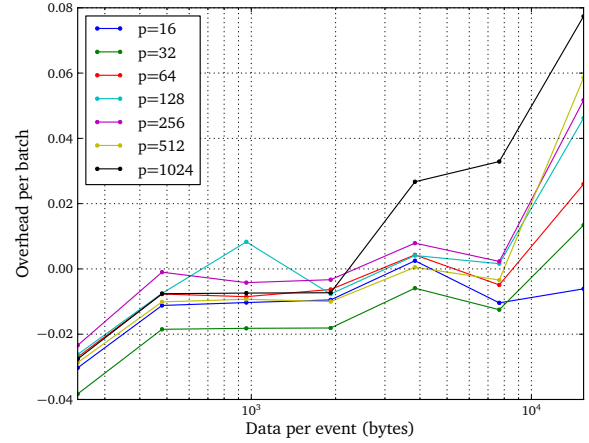


Figure 6-12: Tally server overhead on Titan Cray XK7 as a function of data per event with $c/s = 15$.

the cases with $c/s = 1$ are clearly outliers with much higher overhead than the other cases. This is likely due to network contention since the $c/s = 1$ cases result in half of the processor cores on each node sending messages simultaneously. To understand in greater depth the variability of the overhead as a function of, e.g., the support ratio would likely require a deeper investigation of a particular architecture, including topology-aware algorithms and a more sophisticated model for network contention. These studies are beyond the scope of the present work and are not central to addressing the key questions we set out to study.

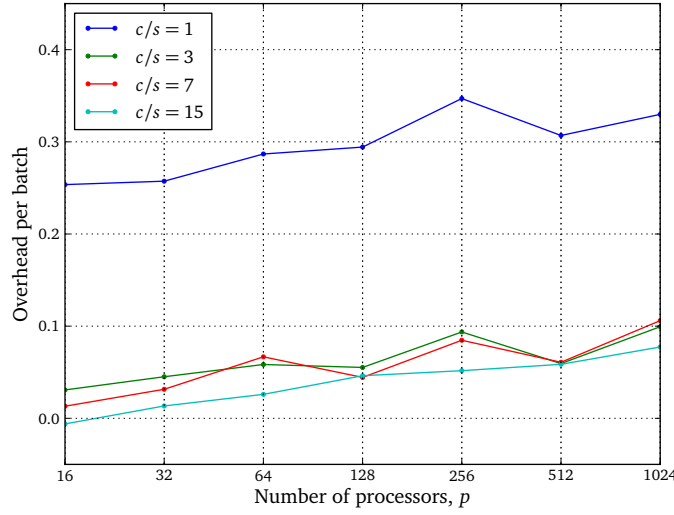


Figure 6-13: Tally server overhead on Titan Cray XK7 as a function of p for $d = 15360$.

6.5 Conclusions

An algorithm for decomposing large tally data in Monte Carlo particle transport simulations was proposed, analyzed, and implemented/tested in OpenMC. The algorithm relies on disjoint sets of compute processes and servers of which the former simulate particles moving through the geometry and the latter runs in a continuous loop receiving scores from the compute processors and incrementing tallies. This algorithm potentially allows the end user to dramatically increase the overall tally memory footprint and therefore enables the potential to carry out full core fuel depletion calculations.

The proposed algorithm is only of practical value if the communication penalty resulting from tally decomposition is reasonable relative to the key timescales of the problem. We carried out an analysis to that end and showed in section 6.2 that for a range of parameters relevant to LWR analysis, the tally server algorithm should perform with minimal overhead on contemporary supercomputers regardless of the message-passing semantics. An implementation of the algorithm in OpenMC was tested on the Intrepid and Titan supercomputers and was demonstrated to perform well over a wide range of the parameters. We can conclude that even with no further improvements in the algorithm or its implementation in OpenMC, it could be successfully used to analyze

LWR models with a level of fidelity that was heretofore not possible due to the need to replicate memory across all processors. It is likely that future developments in Monte Carlo methods for reactor analysis and improvements in computer architectures will only improve the performance of the tally server algorithm over time.

One point that was made earlier was that the algorithm presented here does not reduce the burden of large cross section data. For realistic reactor analysis, cross section data may well reach into the hundreds of gigabytes owing to the fact that cross section libraries would be needed at a multitude of temperatures. In subsection 1.5.2, we had discussed two promising efforts in the area of on-the-fly evaluation of effective cross sections at any temperature — the work of Yesilyurt on on-the-fly Doppler broadening [37] and the work of Viitanen on explicit temperature treatment [40]. The latter development would enable simulation using 0 K cross sections but with a significant performance penalty. In general, this and other improvements in physics methods will likely lead to slower simulations but with higher fidelity. From the perspective of the tally server model, these developments will increase μ and consequently decrease the communication overhead.

On the hardware end, improvements in supercomputer architectures may continue to reduce network latency and improve bandwidth, at least in the short-term. Again, this will largely benefit the tally server algorithm. Since incrementing tallies can naturally be expressed as a fetch-and-add atomic operation, there is also potential to exploit remote direct memory access (RDMA) operations either explicitly (e.g., using MPI-2) or implicitly through a partitioned global address space (e.g., Fortran co-arrays). Modern network interconnects should be able to take advantage of RDMA operations. In addition, the requirement that servers and compute processes be disjoint could be obviated by the use of RDMA, potentially offering further reductions in overhead.

One potential downside to the algorithm presented here is that it considerably complicates the use of threading via OpenMP. The most natural means of obtaining thread-level parallelism in a Monte Carlo particle transport simulation is to divide particles within a batch over multiple threads. Normally, no communication occurs until the end of a batch when it is necessary to synchronize fission bank sites and tallies.

However, with the inclusion of tally servers, it would then be necessary for each thread to participate in message-passing. Further algorithmic innovations will need to be explored to efficiently combine a tally server model with on-node shared-memory parallelism.

As a final comment, one should recognize the fact that the algorithm presented here has primarily been presented with a focus and intent on applications in LWR analysis. For other types of analysis performed with Monte Carlo, it may turn out that the tally server algorithm does not make sense.

Chapter 7

Conclusions

Monte Carlo particle transport methods are being considered as a viable option in the future for high-fidelity simulation of nuclear reactors. This is, in part, thanks to the enormous advances in high performance computing. If parallel methods were not exploited, the sheer number of floating point operations (FLOPs) required to reduce stochastic uncertainty to acceptable levels when using Monte Carlo would require unacceptably long simulation time. However, the present availability of supercomputers with hundreds of thousands or millions of processor cores means that, solely from the perspective of FLOPs required, solution to LWR problems using Monte Carlo could hypothetically be done in a short time.

Lest we be fooled into thinking floating point operations are the only challenge to overcome, let us remind ourselves that they are but one small piece of the puzzle — there are a variety of algorithmic and architectural challenges that will not be easy to solve; an excellent summary of these issues, especially as they apply to full-core LWR calculations, has recently been given by Martin [39]. The objective of this thesis was to make headway towards overcoming some of these challenges.

In chapter 1, an overview of four contemporary issues preventing Monte Carlo simulations of realistic LWR models was given: source convergence, cross section memory requirements, tally memory requirements, and degradation in parallel efficiency. In the following sections, we will summarize the status of and progress that has been made in each area as well as what ongoing work will still be needed in order to reach the goal of

performing reactor analysis with Monte Carlo.

7.1 Source Convergence

One area that has received quite a bit of attention in the last decade is source convergence in Monte Carlo calculations. There are, in a sense, two separate issues relating to source convergence. The first is being able to assess the convergence of the source distribution, i.e. because the source distribution is a collection of finite points in multiple dimensions, how can one assure that it has reached stationarity in the method of successive generations. For a scalar value, such as the global eigenvalue, it is intuitive to merely look a line plot of its value versus the number of batches.

The second issue is accelerating convergence of the source distribution. Until the source has converged in a Monte Carlo eigenvalue calculation, it is not possible to accumulate tallies. Thus, the inactive batches are “wasted” as it were. If a method could be employed to reduce the number of inactive batches, we would save the wasted calculational time. Both issues are made worse by a high dominance ratio; this is unfortunately the case in a full-core reactor where the dominance ratio can be very close to unity.

7.1.1 Status

The pioneering work of Ueki and Brown [106, 75] has helped introduce and gain acceptance of the Shannon entropy, a scalar metric based on information theory, as a proper means for assessing convergence of the source distribution. Shannon entropy has now been implemented in most modern Monte Carlo codes, including OpenMC (see subsection 2.8.2). While Shannon entropy will work for nearly all models, it may be ill-suited for very large, loosely-coupled models such as a spent fuel array; for these problems, research efforts are looking into mesh-based convergence diagnostics [107].

Various methods have been proposed, tested, and implemented in Monte Carlo codes for accelerating source convergence. In the author’s opinion, one of the more promising methods, which is widely employed in deterministic calculations, is coarse mesh finite

difference. The basic idea is to use volume-integrated reaction rates and partial currents on mesh surfaces from Monte Carlo tallies to solve a low-order system. This method has been proven to be quite effective in reducing the number of inactive batches in Monte Carlo eigenvalue calculations [30].

We see then that significant progress has been made in the area of source convergence in Monte Carlo eigenvalue calculations. For full-core LWR models, CMFD can be used to accelerate source convergence, and Shannon entropy can be used to assess source convergence. As a result, it was not an objective of this thesis to pursue further work in the area of source convergence.

7.1.2 Future Work

Nevertheless, there are still a number of interesting areas of research pertaining to source convergence. While source convergence can be assessed using Shannon entropy, there is as-of-yet no viable method for diagnosing undersampling. Undersampling is a phenomenon whereby local tallies may be systematically biased as a result of not using enough particles per batch [33, 34]. To the author's knowledge, only one method for undersampling diagnosis has been proposed in the literature [35], but it unfortunately would not be feasible in a realistic calculation due to memory requirements. Moreover, while the bias in global eigenvalue is fairly well understood [82] and known to be small, no study has systematically looked at biases in local tallies due to undersampling in reactor problems. Very little work on local tally bias has been pursued since the work of Gelbard and Gu in the 1990s [108, 109].

In the area of source convergence acceleration, one current "hot topic" pertaining to CMFD is determining the best way to generate multigroup parameters for the diffusion solver. In particular, generating multigroup diffusion coefficients from a Monte Carlo code can be problematic. A number of research efforts are currently looking at methods for generating diffusion coefficients in the hope that more accurate parameters will lead to better convergence properties [110, 111]. Researchers are also looking at other low-order methods for accelerating convergence.

7.2 Parallel Efficiency

Solution of full-core LWR problems will require an enormous number of floating point operations and will thus necessitate the use of thousands or millions of processors in parallel. However, with current parallel algorithms, a serious degradation in parallel efficiency will likely be experienced when one tries to use even thousands of processors [45]. To reiterate, two of the root causes for this degradation are reduction of tallies and synchronization of the fission source at each batch in an eigenvalue calculation. One of our major objectives in this work has been to develop algorithms that ameliorate the degradation of parallel efficiency at large numbers of processors.

7.2.1 Contributions of Present Work

In chapter 3, a nearest-neighbor algorithm was proposed and subsequently implemented in the OpenMC Monte Carlo code. This algorithm takes advantage of the fact that many of the fission sites produced on one processor can be used as source sites on that same processor — in doing so, it avoids unnecessary communication between processors. A theoretical analysis of the algorithm shows that the expected cost is $O(\sqrt{N})$, N being the number of particles per generation, whereas traditional master-slave algorithms are $O(N)$ at best, and possibly even $O(N \log_2 N)$. The algorithm was tested on two contemporary supercomputers, the Intrepid Blue Gene/P at ANL and the Titan Cray XK7 at ORNL, and demonstrated nearly linear parallel scaling up to 163,840 processor cores. There is no reason to believe that the nearest-neighbor algorithm will not scale to even greater processor counts.

In chapter 4, an algorithm for reducing network communication arising from tally reduction was analyzed and, again, implemented in OpenMC. The basic idea is conceptually very simple — the grouping of particles histories into batches for the sake of calculating variance is arbitrary. The proposed algorithm groups only particle histories on a single processor and in doing so prevents all network communication for tallies until the very end of the simulation. In a large scale parallel calculation of, say, a realistic LWR model, it is likely that enough processors will be used to obtain a sufficient number

of realizations of the random variables. This algorithm was tested in OpenMC on the Monte Carlo performance benchmark on a cluster at MIT, and it was shown that network communication was substantially reduced.

Together, the algorithms presented in chapter 3 and chapter 4 should enable very high parallel efficiencies to be attained for eigenvalue calculations using the method of successive generations. These algorithms have been published in [78] and [86], respectively.

7.2.2 Future Work

There are a few potential shortcomings of the nearest-neighbor fission bank algorithm. One that was mentioned in the conclusions of chapter 3 is that the algorithm would preclude the use of load balancing via existing algorithms for heterogeneous computer architectures. A simple method to provide load balancing in such situations based on “tuning” the algorithm was suggested, but it has never been tested. Additionally, the nearest-neighbor algorithm may be very difficult to combine with any domain decomposition scheme since the order of fission bank sites would necessarily depend on their spatial coordinates. If domain decomposition is ever to be used for calculations with tens of thousands of processors or more, this issue will likely need to be addressed.

The tally reduction algorithm is robust; we see no immediate need to pursue further work on it. Perhaps one downside of the method is that it will not exactly reproduce the variance of a calculation in which particle histories are batched according to single fission generations. However, this is no different than saying that any calculation that uses batching will not reproduce the variance exactly. It was argued that, in the absence of intergenerational correlation, the expected value of the variance is the same regardless of the batching. In fact, batching particle histories across fission generations will produce more reliable estimates of variance in an eigenvalue calculation since intergenerational correlation effects are avoided in doing so.

7.3 Cross Section Memory

In order to perform a realistic simulation of a reactor at power, it is important to account for the dependence of interaction cross sections on temperature. In subsection 1.5.2, this was discussed at length, and we found that the memory requirements resulting from storing cross sections at a multitude of temperatures could be as high as hundreds of gigabytes. Thus, methods are needed to reduce or decompose the cross section data. We reiterate that this thesis has not looked at this particular issue since other research efforts have shown promise.

7.3.1 Status

Two substantial efforts are underway aimed at reducing cross section memory requirements. The first is the work of Yesilyurt, Martin, and Brown on on-the-fly Doppler broadening of cross sections [37, 38]. In this method, the cross section at any temperature is represented as a series expansion — thus only the series expansion coefficients need to be stored in memory. Preliminary work on this method looks promising, but it has yet to be demonstrated for a realistic problem with hundreds of nuclides at many temperatures.

The other more recent research effort is an explicit temperature treatment by Viitanen and Leppänen [40]. This is a fundamentally different approach wherein cross sections are only stored at 0 K and the effect of the thermal motion of the target material is accounted for by using a rejection sampling technique. This would reduce the necessary cross section storage to that of a single temperature. The work is still in a preliminary state; however, it has been demonstrated rigorously that this method can account for the thermal motion of nuclides in material at a temperature greater than 0 K.

7.3.2 Future Work

In both the on-the-fly Doppler broadening and explicit temperature methods, the temperature dependence of $S(\alpha, \beta, T)$ data and unresolved resonance probability tables can not

be accounted for. For any realistic reactor simulation, accounting for the temperature dependence of $S(\alpha, \beta, T)$ is absolutely essential to obtaining accurate results. It should be noted however that $S(\alpha, \beta, T)$ and probability table data is typically a very small fraction of the overall cross section data. As such, it may be feasible to simply store these data at very fine temperature intervals. However, this has not been studied.

The explicit temperature method has been shown to produce unbiased results [40]. However, no results in the literature have demonstrated what the effect on the figure of merit for tallies would be, i.e. while the absolute performance cost was shown to be reasonable [41], does the method require significantly more particles to obtain comparable statistics? Until that question is answered, it is not possible to assess the performance penalty of the method versus using normal Doppler broadened cross sections.

7.4 Tally Memory — Domain Decomposition

In the current SPMD parallel technique for Monte Carlo particle transport, all problem data stored in memory must be replicated on each process in a simulation. For the simulation of a light-water reactor, the memory requirements for tallies may be enormous, likely exceeding terabytes. A method for decomposing tally memory across many processors is critical in such a scenario. In this thesis, we have looked at two different schemes for decomposing tally memory, domain decomposition and data decomposition.

7.4.1 Contributions of Present Work

A theoretical framework for analyzing domain decomposition of Monte Carlo particle transports has only been posed in the last year or so [95]. In chapter 5, we presented a theoretical analysis of domain decomposed Monte Carlo particle transport simulations looking at the effect of load imbalances on the total simulation time relative to a perfectly load balanced simulation¹. The analysis demonstrated that load imbalances in domain decomposed simulations arise from two different phenomena: non-uniform particle

¹This is analogous to a simulation performed with no domain decomposition.

densities and non-uniform spatial leakage. One of the interesting facts we can glean from the analysis is that the dominant performance penalty in domain decomposition comes not from network communication but from these load imbalances. Importantly, the penalty from non-uniform spatial leakage is a function of the subdomain size — smaller partitions lead to a larger penalty from the load imbalance. This may limit the utility of domain decomposition for reactor analysis.

The analysis and results from chapter 5 were published in [96].

7.4.2 Future Work

In chapter 5, the assessment of the load imbalance penalty was done based on measurements of the Monte Carlo performance benchmark using OpenMC. We suggest that future work look at measurements on an actual reactor model, such as the MIT PWR benchmark. The enrichment zoning will likely result in a smaller load imbalance penalty from non-uniform particle densities (since the power distribution should be flatter), but greater material heterogeneities could mean that the load imbalance penalty from non-uniform spatial leakage is worse.

Additionally, while the analysis in chapter 5 looked at the load imbalance penalty for various domain sizes, it was not mentioned what domain size will really be necessary for reactor analysis. This will be largely determined by the tally memory requirements since they will impose a limit on the size of a spatial subdomain. Other methods proposed in the literature such as overlapping domains and domain replication should also be accounted for.

Spatial leakage rates may also be sensitive to the use of survival biasing or other weight adjustment methods used in Monte Carlo eigenvalue calculations. This effect should be quantified to assess whether this would substantially change the results we arrived at in chapter 5.

7.5 Tally Memory — Data Decomposition

The main alternative to domain decomposition for reducing tally memory requirements is data decomposition. Although this idea has existed in the literature for eight years [100], little to no work or analysis has been carried out until now. The last objective of this thesis was to enhance our understanding of data decomposition algorithms to determine whether they might enable realistic reactor analysis using Monte Carlo.

7.5.1 Contributions of Present Work

In chapter 6, an algorithm for decomposing large tally data in Monte Carlo particle transport simulations was proposed, analyzed, and implemented/tested in OpenMC. The algorithm relies on disjoint sets of compute processes and servers of which the former simulate particles moving through the geometry and the latter runs in a continuous loop receiving scores from the compute processors and incrementing tallies. The analysis in section 6.2 showed that for a range of parameters relevant to LWR analysis, the tally server algorithm should perform with minimal overhead on contemporary supercomputers. The implementation of the algorithm in OpenMC was tested on the Intrepid and Titan supercomputers and was demonstrated to perform well over a wide range of the parameters. We thus conclude that the tally server algorithm is a successful approach to circumventing classical on-node memory constraints en route to unprecedentedly detailed Monte Carlo reactor simulations.

The work presented on the tally server algorithm has been submitted for publication in [103].

7.5.2 Future Work

The first implementation of the tally server algorithm in OpenMC relied on blocking communication semantics. It would be worthwhile to implement non-blocking communication to further reduce the overhead from the tally server algorithm. While the algorithm performed well on contemporary supercomputers, on a machine more within

the reach of a typical user, such as a small cluster, network communication may become a major problem.

One of the important parameters in the theoretical analysis of the tally server algorithm is the number of events per particle. This parameter will be affected by the use of survival biasing and other variance reduction techniques. Namely, survival biasing will increase the number of events per particle. However, the absolute simulation time will also increase as a result of the use of survival biasing. In any event, the effect of survival biasing on this parameter and the feasibility of the tally server algorithm should be quantified.

The number of events per particle will also be affected by the discretization of a fuel pin into axial and radial segments. Such discretization will be necessary for detailed depletion calculations. Thus, this effect should also be quantified and its impact on the overhead assessed.

The tests of the tally server algorithm on Intrepid and Titan were only performed on up to 1,024 processors. Although the performance showed little dependence on the number of processors (as predicted), it would nevertheless be instructive to perform a very large simulation on many processors and with very large tally requirements.

7.6 Other Future Work

One area that has received, undeservedly, little attention in this thesis is the coupling of neutronics to other fields such as thermal-hydraulics, transients, fuel performance, and mechanics. Without feedback from these fields, one can only obtain a solution to the *wrong* problem. For the purpose of realistic reactor analysis using Monte Carlo, much work will be needed to best account for multi-physics feedback. We refer the reader to [39] for a review of current work in this area.

Neutronic simulations are typically performed assuming no coupling between neutron and photon physics. As a result, it is necessary to make assumptions regarding the distribution of photon energy deposition. A typical procedure is to “smear” the photon energy deposition over the problem. Again, to truly obtain an accurate solution, explicit

coupling of neutron and photon transport is needed.

Many Monte Carlo codes do not account for physics effects that may be important in certain situations: to name a few, the impact of low-energy resonance scattering from heavy nuclides [112, 113], the epithermal scattering of neutrons from Hydrogen via the short collision time approximation [114], and a continuous $S(\alpha, \beta, T)$ treatment [115]. To the author's knowledge, MC21 is the only code that can account for all these effects. Wider acceptance and implementation of these methods will be needed for reactor analysis.

The last issue we will mention is that the memory required to store material compositions may become non-trivial for depletion calculations. Consider a reactor with 193 assemblies, 264 pins in each assembly, and a subdivision of each pin into 100 axial segments and 10 radial rings: a total of about 254 million materials. For a depletion calculation, the densities of up to 300 nuclides would need to be stored for each material. The material compositions alone would therefore require over 120 GB of memory. This problem would affect not only Monte Carlo methods but deterministic methods as well.

References

- [1] B. G. CARLSON and K. D. LATHROP, *Transport Theory: The Method of Discrete Ordinates*, Los Alamos Scientific Laboratory of the University of California (1965).
- [2] G. I. BELL and S. GLASSTONE, *Nuclear Reactor Theory*, Van Nostrand, Princeton, New Jersey (1970).
- [3] K. S. SMITH and J. D. RHODES, “Full-Core, 2-D, LWR Core Calculations with CASMO-4E,” *Proc. PHYSOR*, Seoul, South Korea, Oct. 7-10, 2002.
- [4] N. METROPOLIS and S. ULAM, “The Monte Carlo Method,” *J. Am. Stat. Assoc.*, **44**, 247, 335 (1949).
- [5] E. TROUBETZKOY, H. STEINBERG, and M. KALOS, “Monte Carlo Radiation Penetration Calculations on a Parallel Computer,” *Trans. Am. Nucl. Soc.*, **17**, 260 (1973).
- [6] F. B. BROWN and W. R. MARTIN, “Monte Carlo Methods for Radiation Transport Analysis on Vector Computers,” *Prog. Nucl. Energy*, **14**, 3, 269 (1984).
- [7] F. DAREMA, “The SPMD Model: Past, Present and Future,” in *Recent Advances in Parallel Virtual Machine and Message Passing Interface*, volume 2131 of *Lecture Notes in Computer Science*, p. 1–1, Springer Berlin / Heidelberg, 2001.
- [8] A. BEGUELIN, J. DONGARRA, A. GEIST, R. MANCHEK, and V. SUNDERAM, “A Users’ Guide to PVM (Parallel Virtual Machine),” ORNL/TM-11826, Oak Ridge National Laboratory (1991).
- [9] W. GROPP, E. LUSK, and A. SKJELLUM, *Using MPI: Portable Parallel Programming with the Message Passing Interface*, volume 1, MIT Press (1999).
- [10] P. K. ROMANO, B. FORGET, and J. THOMAS H. NEWTON, “Development of a Graphical User Interface for In-Core Fuel Management Using MCODE,” *Proc. Advances in Nuclear Fuel Management IV*, Hilton Head Island, South Carolina, April 12–15, 2009.
- [11] K. SMITH, “Reactor Core Methods,” *Proc. M&C 2003*, Gatlinburg, Tennessee, April 6–10, 2003, Plenary Presentation.

- [12] W. R. MARTIN, “Advances in Monte Carlo Methods for Global Reactor Analysis,” *Proc. Joint International Topical Meeting on Mathematics & Computation and Supercomputing in Nuclear Applications*, Monterey, California, April 15–19, 2007, Invited Lecture.
- [13] J. E. HOOGENBOOM and W. R. MARTIN, “A Proposal for a Benchmark to Monitor the Performance of Detailed Monte Carlo Calculation of Power Densities in a Full Size Reactor Core,” *Proc. Int. Conf. Mathematics, Computational Methods, and Reactor Physics*, Saratoga Springs, New York, May 3–7, 2009.
- [14] J. E. HOOGENBOOM, W. R. MARTIN, and B. PETROVIC, “The Monte Carlo Performance Benchmark Test - Aims, Specifications and First Results,” *Proc. Int. Conf. Mathematics and Computational Methods Applied to Nuclear Science and Engineering*, Rio de Janeiro, Brazil, May 8–12, 2011.
- [15] D. J. KELLY, T. M. SUTTON, T. H. TRUMBULL, and P. S. DOBREFF, “MC21 Monte Carlo Analysis of the Hoogenboom-Martin Full-Core PWR Benchmark Problem,” *Proc. PHYSOR – Advances in Reactor Physics to Power the Nuclear Renaissance*, Pittsburgh, Pennsylvania, May 9–14, 2010.
- [16] T. M. SUTTON et al., “The MC21 Monte Carlo Transport Code,” *Proc. Joint International Topical Meeting on Mathematics & Computation and Supercomputing in Nuclear Applications*, Monterey, California, April 15–19, 2007.
- [17] J. LEPPÄNEN, “Development of a New Monte Carlo Reactor Physics Code,” P640, VTT Technical Research Centre of Finland (2007).
- [18] J. LEPPÄNEN, “Use of the Serpent Monte Carlo Reactor Physics Code for Full-Core Calculations,” *Proc. Joint International Conference on Supercomputing in Nuclear Applications and Monte Carlo*, Tokyo, Japan, October 17–21, 2010.
- [19] D. J. KELLY, T. M. SUTTON, and S. C. WILSON, “MC21 Analysis of the Nuclear Energy Agency Monte Carlo Performance Benchmark Problem,” *Proc. PHYSOR – Advances in Reactor Physics – Linking Research, Industry, and Education*, Knoxville, Tennessee, April 15–20, 2012.
- [20] F. B. BROWN, “Fundamentals of Monte Carlo Transport,” LA-UR-05-4983, Los Alamos National Laboratory (2005).
- [21] P. K. ROMANO and B. FORGET, “The OpenMC Monte Carlo Particle Transport Code,” *Ann. Nucl. Energy*, **51**, 274 (2013).
- [22] J. DUFEK and W. GUDOWSKI, “Fission matrix based Monte Carlo criticality calculations,” *Ann. Nucl. Energy*, **36**, 8, 1270 (2009).
- [23] S. E. CARNEY, F. B. BROWN, B. C. KIEDROWSKI, and W. R. MARTIN, “Fission Matrix Capability for MCNP Monte Carlo,” LA-UR-12-24533, Los Alamos National Laboratory (2012).

- [24] T. YAMAMOTO and Y. MIYOSHI, “Reliable Method for Fission Source Convergence of Monte Carlo Criticality Calculation with Wielandt’s method,” *J. Nucl. Sci. Technol.*, **41**, 2, 99 (2004).
- [25] F. BROWN, “Wielandt Acceleration for MCNP5 Monte Carlo Eigenvalue Calculations,” *Proc. Joint International Topical Meeting on Mathematics & Computation and Supercomputing in Nuclear Applications*, Monterey, California, April 15–19, 2007.
- [26] D. P. GRIESHEIMER and B. E. TOTH, “A Novel Source Convergence Acceleration Scheme for Monte Carlo Criticality Calculations, Part I: Theory,” *Proc. Joint International Topical Meeting on Mathematics & Computation and Supercomputing in Nuclear Applications*, Monterey, California, April 15–19, 2007.
- [27] B. E. TOTH and D. P. GRIESHEIMER, “A Novel Source Convergence Acceleration Scheme for Monte Carlo Criticality Calculations, Part II: Implementation & Results,” *Proc. Joint International Topical Meeting on Mathematics & Computation and Supercomputing in Nuclear Applications*, Monterey, California, April 15–19, 2007.
- [28] M. J. LEE, H. G. JOO, D. LEE, and K. SMITH, “Investigation of CMFD Accelerated Monte Carlo Eigenvalue Calculation with Simplified Low Dimensional Multigroup Formulation,” *Proc. PHYSOR – Advances in Reactor Physics to Power the Nuclear Renaissance*, Pittsburgh, Pennsylvania, May 9–14, 2010.
- [29] M.-J. LEE, H. G. JOO, D. LEE, and K. SMITH, “Multigroup Monte Carlo Reactor Calculation with Coarse Mesh Finite Difference Formulation for Real Variance Reduction,” *Proc. Joint International Conference on Supercomputing in Nuclear Applications and Monte Carlo*, Tokyo, Japan, October 17–21, 2010.
- [30] M. J. LEE, H. G. JOO, D. LEE, and K. SMITH, “Monte Carlo Reactor Calculation with Substantially Reduced Number of Cycles,” *Proc. PHYSOR – Advances in Reactor Physics – Linking Research, Industry, and Education*, Knoxville, Tennessee, April 15–20, 2012.
- [31] M. T. YOUNG, F. B. BROWN, B. C. KIEDROWSKI, and W. R. MARTIN, “Coarse Mesh Finite Difference in MCNP5,” LA-UR-11-04834, Los Alamos National Laboratory (2011).
- [32] P. K. ROMANO et al., “Progress and Status of the OpenMC Monte Carlo Code,” *Proc. International Conference on Mathematics and Computational Methods Applied to Nuclear Science & Engineering*, Sun Valley, Idaho, May 5–9, 2013.
- [33] T. UEKI, “Information Theory and Undersampling Diagnostics for Monte Carlo Simulation of Nuclear Criticality,” *Nucl. Sci. Eng.*, **151**, 283 (2005).
- [34] T. UEKI, “On-the-Fly Diagnostics of Particle Population in Iterated-Source Monte Carlo Methods,” *Nucl. Sci. Eng.*, **158**, 15 (2008).

- [35] T. UEKI and B. S. CHAPMAN, "Particle Population Diagnosis and Euclidean Minimum Spanning Tree in Monte Carlo Calculation of Power Distribution," *J. Nucl. Sci. Technol.*, **48**, 2, 292 (2011).
- [36] T. H. TRUMBULL, "Treatment of Nuclear Data for Transport Problems Contained Detailed Temperature Distributions," *Nucl. Technol.*, **156**, 1, 75 (2006).
- [37] G. YESILYURT, W. R. MARTIN, and F. B. BROWN, "On-the-Fly Doppler Broadening for Monte Carlo codes," *Nucl. Sci. Eng.*, **171**, 239 (2012).
- [38] F. B. BROWN, W. R. MARTIN, G. YESILYURT, and S. WILDERMAN, "Progress with On-The-Fly Neutron Doppler Broadening in MCNP," *Trans. Am. Nucl. Soc.*, **106**, 708 (2012).
- [39] W. R. MARTIN, "Challenges and Prospects for Whole-Core Monte Carlo Analysis," *Nucl. Eng. Technol.*, **44**, 2, 151 (2012).
- [40] T. VIITANEN and J. LEPPÄNEN, "Explicit Treatment of Thermal Motion in Continuous-Energy Monte Carlo Tracking Routines," *Nucl. Sci. Eng.*, **171**, 165 (2012).
- [41] T. VIITANEN and J. LEPPÄNEN, "Explicit Temperature Treatment in Monte Carlo Neutron Tracking Routines — First Results," *Proc. PHYSOR – Advances in Reactor Physics – Linking Research, Industry, and Education*, Knoxville, Tennessee, April 15–20, 2012.
- [42] B. GASTER et al., "Preparing the World for Ubiquitous Parallelism," *Proc. Supercomputing*, Portland, Oregon, November 14–20, 2009, Panel.
- [43] J. CETNAR, "General solution of Bateman equations for nuclear transmutation," *Ann. Nucl. Energy*, **33**, 640 (2006).
- [44] T. GOORLEY et al., "Initial MCNP5 Release Overview," *Nucl. Technol.*, **180**, 3, 298 (2012).
- [45] J. E. HOOGENBOOM, "Is Monte Carlo Embarassingly Parallel?," *Proc. PHYSOR – Advances in Reactor Physics – Linking Research, Industry, and Education*, Knoxville, Tennessee, April 15–20, 2012.
- [46] L. M. PETRIE and N. F. LANDERS, "SCALE: A Modular Code System for Performing Standardized Computer Analyses for Licensing Evaluation.," NUREG/CR-0200, Rev. 4, U.S. Nuclear Regulatory Commission (1990).
- [47] P. K. ROMANO, B. FORGET, and F. BROWN, "Data Decomposition for Monte Carlo Transport Applications: Initial Results and Findings," LA-UR-09-05721, Los Alamos National Laboratory (2009).
- [48] X-5 Monte Carlo Team, "MCNP - A General Monte Carlo N-Particle Transport Code, Version 5," LA-UR-03-1987, Los Alamos National Laboratory (2008).

- [49] P. K. ROMANO, “GitHub - Reactor Physics Benchmark Models,” <https://github.com/mit-crpg/benchmarks>, accessed October 26, 2012.
- [50] P. K. ROMANO, “The OpenMC Monte Carlo Code — OpenMC Documentation,” <http://mit-crpg.github.com/openmc>, accessed October 26, 2012.
- [51] X-5 Monte Carlo Team, “MCNP - A General Monte Carlo N-Particle Transport Code, Version 5, Volume III: Developer’s Guide,” LA-CP-03-0284, Los Alamos National Laboratory (2008).
- [52] R. E. MACFARLANE and A. C. KAHLER, “Methods for Processing ENDF/B-VII with NJOY,” *Nucl. Data Sheets*, **111**, 2739 (2010).
- [53] M. B. CHADWICK et al., “ENDF/B-VII.1 Nuclear Data for Science and Technology: Cross Sections, Covariances, Fission Product Yields and Decay Data,” *Nucl. Data Sheets*, **112**, 12, 2887 (2011).
- [54] J. LEPPÄNEN, “Serpent — a Continuous-energy Monte Carlo Reactor Physics Burnup Calculation Code, User’s Manual,” VTT Technical Research Centre of Finland (2012).
- [55] J. LEPPÄNEN, “Two practical methods for unionized energy grid construction in continuous-energy Monte Carlo neutron transport calculation,” *Ann. Nucl. Energy*, **36**, 878 (2009).
- [56] D. E. KNUTH, *The Art of Computer Programming*, Addison-Wesley (2006).
- [57] P. L’ECUYER, “Tables of Linear Congruential Generators of Different Sizes and Good Lattice Structures,” *Math. Comput.*, **68**, 225, 249 (1999).
- [58] F. B. BROWN, “Random Number Generation with Arbitrary Strides,” *Trans. Am. Nucl. Soc.*, **71**, 202 (1994).
- [59] M. HERMAN and A. TRKOV, “ENDF-6 Formats Manual. Data Formats and Procedures for the Evaluated Nuclear Data File ENDF/B-VI and ENDF/B-VII,” BNL-90365-2009, Brookhaven National Laboratory (2009).
- [60] R. J. DOYAS and S. T. PERKINS, “Interpolation of Tabular Secondary Neutron and Photon Energy Distributions,” *Nucl. Sci. Eng.*, **50**, 390 (1972).
- [61] A. FODERARO, *The Elements of Neutron Interaction Theory*, MIT Press, Cambridge, Massachusetts (1971).
- [62] C. J. EVERETT and E. D. CASHWELL, “A Third Monte Carlo Sampler,” LA-9721-MS, Los Alamos National Laboratory (1983).
- [63] B. E. WATT, “Energy Spectrum of Neutrons from Thermal Fission of U^{235} ,” *Phys. Rev.*, **87**, 6, 1037 (1952).

- [64] D. E. CULLEN and C. R. WEISBIN, "Exact Doppler Broadening of Tabulated Cross Sections," *Nucl. Sci. Eng.*, **60**, 199 (1976).
- [65] D. E. CULLEN, "PREPRO 2012 - 2012 ENDF-6 Pre-processing Codes," IAEA-NDS-39, Rev. 15, International Atomic Energy Agency (2012).
- [66] E. M. GELBARD, "Epithermal scattering in VIM," FRA-TM-123, Argonne National Laboratory (1979).
- [67] M. M. R. WILLIAMS, *The Slowing Down and Thermalization of Neutrons*, North-Holland Publishing Co., Amsterdam, Netherlands (1966).
- [68] G. L. SQUIRES, *Introduction to the Theory of Thermal Neutron Scattering*, Cambridge University Press, Cambridge, United Kingdom (1978).
- [69] L. B. LEVITT, "The Probability Table Method for Treating Unresolved Neutron Resonances in Monte Carlo Calculations," *Nucl. Sci. Eng.*, **49**, 450 (1972).
- [70] R. E. MACFARLANE and D. W. MUIR, "The NJOY Nuclear Data Processing System, Version 91," LA12740-M, Los Alamos National Laboratory (1994).
- [71] T. M. SUTTON and F. B. BROWN, "Implementation of the Probability Table Method in a Continuous-Energy Monte Carlo Code System," *Proc. Int. Conf. Physics of Nuclear Science and Technology*, Long Island, New York, October 5–8, 1998.
- [72] E. E. O. GEORGE and M. SIVARAM, "A modification of the Fisher-Cornish approximation for the student t percentiles," *Communication in Statistics - Simulation and Computation*, **16**, 4, 1123 (1987).
- [73] P. J. ACKLAM, "An algorithm for computing the inverse normal cumulative distribution function," <http://home.online.no/~pjacklam/notes/invnorm/>, accessed October 4, 2012.
- [74] J. LIEBEROTH, "A Monte Carlo Technique to Solve the Static Eigenvalue Problem of the Boltzmann Transport Equation," *Nukleonik*, **11**, 5, 213 (1968).
- [75] F. B. BROWN, "On the Use of Shannon Entropy of the Fission Distribution for Assessing Convergence of Monte Carlo Criticality Calculations," *Proc. ANS Topical Meeting on Reactor Physics*, Vancouver, British Columbia, Canada, September 10–14, 2006.
- [76] P. K. ROMANO, "Application of the Stochastic Oscillator to Assess Source Convergence in Monte Carlo Criticality Calculations," *Proc. Int. Conf. Mathematics, Computational Methods, and Reactor Physics*, Saratoga Springs, New York, May 3–7, 2009.
- [77] T. UEKI, "On-the-Fly Judgments of Monte Carlo Fission Source Convergence," *Trans. Am. Nucl. Soc.*, **98**, 512 (2008).

- [78] P. K. ROMANO and B. FORGET, "Parallel Fission Bank Algorithms in Monte Carlo Criticality Calculations," *Nucl. Sci. Eng.*, **170**, 2, 125 (2012).
- [79] F. BROWN and T. SUTTON, "Reproducibility and Monte Carlo Eigenvalue Calculations," *Trans. Am. Nucl. Soc.*, **65**, 235 (1992).
- [80] R. THAKUR, R. RABENSEIFNER, and W. GROPP, "Optimization of Collective Communication Operations in MPICH," *Int. J. High Perf. Comput. Appl.*, **19**, 1, 119 (2005).
- [81] M. BARNETT et al., "Interprocessor Collective Communication Library (Inter-Com)," *Proc. Supercomputing '94*, November 14–18, 1994.
- [82] R. J. BRISSENDEN and A. R. GARLICK, "Biases in the Estimation of k_{eff} and its Error by Monte Carlo Methods," *Ann. Nucl. Energy*, **13**, 2, 63 (1986).
- [83] B. NEASE, T. UEKI, T. SUTTON, and F. BROWN, "Instructive Concepts about the Monte Carlo Fission Source Distribution," *Proc. Int. Conf. Mathematics, Computational Methods, and Reactor Physics*, Saratoga Springs, New York, May 3–7, 2009.
- [84] R. C. GEARY, "The Frequency Distribution of the Quotient of Two Normal Variates," *J. Roy. Stat. Soc.*, **93**, 3, 442 (1930).
- [85] S. S. SHAPIRO and M. B. WILK, "An analysis of variance test for normality (complete samples)," *Biometrika*, **52**, 3–4, 591 (1965).
- [86] P. K. ROMANO and B. FORGET, "Reducing Parallel Communication in Monte Carlo Simulations via Batch Statistics," *Trans. Am. Nucl. Soc.*, **107**, 519 (2012).
- [87] E. M. GELBARD and R. PRAEL, "Computation of Standard Deviations in Eigenvalue Calculations," *Prog. Nucl. Energy*, **24**, 237 (1990).
- [88] H. J. ALME, "Domain Decomposition Models for Parallel Monte Carlo Transport," *J. Supercomput.*, **18**, 1, 5 (2001).
- [89] R. PROCASSINI et al., "New Capabilities in Mercury: A Modern, Monte Carlo Particle Transport Code," *Proc. Joint International Topical Meeting on Mathematics & Computation and Supercomputing in Nuclear Applications*, Monterey, California, April 15–19, 2007.
- [90] R. PROCASSINI, M. O'BRIEN, and J. TAYLOR, "Load Balancing of Parallel Monte Carlo Transport Calculations," *Proc. Mathematics and Computation, Supercomputing, Reactor Physics and Nuclear and Biological Applications*, Avignon, France, September 12–15, 2005.
- [91] G. GREENMAN, M. O'BRIEN, R. PROCASSINI, and K. JOY, "Enhancements to the combinatorial geometry particle tracker in the Mercury Monte Carlo transport code: Embedded meshes and domain decomposition," *Proc. International*

Conference on Mathematics, Computational Methods and Reactor Physics, Saratoga Springs, New York, May 3–7, 2009.

- [92] T. A. BRUNNER, T. J. URBATSCH, T. M. EVANS, and N. A. GENTILE, “Comparison of four parallel algorithms for domain decomposed implicit Monte Carlo,” *J. Comput. Phys.*, **212**, 527 (2006).
- [93] T. A. BRUNNER and P. S. BRANTLEY, “An efficient, robust, domain-decomposition algorithm for particle Monte Carlo,” *J. Comput. Phys.*, **228**, 3882 (2009).
- [94] N. C. SLY et al., “Verification of the Shift Monte Carlo Code with the C5G7 Reactor Benchmark,” *Proc. PHYSOR – Advances in Reactor Physics – Linking Research, Industry, and Education*, Knoxville, Tennessee, April 15–20, 2012.
- [95] A. SIEGEL, K. SMITH, P. FISCHER, and V. MAHADEVAN, “Analysis of communication costs for domain decomposed Monte Carlo methods in nuclear reactor analysis,” *J. Comput. Phys.*, **231**, 3119 (2012).
- [96] A. R. SIEGEL, K. SMITH, P. K. ROMANO, B. FORGET, and K. FELKER, “The effect of load imbalances on the performance of Monte Carlo codes in LWR analysis,” *J. Comput. Phys.* (2012).
- [97] L. R. SCOTT, T. CLARK, and B. BAGHERI, *Scientific Parallel Computing*, Princeton University Press, Princeton, New Jersey (2005).
- [98] A. J. WALLCRAFT, “SPMD OpenMP versus MPI for ocean models,” *Concurrency - Practice and Experience*, **12**, 12, 1155 (2000).
- [99] Y. G. PASHKIN, “Accuracy of the Wigner approximation,” *Atomic Energy*, **28**, 2, 184 (1970).
- [100] F. B. BROWN and W. R. MARTIN, “High Performance Computing and Monte Carlo,” *Trans. Am. Nucl. Soc.*, **91**, 1, 279 (2004).
- [101] P. ROMANO, B. FORGET, and F. BROWN, “Towards Scalable Parallelism in Monte Carlo Transport Codes Using Remote Memory Access,” *Prog. Nucl. Sci. Technol.*, **2**, 670 (2011).
- [102] Q. NIU et al., “A Global Address Space Approach to Automated Data Management for Parallel Quantum Monte Carlo Applications,” *Proc. IEEE International Conference on High Performance Computing*, Pune, India, December 18–21, 2012.
- [103] P. K. ROMANO, A. R. SIEGEL, B. FORGET, and K. SMITH, “Data decomposition of Monte Carlo particle transport simulations via tally servers,” *J. Comput. Phys.* (2012), Submitted.
- [104] S. ALAM et al., “Early Evaluation of IBM BlueGene/P,” *Proc. SC08: International Conference of High Performance Computing, Networking, Storage, and Analysis*, Austin, Texas, November 15–21, 2008.

- [105] J. BEECH-BRANDT, “Gemini description, MPI,” *Proc. HLRS Cray XE6 Optimization Workshop*, Stuttgart, Germany, February 2–4, 2011.
- [106] T. UEKI and F. B. BROWN, “Stationarity Diagnostics Using Shannon Entropy in Monte Carlo Criticality Calculation I: F Test,” *Trans. Am. Nucl. Soc.*, **87**, 156 (2002).
- [107] B. SHI and B. PETROVIC, “Convergence Diagnostics for Eigenvalue Problems with Linear Regression Model,” *Proc. International Conference on Mathematics and Computational Methods Applied to Nuclear Science and Engineering*, Rio de Janeiro, Brazil, May 8–12, 2011.
- [108] E. M. GELBARD, F. B. BROWN, and A. G. GU, “Estimation of Fission Source Bias in Monte Carlo Eigenvalue Calculations,” *Trans. Am. Nucl. Soc.*, **69**, 201 (1993).
- [109] E. M. GELBARD and A. G. GU, “Biases in Monte Carlo Eigenvalue Calculations,” *Nucl. Sci. Eng.*, **117**, 1 (1994).
- [110] E. FRIDMAN and J. LEPPÄNEN, “On the use of the Serpent Monte Carlo code for few-group cross section generation,” *Ann. Nucl. Energy*, **38**, 6, 1399 (2011).
- [111] J. M. POUNDERS and F. RAHNEMA, “On the Diffusion Coefficients for Reactor Physics Applications,” *Nucl. Sci. Eng.*, **163**, 3, 243 (2009).
- [112] B. BECKER, R. DAGAN, and G. LOHNERT, “Proof and implementation of the stochastic formula for ideal gas, energy dependent scattering kernel,” *Ann. Nucl. Energy*, **36**, 4, 470 (2009).
- [113] E. E. SUNNY, F. B. BROWN, B. C. KIEDROWSKI, and W. R. MARTIN, “Temperature Effects of Resonance Scattering for Epithermal Neutrons in MCNP,” *Proc. PHYSOR – Advances in Reactor Physics – Linking Research, Industry, and Education*, Knoxville, Tennessee, April 15–20, 2012.
- [114] T. M. SUTTON, T. H. TRUMBULL, and C. R. LUBITZ, “Comparison of Some Monte Carlo Models for Bound Hydrogen Scattering,” *Proc. International Conference on Mathematics, Computational Methods and Reactor Physics*, Saratoga Springs, New York, May 3–7, 2009.
- [115] A. T. PAVLOU, F. B. BROWN, W. R. MARTIN, and B. C. KIEDROWSKI, “Comparison of Discrete and Continuous Thermal Neutron Scattering Treatments in MCNP5,” *Proc. PHYSOR – Advances in Reactor Physics – Linking Research, Industry, and Education*, Knoxville, Tennessee, April 15–20, 2012.